2009

Cortical Bone Tissue Engineering;Scaffold Design and Cell Selection

Demin Wen
Cleveland State University

CORTICAL BONE TISSUE ENGINEERING:

SCAFFOLD DESIGN AND CELL SELECTION

DEMIN WEN

Bachelor of Science in Biochemical Engineering

East China University of Science and Technology

June, 2000

Master of Science in Biochemical Engineering

East China University of Science and Technology

June, 2003

Submitted in partial fulfillment of requirement for the degree

DOCTORATE OF ENGINEERING

At the

CLEVELAND STATE UNIVERSITY

May, 2009

This dissertation has been approved

for the Department of CHEMICAL AND BIOMEDICAL ENGINEERING

and the College of Graduate Studies by

_____

Dissertation Chairperson, Ronald J. Midura

_____

Department & Date

_____

Joanne M. Belovich

_____

Department & Date

_____

Kathleen A. Derwin

_____

Department & Date

_____

Shuvo Roy

_____

Department & Date

_____

Crystal Weyman

_____

Department & Date

CORTICAL BONE TISSUE ENGINEERING:

SCAFFOLD DESIGN AND CELL SELECTION

DEMIN WEN

ABSTRACT

Cortical bone tissue engineering provides a promising approach to generate graft materials needed to treat the large sized bone defects. The underling premise of tissue engineering is to mimic the *in vivo* microenvironment as best as possible *in vitro* culture system. To select an appropriate scaffold material used in this model system, mechanical and hydraulic permeability properties of 316L porous stainless steel and polymethylmethacrylate (PMMA) were studied, as well as their biocompatibility in short and long term cell culture. Results showed that scaffolds made of both stainless steel and PMMA: (1) could be manufactured to have similar permeability as that cortical bone, (2) exhibited biocompatibility in short term cell culture; and that as the ultimate tensile strength was concerned, the scaffold made of stainless steel was similar to cortical bone while not PMMA; and that as the elastic modulus was concerned, neither scaffolds made of stainless steel or PMMA was similar to cortical bone. To establish an optimal culture condition and select an appropriate cell source, the influence of an artificial osteoid layer made from type I collagen and fibronectin on the osteogenesis of bone marrow and periosteum cells were studied. Results showed that more extracellular matrix and calcium minerals were deposited in cultures on the artifical osteoid layer than on conventional 2D plastic; and that polarity of cell density distribution occurred in cultures on the artifical osteoid layer while not on 2D plastic; and that there was no significant difference of the osteogenesis between the cultures of bone marrow cells and periosteum cells.

TABLE OF CONTENTS

LIST OF FIGURES

x

LIST OF TABLES

LIST OF ABBREVIATIONS

ARS: Alizarin Red

BSP: Bone Sialoprotein

DAPI: 4',6-diamidino-2-phenylindole

DMEM: Dulbecco's Modification of Eagle's Medium

H&E: Hematoxylin and Eosin

MEM: Minimum Essential Media

PBS: Phosphate buffered saline

PMMA: Polymethyl methacrylate

SPARC: Secreted protein, acidic, cysteine-rich

TBS: Tris Buffered Saline

CHAPTER I

INTRODUCTION

Damage to weight bearing bones either due to pathologies or trauma is a common occurrence and represents a significant problem in orthopedics [1, 4]. Large-sized bone defects and recalcitrant fractures often require surgical intervention using grafting materials to provide the best potential for healing. More than 500,000 bone-grafting procedures are performed annually in the United States as well as 1.2 million worldwide. For the average procedure, the initial surgical cost is around $20,000 US [4]. Therefore around 10 billion dollars in United States and 24 billion dollars worldwide are expended annually to treat large-sized bone damage. Among the bone grafts used in these procedures, about 55% are autografts and 35% are allografts [4, 39, 69]. The limitations of these two grafts are that (1) autografts are not always available and require a second operation, and (2) allografts are sometimes susceptible to disease transmission from donor to recipient. The other 10% bone graft substitutes include metals, natural and

synthetic polymers, ceramics and composite materials [66]. The criteria for the success of bone graft substitutes to regenerate new bone are: (1) biocompatibility, (2) osteoconductivity – permitting cells to attach, proliferate and migrate and allowing nutrient-waste exchange and vessel penetration, (3) osteoinductivity – inducing the osteoprogenitors to differentiate into osteoblasts, and (4) osteogenicity – producing mineralized tissue matrix [1, 4, 28, 39, 95]. Unfortunately, not all of existing substitutes satisfy all of the criteria required to regenerate substantial amounts of new osseous tissue. Therefore new bone graft substitutes still need to be designed and generated to fully match these criteria. Bone tissue engineering provides a promising new approach to generate novel graft substitutes combining cells, scaffolds, growth factors and mechanical loads that should satisfy all of the above criteria in a cost effective manner [1, 4, 28, 29, 33, 39, 51, 75, 95].

An underlining premise of bone tissue engineering is to mimic key aspects of the *in vivo* microenvironment as best as possible within *in vitro* bioreactor culture systems. Several laboratories are developing bone culture systems in attempts to generate functional bone tissue *in vitro* using tissue engineering principles [6, 22, 30, 33, 49, 50], though none of them have been able to generate cortical bone tissue in a bioreactor system. This is in stark contrast to ample formation of functional cortical bone tissue *in vivo.* We surmise from this discrepancy that there must be some key attributes lacking in current *in vitro* bone bioreactor systems which are necessary for bone cells to behave as they do *in vivo*.

One attribute that still needs to be addressed is hydraulic permeability of cortical bone. Permeability is defined as the ease with which a fluid passes through a porous material and can be determined from Darcy's Law [69, 74]. The permeability of cortical bone is important for nutrient and growth factor transport, and waste product exchange. This places permeability critically important to maintain osteocyte viability and regulate the physiological processes of bone remodeling and homoestasis [17, 69].

Secondly, osteoid is the densely packed organic matrix secreted by mature surface osteoblasts that eventually becomes mineralized and forms bone tissue [9, 44]. Osteoblasts express receptors that engage two key molecules in osteoid, type I collagen and fibronectin. These receptors modulate interactions that have been reported to promote the process of osteogenesis [22, 27, 30, 33, 54, 62, 65, 87, 92, 93]. Thus the permeability of cortical bone and the assembly of an osteoid layer may be important for osteoblasts to optimize the formation of bone tissue *in vivo*. Accordingly, this dissertation will focus on cortical bone permeability and the interaction of osteoblasts with osteoid as two potential attributes that need to be investigated in a tissue engineering approach to form functional cortical bone tissue *in vitro*. The following chapters of this dissertation will focus on testing these attributes.

Chapter III-- Stainless steel and poly(methyl methacrylate) (PMMA) are commnonly used in orthopaedic procedures [66]. They were selected as candidate scaffold materials to be used in bone tissue engineering since they are inexpensive materials that can be fabricated in varying shapes and exhibit acceptable biocompatibility. Still their

mechanical properties (elastic modulus, ultimate tensile strength) and hydraulic permeability need to be investigated in order to choose those scaffold materials that best mimic key cortical bone properties. In addition, their biocompatibility needs to be tested by culturing bone cells on these scaffold materials.

In Chapter III, we proposed that (1) stainless steel and PMMA could be manufactured to exhibit similar pore size, permeability and mechanical properties as cortical bone, and (2) stainless steel and PMMA would exhibit sufficient biocompatibility in the cultures. To test the first hypothesis, the pore size, permeability and mechanical properties (elastic modulus, ultimate tensile strength) of stainless steel and PMMA were measured and compared with authentic cortical bone. To test the second hypothesis, for short term biocompatibility test, the cell attachment percentage and proliferation of UMR osteoblastic cells cultured on PMMA and stainless steel scaffolds for 14 days were compared with cultures on conventional plastics. Also, for long term biocompatibility test, MC-4 pre-osteoblasts and periosteum- derived primary bone cells were cultured on stainless steel scaffolds for 25 days and the cell morphology and cell numbers were analyzed by histology and histomorphometry.

Chapter IV-- The permeability of cortical bone still needs to be accurately measured since few studies have experimentally measured the hydraulic permeability of adult cortical bone. In addition, there are no reports in the literature establishing what chemical components of cortical bone tissue regulate its hydraulic permeability. Knowledge regarding the permeability of cortical bone and the chemical components that may affect

cortical bone permeability is needed to help select scaffold materials that best mimic this property of cortical bone. Ultimately we intend to use this information in order to promote functional cortical bone tissue formation *in vitro*. Therefore, studies were completed to (1) accurately measure the permeability of adult cortical bone, and (2) determine the contribution of lipids and densely packed collagen matrix to the permeability of cortical bone.

In Chapter IV, we hypothesize that: (1) the presence of hydrophobic molecules within the porous compartment of cortical bone would reduce its permeability, and that removal of such hydrophobic materials would increase its permeability; and (2) the presence of a densely packed pericellular matrix (mostly type I collagen) within the porous compartment of cortical bone would reduce its permeability, and that removal or loosening of such collagen matrix would increase its overall permeability. To test these hypotheses, a new device with a detection limit of $4 \times 10^{-17} \text{ m}^2$ was designed to sequentially measure radial hydraulic permeability of the cortical bone wafers (1.5 mm thickness), before and after removing lipids, and digesting with bacterial collagenase. Confirmation of lipid extraction was done using gas chromatography and mass spectroscopy, while collagen digestion was monitored by a colorimetric method to measure hydroxyproline.

Chapter V-- Nutrient and waste product transport in bone tissue are controlled by both hydraulic permeability (a measure of the ability of a material to transmit fluids) and molecular diffusion (a net transport of molecules from a region of higher concentration to

one of lower concentration by random molecular motion). Knowing which property has a greater influence on nutrient transport in cortical bone tissue should aid in the selection of appropriate scaffolds for bone tissue engineering. Therefore, In Chapter V, the diffusion coefficient of glucose in cortical bone in radial direction was measured with diffusion cell. And a mathematical model was established to calculate the glucose concentration profile in the cultures with the scaffold material.

Chapter VI-- As previously mentioned, the presence of osteoid in long bone surfaces may be an important characteristic that needs to be mimicked *in vitro* in order to promote optimal osteogenesis leading to functional bone tissue formation. Osteoid is composed of collagen fibers and several non-collagenous proteins. The predominant fibrillar collagen in osteoid is type I collagen. In addition, an important matricellular protein, fibronectin, is found in the osteoid layer and is required for osteoblast differentiation and vitality.

Therefore in Chapter VI, we attempted to mimic this osteoid structure with a 3-D hydrogel made of native type I collagen and fibronectin. The osteogensis of different types of natural osteoprogenitor cells (bone marrow and periosteum derived cells) were measured on these 3D hydrogels and compared with conventional 2D plastic culture dishes. In this system the following hypotheses were tested: (1) osteo- progenitors derived from bone marrow and periosteum cells exhibit equivalent osteogenesis; (2) cell morphology at different stages of osteogenesis would be different; (3)more extracellular matrix would be deposited in the cultures of both periosteum and bone marrow cells on collagen-fibronectin hydrogels compared with cultures on conventional plastic, and a

more basal lateral deposition pattern of extracellular matrix would be observed collagen-fibronectin hydrogel cultures while less so on conventional plastic; (4) and more mineral would be deposited in cultures of periosteum and bone marrow cells on collagen-fibronectin hydrogels compared with cultures on conventional plastic, and a more basal lateral deposition pattern of mineral would be observed in collagen-fibronectin hydrogel cultures while less so on conventional plastic. To test these hypotheses, bone marrow and periosteum cells were cultured both on 3D collagen fibronectin hydrogels and 2D plastic. The amount and distribution of extracellular matrix (Bone sialoprotein (BSP) and Sereted protein acid rich with cysteines (SPARC)) and calcium mineral deposited in the cultures were measured by histomorphometry.

Chapter VII-- This chapter summarizes the novel findings from my investigations. It attempts to explain the limitations of these findings, provides conclusions stemming from these findings and discusses the physiological and tissue engineering relevance of the findings. Finally, comments are made on the next level of investigation that would logically build on these current data for future experimentation.

In all our approach and system design may provide a means for studies to be conducted towards the development of functional bone tissue *in vitro*. Our ultimate goal is to generate a functional bone tissue on a biocompatible scaffold, which will be peeled off from the scaffold and used as bone scaffold material to treat large size bone defect. The contents included in this dissertation provide the first step (scaffold and cell source selection) to develop the model system. And in the future growth factors and/or

biophysical stimuli will be incorporated into this system to promote sustained bone

formation *in vitro*.

CHAPTER II

BACKGROUND

2.1 Overview of Bone Tissue Engineering

Bone damage due to pathologies or traumas is a common occurrence and the repair of this damage represents a major concern in orthopedics. Large size defects in load bearing bones with limited healing capacity often require graft intervention to provide the best potential for healing [4, 39]. The choices of bone graft include autografts, allografts and synthetic bone graft substitutes. Autografts, bone tissue taken from another part of a patients' own body (e.g., grafts taken from the patient's iliac crest) set a gold standard for bone graft choices. A patient's overall health and the pain and morbidity of a second operation site restrict autograft applications. Allografts are bone tissues taken from cadavers. In addition to a limited availability, allografts involve the risk of blood-borne diseases and must be correctly donor-receiver immune matched [4, 28, 95]. Synthetic bone grafts are readily available, but from a mechanical aspect, they do not have the same

toughness and stiffness properties as cortical bone. From a biocompatibility aspect, some synthetic grafts lack either osteoconductive or osteoinductive properties [1, 28]. Therefore new bone graft substitutes with improved osteogenic properties are still needed. To these ends, one approach is bone tissue engineering, which may produce variably sized bone graft substitutes in the laboratory using a patient's own source of bone cells from either periosteum [30, 39,, 42, 89], or bone marrow [5, 6, 13, 33, 39, 50, 51, 76-79].

Tissue engineering is "an interdisciplinary field of research that applies the principles of engineering and life sciences towards the development of biological substitutes that restore, maintain, or improve tissue function"[29]. For bone tissue engineering an underlining premise is to mimic essential aspects of the *in vivo* bone tissue microenvironment as best as possible in an *in vitro* culture environment. Four different parameters affecting bone tissue engineering need to be investigated and optimized: bone cells, scaffold materials, growth factors and mechanical load [29, 33, 66].

2.2 Bone

Bone is a living, highly vascular and dynamic mineralized connective tissue. It is characterized by it hardness, growth mechanisms, resilience and its ability to remodel and repair itself with high fidelity [9]. Its four main components are bone matrix, bone cells, bone marrow and its associated vascular network (Figure 2-1). Bone tissue matrix is comprised of organic and inorganic molecules. This biocomposite nature provides mechanical strength and a mineral store for the body [9, 17]. Various types of bone cells form (osteoblast), maintain (osteocytes), or resorb (osteoclast) this tissue matrix [9]. Bone

10

marrow, periosteum and associated vasculature provide sources of osteogenic stem cells. At the organ and tissue levels, bone is subjected to dynamic mechanical deformation. Mechanical stress or "load" has important consequences for the health of this tissue since bone loss occurs in the absence of mechanical load. The physiological range of mechanical strains in cortical bone tissue is 0.04~0.3% [17, 23, 31].
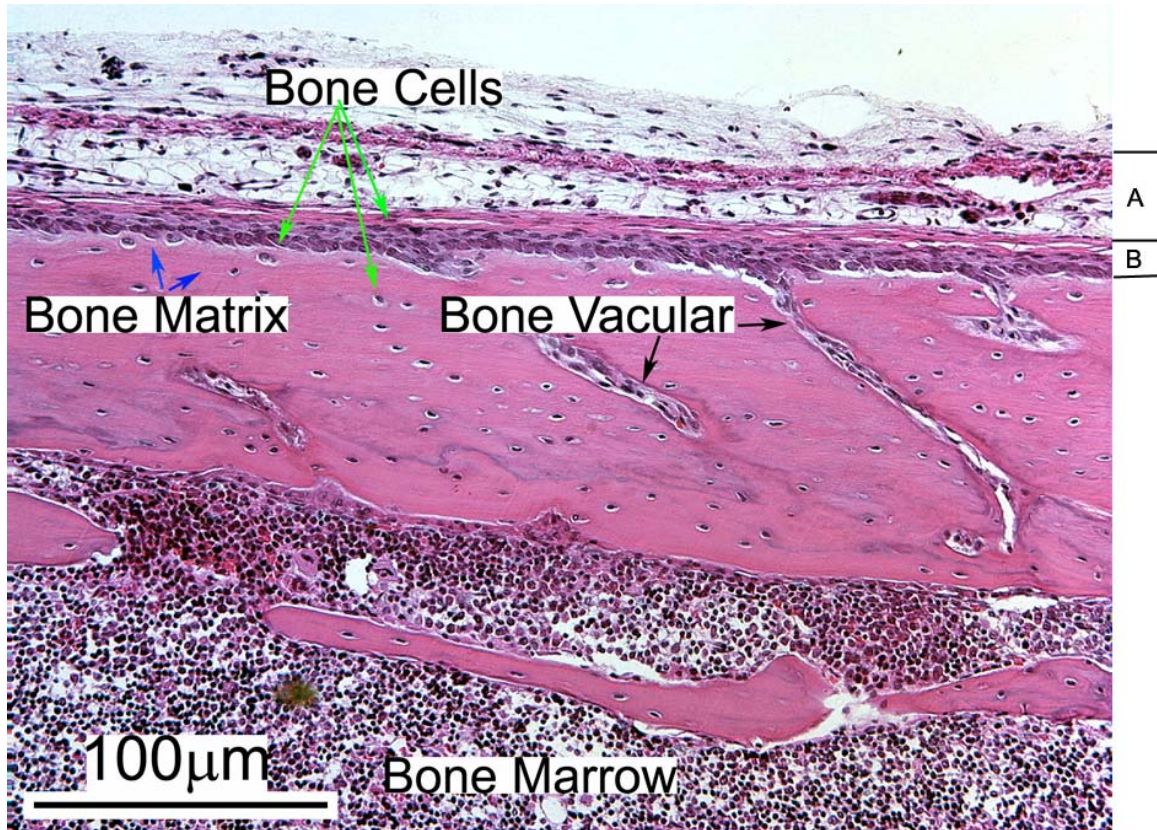
Figure 2-1 Hematoxylin and eosin (H&E) staining image of tibial diaphysis from a juvenile rat. A: Periosteum fibrous layer. B: Osseous cambium layer, done in Midura lab

The formation of bone during the fetal stage of development occurs by two general processes: intramembranous and endochondral ossification [9]. Intramembranous

11

ossification mainly occurs during formation of the flat bones of the skull; the bone is formed directly from mesenchyme tissue without a cartilaginous intermediate. Endochondral ossification, on the other hand, occurs in long bones, and forms using a cartilage tissue template. Remodeling is the process of resorption followed by replacement of new bone with little change in shape and occurs throughout a person's life [9]. Osteoblasts and osteoclasts, coupled together via paracrine cell signalling, are referred to as bone remodeling units. The purpose of remodeling is to regulate calcium homeostasis, repair micro-damaged bones (from everyday stress) but also to shape and sculpture the skeleton during growth. Bone resorption is done by osteoclasts [9].

Bone formation is done by osteoblasts through secretion of osteoid, which is stimulated by the secretion of several hormones and growth factors including growth hormone, thyroid hormone and the sex hormones (estrogens and androgens) [9]. Osteoid is the densely packed organic matrix that eventually becomes mineralized and forms bone tissue. Osteoid is composed of collagen fibers (mainly type I collagen) and several non-collagenous proteins (such as fibronectin). Receptors expressed on osteoblasts can interact with the molecules in the osteoid layer to promote the process of osteogenesis [9]. Moreover, the osteoid layer is always deposited underneath the osteoblast (basal deposition pattern). This basal deposition pattern is important for osteoblasts to continue to form new cortical bone to widen the girth of long bone shafts [9]. This pattern may influence the packing and assembling of extracellular matrix deposited by osteoblasts,

12

and thereby influences the interactions of matrix receptors on osteoblasts and their extracellular matrix molecules, ultimately influencing the entire osteogenesis process [9].

2.3 Cells used in bone tissue engineering field

Sources of cells used in bone tissue engineering includes mesenchymal stem cells derived from different tissues, such as bone marrow, periosteum, human umbilical cord blood[5, 6, 13, 29, 30, 33, 39, 42, 50, 51, 76-79, 89], and mature osteoblast cells, such as primary cells from human trabecular bone obtained during iliac crest biopsies [60]. Mesenchymal stem cells are mostly used in tissue engineering since compared to mature 30 osteoblasts cells, they proliferate quicker and have longer population doubling limits [66]. Specifically, mesenchymal stem cells from bone marrow and periosteum are two sources widely used by investigators.

Bone marrow is the highly cellular tissue found in the medullary cavity of long bones (Figure 2-1) [9]. Cells from bone marrow comprise a heterogeneous group of phenotypes including hematopoietic stem cells, mesenchymal stem cells and endothelial stem cells [9]. Mesenchymal stem cells, a source of primary cells used in bone tissue engineering, can be separated from the other two stem cell populations by a colony forming adhesion assay [66]. Studies have shown the osteogenesis potential of bone marrow cells. For example, Barralet et al. cultured bone marrow cells on type I collagen gels for 21-28 days and showed new osteoid-like tissue formation by these cells [6]. Sikavitsas et al. cultured bone marrow cells in a flow perfusion bioreactor and showed that such a fluid-flow bioreactor culture system minimized diffusion constraints and

provided mechanical stimulation to the bone marrow cells, leading to the accumulation of a cancellous bone-like mineralized tissue [78]. Although these studies demonstrated the osteogenic nature of these cells, they were not able to generate cortical-bone like tissue *in vitro*.

Periosteum is the layer of cells that lines the outer surface of all bones, except at the joints of long bones (Figure. 2-1).[9] It consists of an irregular type of dense connective tissue and is divided into an outer "fibrous layer" and inner "cambium layer". The fibrous layer contains fibroblasts, adipocytes, and blood vessels, while the cambium layer contains osteo-progenitor cells which develop into osteoblasts.[9] These osteoblasts are responsible for increasing the width of a long bone and the overall size of other bone types. Osteo-progenitor cells within the periosteal cambium layer can be isolated, which provides another source of primary osteoblastic cells for bone tissue engineering [30, 89]. Several studies have reported on the osteogenic properties of periosteal cells. Wiesmann et al. cultured periosteal derived osteoblasts on Petri dishes as well as within 3D collagen constructs. They showed that these cells can form 'bone like' mineral deposits in both 2- and 3-D environments and formed an extracellular matrix containing osteocalcin, SPARC (osteonectin), and newly synthesized collagen type I in both environments [89].Koshihara et al showed that periosteum cells are osteoblastic cells and could differentiat into osteocytes and deposited calcified mineral in response to 1, 25 dihydroxyvitamin D_3 [48].

2.4 Scaffolds used in bone tissue engineering

One of the four key elements in bone tissue engineering is a scaffold. The gold standard used in bone tissue engineering is autograft. Generally speaking, the criteria for selecting a scaffold includes[4, 30, 66 95]: (1) biocompatibility, (2) osteoconductivity – permitting cells to attach, proliferate and migrate and allowing nutrient-waste exchange and vessel penetration, (3) osteoinductivity – inducing osteoprogenitors to differentiate into osteoblasts, and (4) osteogenicity – producing ample amounts of mineralized tissue matrix. Besides these criteria, there are two more issues to be considered: (1) they should have similar mechanical properties as bone tissue; and (2) they should have similar hydraulic permeability as bone so that they can have proper nutrient/waste product exchange rates.

Currently many kinds of materials have been used in bone tissue engineering, which include demineralized allograft bone matrix, ceramics and ceramic composites [4, 30], collagen-mineral composites [86], bioactive glass [52], synthetic biodegradable polymers [108] and metals [3]. Demineralized allograft bone matrix is a biologically derived material exhibiting both osteoconductive and osteoinductive properties. Yet it lacks stiffness and in some cases may cause an immune-reaction [39, 66, 95]. Ceramics and ceramic composites are synthetic materials exhibiting osteoconductive properties and have a similar stiffness as that of bone. Yet they are limited by a lack of osteoinductivity and do not exhibit the same elastic modulus as that of bone [39, 66, 95]. Collagen-mineral composites are matrices that exhibit the advantages of ceramics and demineralized allograft bone matrix, but still do not exhibit the same elastic modulus as

that of bone [39, 66, 95]. Bioactive glass exhibits both osteoconductive and osteoinductive properties, but does not have the same stiffness or toughness of bone [39, 66, 95]. Synthetic polymers exhibit osteoconductive properties and are biodegradable [39, 66, 95]. Yet, several such polymers can elicit metabolic side effects as they decompose to monomers. Metals, such as stainless steel or titanium, exhibit osteoconductive but no osteoinductive properties [39, 66, 95]. Thus the selection of an optimal bone scaffold material has not reached a single consensus and still requires careful consideration.

2.5 Biophysical stimuli used in bone tissue engineering

At the organ and tissue levels, bone is subjected to dynamic mechanical deformation [17]. Mechanical stress or "load" has important consequences for the health of bone tissues [12, 16, 17]. Studies have shown that *in vitro*, application of dynamic mechanical forces influence bone cell proliferation and osteogenesis [33, 34, 50, 81]. Two different mechanisms have been investigated for explaining a bone cell's response to mechanical load. One states that mechanical load drives nutrient and metabolite transport within bone tissue via fluid flow [18]. Such induced fluid flow can generate streaming potentials caused by fluid moving back and forth across fixed charges in the tissue matrix that generate electrical potentials. These streaming potentials are thought to play an important role in modulating bone cell activity [18, 33].

Another mechanism states that mechanical load is sensed directly by mechanoreceptors on the surface of bone cells leading to intracellular signaling in a manner referred to as the mechanotransduction pathway [32]--one common pathway for

16

force transmission is via the focal adhesions. Transmembrane proteins including mechanosensitive ion channels and signaling molecules such as integrins, form focal cell adhesions with the extracellular matrix. These focal adhesions constitute a primary pathway for intracellular force transmission and therefore have been viewed as likely candidates for an initiating mechanosensing event. On the intracellular side, many proteins tend to localize to focal adhesions, binding directly to either the α- or β-subunits of the integrin heterodimer. Other proteins link integrins to the actin cytoskeleton, having binding domains for both integrins and actin. Cell-cell junctional complexes and cell-matrix interactions transmit mechanical stimuli to the internal cellular structures via cytoskeletal components. Some pathways of mechanotransduced signals lead to gene activation at the nucleus via nuclear junctions [32].

In vitro, mechanical loads are applied by an actuator device in a bioreactor system. Ideally, a bone tissue engineering bioreactor system should support rapid and orderly development of functional bone tissue by providing control over the entire cellular microenvironment (eg., temperature, pH, osmolality, levels of oxygen, nutrients, metabolite and regulatory molecules) [66, 78]. Such control would facilitate mass transfer to and from cells, and provide physiologically relevant stimuli and signals (eg., streaming potentials, mechanotransduction) [69]. Different bioreactor designs have been used in attempts to make tissue-engineered bone utilizing different scaffold materials and bone cell sources, and these designs include spinner flasks, rotating wall vessels, flow perfusion and mechanical loading devices [77, 78]. Mauney et al. applied mechanical

loads in a 3-D bioreactor system and showed that mechanical stimulation significantly reduced apoptosis and improved osteocyte viability in human bone tissue samples obtained from human patients [50]. Gomes et al. cultured bone marrow cells on porous fiber mesh scaffolds obtained from a blend of starch and poly(-caprolactone) in a fluid flow perfusion bioreactor. They showed that levels of alkaline phosphatase activity were higher in flow cultures compared to static ones, and that pore-like structures were formed within the extracellular matrix which were not observed in static cultures [25]. Meinel et al. cultured bone marrow derived mesenchymal stem cells in spinner flasks and observed that a dynamic flow environment upregulated their osteogenesis [51]. Yu et al cultured rat calvarial osteoblast cells in a dynamic flow culture system using high-aspect-ratio rotating vessel bioreactors and 3D scaffolds. They showed that a 3D dynamic flow environment affected bone cell distribution, enhanced osteogenic gene expression and increased the production of a mineralized matrix compared to static conditions [94]. Sikavitsas et al. cultured bone marrow stromal cells in spinner flasks and demonstrated enhanced cell proliferation at the end of the first week in spinner flasks as compare to static cultures [79].

2.6 Our proposed bone model system

Native cortical bone can be separated into three layers: periosteum tissue layer, osteoid layer and bone tissue layer (Figure 2-2). In our tissue engineering bone system, we attempt to mimic these three layers in order to promote bone formation *in vitro* as described in Figure 2-2. Specifically, periosteum tissue layer will be mimicked by

isolated bone marrow or periosteum cells since these two cell types are primary bone cells and exhibit osteogenesis *in vitro*. The osteoid layer will be mimicked by a native type I collagen gel and fibronectin coating, as type I collagen is the main component in bone extracellular matrix, and fibronectin is an extracellular matrix protein with a collagen binding domain. Fibronectin also promotes bone cell adherence, proliferation and osteogenic differentiation. The bone layer will be mimicked by a long term biocompatible scaffold material with similar mechanical and permeability properties as cortical bone.
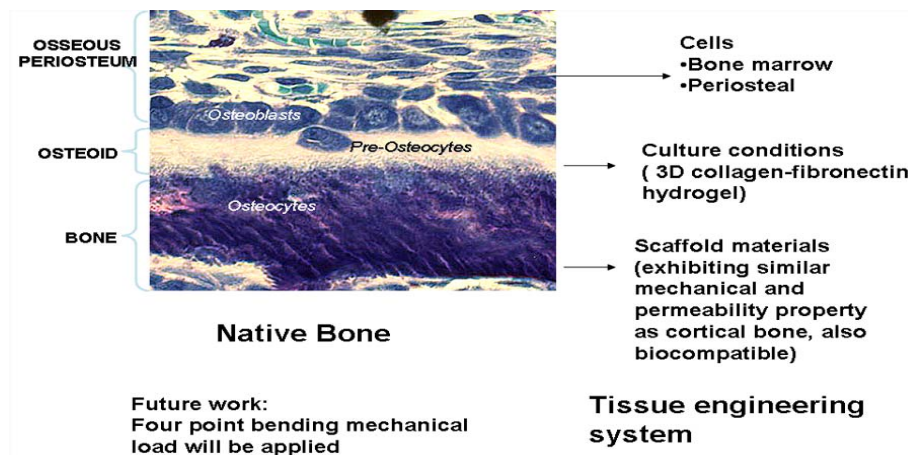
Figure 2-2 Cortical bone tissue engineering system.

2.7 Summary

In summary, to build our bone model system, firstly the selected scaffold should have similar mechanical and permeability properties as cortical bone, and should be biocompatible; therefore the mechanical, the permeability and biocompatible properties of PMMA and stainless steel were investigated in Chapter III. Secondly, the contribution

of bone components to its permeability can be used to modify the permeability scaffold to obtain the similar permeability as bone; therefore the permeability of cortical bone and contribution of lipids and collagen matrix to its permeability were investigated in Chapter IV. Thirdly, nutrient supply was important issue to be considered in culture system and diffusion was the only way for the glucose transport in the static culture system; therefore the diffusion coefficient of glucose in cortical bone was investigated and a mathematical model was established to predict the glucose concentration profile in the static culture system in Chapter V. Fourthly, osteoid layer was bone mineralization front and promoted osteogenesis *in vivo*; therefore an artificial osteoid layer made of type I collagen and fibronectin was investigated as a culture condistion to promotes the osteogenesis *in vitro* culture system in Chapter VI. Fifthly, osteoblasts derived from periosteum and bone marrow tissues showed their osteogenesis *in vitro* culture system; to select cells used in the model system, osteogenesis of these two cell types were investigated in Chapter VI.

In all our approach and system design may provide a means for studies to be conducted towards the development of functional bone tissue *in vitro*. Specifically, our design incorporates the use of a biocompatible bone–like scaffold layer coated with a bioartifical " osteoid" layer of type I collagen and fibronectin, and primary osteogenitor cells as our first step to develop bone tissue *in vitro*. Based on this, in the future we may incorporate growth factors and/or biophysical stimuli into this system to promote sustained bone formation *in vitro*.

CHAPTER III

PROPERTIES OF PMMA AND STAINLESS STEEL SCAFFOLDS

3.1 Introduction:

Scaffold is one of four components (cells source, scaffolds, growth factors and biophysical stimuli) that needs to be considered in bone tissue engineering. Key criteria for choosing appropriate biomaterials as scaffolds to be used in cortical bone tissue engineering are: (1) they should have similar mechanical properties as bone so that they can restore immediate mechanical function; (2) they should have similar permeability as authentic bone to maintain proper nutrient/waste product exchange rates; and (3) they should exhibit full biocompatibility so that they do no harm to surrounding cells and tissues in a patient [39, 66, 95].

Elastic modulus and ultimate tensile strength are two parameters used to evaluate the mechanical properties of bone [17]. An elastic modulus, or modulus of elasticity, is the

mathematical description of an object or substance's tendency to be deformed elastically when a force is applied to it. The elastic modulus of an object is defined as the slope of its stress-strain curve in the elastic deformation region [17]. Stress is the force causing the deformation divided by the area to which the force is applied; and strain is the ratio of the change caused by the stress to the original state of the object. Tensile strength is the stress at which a material breaks or permanently deforms [17]. Ultimate tensile strength is the maximum stress a material can withstand when subjected to tension, compression or shearing. It is the maximum stress on the stress-strain curve [17].

The permeability of cortical bone is the measurement of the ease of fluid flow through cortical bone and can be determined by Darcy's law: $P = \dfrac{\mu L v}{A \Delta p}$. Here, P (m^2) is the hydraulic permeability of the material, μ (1 cp = 0.001 kg / (m·s)) is the viscosity of the fluid flowing through the material, L (mm) is the thickness of the material, v (mL / hr) is the fluid flow rate, A (mm^2) is the area fluid flowing through, Δp (kpa) is the pressure difference between upstream flow and downstream flow.

The definition of biocompatibility has been refined over the last sixty years from "do no harm" to that of being clinically beneficial [28]. In 1940, an early definition of biocompatibility was to be 'non-toxic, non-immunogenic, non-thrombogenic, non-carcinogenic, non-irritant' [28]. In 1987, biocompatibility was redefined as 'the ability of a material to perform with an appropriate host response in a specific situation'[28]. The current definition (2008) of biocompatibility is the 'ability of a biomaterial to perform its

22

desired function with respect to a medical therapy, without eliciting any undesirable local or systemic effects in the recipient or beneficiary of that therapy, but generating the most appropriate beneficial cellular or tissue response in that specific situation, and optimizing the clinically relevant performance of that therapy' [28].

Different biomaterials have been used in bone tissue engineering. They include metals (such as cobalt-chromium alloys, stainless steel and titanium), synthetic polymers (such as PMMA), ceramics, natural collagens and their bio-composites [39, 66, 95]. In the mid 1920's, 316 L stainless steel was developed for surgical implants due to its higher stiffness and higher resistance to corrosion *in vivo* [20]. As of today 316 L stainless steel is still widely used in the field of orthopaedic applications since it has acceptable biocompatibility and physical properties, and can be fabricated into a variety of shapes and sizes for wires, screws and implants [3, 11]. Several studies have been done on the biocompatibility of stainless steel. Puleo et al. [61] showed that stainless steel exhibits good short term biocompatibility. However, Jocobs et al.[36] stated that 316 L stainless steel containing chromium (16-18%) and nickel (10-14%) was a probable source of long-term complications, and their findings suggested caution for its use as an implant. Kraft et al. reported that stainless steel wear debris had a marked and persistent negative effect on leukocyte-endothelium interaction leading to chronic low levels of inflammation [41]. Bailey et al. also reported an immune response of the body to wear debris from stainless steel [3]. There is still no full agreement on the biocompatibility of stainless steel,

23

presumably which may because of the difference in manufacture process and the concentration of its heavy metal components (such as chromium and nickel).

PMMA is another biomaterial widely used in bone tissue engineering since it also exhibits acceptable biocompatibility and is easily to be manufactured [66]. The biocompatibility of PMMA has also been called into question. Chiu et al. showed that PMMA inhibits the proliferation and osteogenic differentiation of bone marrow cells suggesting that PMMA may not always exhibit high levels of biocompatibility [13]. In contrast, Ramachandran et al. showed that osteoblasts exhibited phenotypic stability when cultured on PMMA suggesting that PMMA exhibits adequate biocompatibility [63].

In this part of my study I addressed the selection of a suitable biomaterial as a bone scaffold in attempts to mimic cortical bone properties that may promote bone formation in our bioreactor design. As mentioned in previous chapters, a suitable biomaterial should have similar permeability and mechanical properties as cortical bone, and should be biocompatible in long term cultures. Stainless steel and PMMA were selected as candidates since they are relatively inexpensive to fabricate into any desired size and porosity, are stiff materials and are biocompatible. Therefore I hypothesized that (1) stainless steel and PMMA could be manufactured to exhibit similar porosity, permeability and mechanical properties as cortical bone, and that (2) stainless steel and PMMA would exhibit sufficient biocompatibility in cultures. To test the first hypothesis, the porosity, permeability and mechanical properties (elastic modulus, ultimate tensile strength) of stainless steel and PMMA were measured and compared with cortical bone.

To test the second hypothesis, for short term biocompatibility, the cell attachment percentage and proliferation of osteoblastic cells cultured on PMMA and stainless steel scaffolds for up to 14 days were compared with cultures on conventional tissue culture plastic. Also, for long term biocompatibility test, a pre-osteoblast cell line and periosteum derived primary bone cells were cultured on stainless steel scaffolds for up to 25 days and the cell morphology and cell numbers were analyzed by H&E and DAPI staining.

3.2 Materials and methods

3.2.1 Synthesis of PMMA Scaffolds

Described below is the protocol used to create PMMA scaffolds that have a pore size structure that ranges from 28 -100 μm in diameter. A 'layering' approach utilizing PMMA/Sodium Chloride solutions of two bead diameters (28 μm and 100 μm) was used to create scaffolds with similar porosity property as native cortical bone.

1. Preparation of PMMA Layer Solutions

PMMA layer solutions of varying pore size were prepared as follows: (a) Solution 1 - 0.66 g of PMMA beads (bead diameter of 10-50 μm, Scientific Polymer Products, Inc., Ontario, NY) and 0.66 g of NaCl (sieved to 28 μm mean diameter, Scientific Polymer Products, Inc., Ontario, NY) were combined in a 50 mL conical test tube; (b) Solution 2 - 0.66 g of PMMA beads (as above) and 0.66 g NaCl (sieved to 100 μm mean diameter, Scientific Polymer Products, Inc., Ontario, NY) were combined in a 50 mL conical tube; three tubes of solution 2 were required; and (c) Solution 3 - 0.66 g NaCl (either size)

was placed into a fifth 50 mL conical tube. Test tubes containing solutions 1 and 2 were mixed for 20 s with a spatula, then vortexed for 20 s, followed by incubation at 37°C in a humidified incubator for 48 hr. The solution 3 test tube was incubated in a 60°C dry oven for 48 hr.

2. Preparation of PMMA Scaffolds

In an airflow hood, solution 1 PMMA mixture was spread onto a clean, dry silicone mold evenly along the surface of mold. One mL of acrylic solvent (methylene chloride and diacetone alcohol, Craftics Plastick Acrylic Solvent Cement, Albuquerque, NM) was added wetting the entire surface of layer. Acrylic was used to glue the layers together. This was followed by spreading the first test tube of the solution 2 PMMA mixture evenly over the first layer. This was followed by adding one mL acrylic solvent on top of the second layer. Repeat the same process with the remaining two test tubes of solution 2. Then solution 3 was spread evenly over the fourth layer of PMMA. This fifth layer was spread and evenly distributed with a spatula. Finally the mold was put in place and a 5 pound weight placed on top of the mold cover for a 48 hr period to dry.

After 48 hr, the PMMA scaffold was removed from the mold, then the excess salt crystal was shake off, and the scaffold was placed in a Petri dish. This was followed by a serial washing of the scaffold, first with a 12 mL of 100% ethanol for 30 min, then with a 12 mL 70% ethanol for 30 min. Then they were placed into a 1 L beaker and washed with Milli Q water until the conductivity of the wash water no longer changed (approximately

3-4 days with daily changes of the water in the 1 L beaker). At this point, the PMMA scaffold was ready for permeability and mechanical testing.

3.2.2 Stainless Steel Scaffolds

316L stainless steel disc scaffolds with 0.750 ± 0.05 inch (1.90 ± 0.01 cm) diameter, 1/16 inch (1.5 mm) thick and 0.5 μm pore size were purchased from Mott Corporation (Farmington, CT). The following table (Table 3-1) was the information they provided.

316L SS	Pore size (μm)	Thickness (Inches)	Density (mg/cm^3)	Porosity (%)	Permeability (Darcy Value)
Characteristics	0.5	1.5 mm	5.83	16.8	0.103

Table 3-1: Media Characterization – Mott porous 316LSS disc
*. 1) Darcy value of 1.00 = the flow of 1 cc (mL) of 1 cp (centipoise, 1 cp = 0.001 kg/(m·s)) fluid in 1 second at 1 atmosphere pressure (1atm = 101.3 kpa) through 1 cm^2 x 1 cm thick section of porous media. (1 Darcy = 9.9 x 10^{-14} m^2, therefore, the permeability of stainless steel is 1.02 x 10^{-14} m^2)

3.2.3 Processing for scanning electron microscope (SEM)

Scanning electron microscope (SEM) was used to view the micro-structure of PMMA, stainless steel and cortical bone. For SEM, specimens were fixed, dehydrated and coated with gold. In this study, stainless steel (n=3), PMMA (n=3) and cortical bone (n=3) were submitted for SEM.

1. Fixation.

Specimens were placed into a fixative solution (2% glutaraldehyde (EMS), 3% sucrose (EMS), in 0.1M phosphate buffer (Cellgro) at pH 7.4) for overnight (the volume ratio of specimen to solution was 1:20). This was followed by a serial washing of the

specimen, first with PBS solution, 30 min each time for two times, then with milli Q water, 5 min each time for two times.

2. Dehydration

The specimen was dehydrated with a series of ethanol (Fisher) solutions made from absolute ethanol (v/v) (50%, 70%, 80%, 90%, 95%, 100%, 100%), 15 min in each solution. The specimen was then dried using a series of Hexamethyldisolazane (HMDS) (Electron Microscopy Sciences) in ethanol solution (v/v) (1:1 HMDS-ethanol, 1:1 HMDE-ethanol, 100% HMDS, 100% HMDS, 100% HMDS), 10 min in each solution. Then the specimen stayed in the air-flow hood for 2 hr to evaporate residual HMDS.

3. Images taken

The dehydrated specimen was sputter coated with gold in SPI-Module Sputter Coater (Structure Probe Inc., West Chester, PA).to increase the ability of a specimen to conduct electricity and emit secondary electrons. Then the specimen was ready for SEM imaging.

SEM images were taken with a scanning electron microscope (SEM) (S570, Hitachi, Japan).

3.2.4 Mechanical property measurement

The elastic modulus and ultimate tensile strength of stainless steel (sample size n=3), PMMA (sample size n=3) and cortical bone (sample size n=3) were measured using a 4 point bending holder device. Specifically, specimens were placed in the holder, and a mechanical load was applied on the specimen using an Instron Model 8500 tensile test machine as depicted in Figure 3-1. The load and displacement data were recorded with

time. The elastic modulus and ultimate tensile strength were calculated based on the load and displacement curve generated using the standard equation as below. If we set the dimensions of the specimen and experiment parameters as: length = L, width = b, height = h, the distance between loading site = a, the load = P and the displacement = D.

The moment of inertia (I) of the specimen can be calculated as equation (1);

$$I = \frac{b \times h^3}{12} \ (1),$$

Strain can be calculated as equation (2)

$$Strain = \frac{12 \times D \times h/2}{2a \times (3L - 2a)} \ (2),$$

And Stress can be calculated as equation (3)

$$Stress = \frac{P \times 2a \times h/2}{4I} \ (3).$$ Therefore, stress-strain curves were generated (Figure 3-2); and the elastic modulus

Assume for the specimen
Length L, width b, Height h
Moment of Inertia, I
I=b x h3
Load = P
Displacement =D
Loading point distance = a

Figure 3-1 Schematic of mechanical load on the specimen.
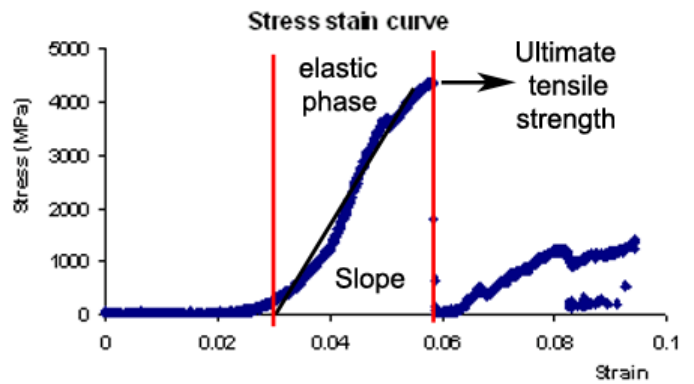
Figure 3-2 Stress strain curve of a specimen

was calculated as the slope of the stress –strain curve in the elastic phase and the ultimate tensile strength was the stress at the breaking point.

3.2.5 Permeability measurement

The permeability of stainless steel (n=3) and PMMA (n=3) was measured three independent times in a radial flow direction using a custom built device (same as the device used to measure bone permeability, detailed in Chapter IV). All the samples were completely sealed in the holder and tested in the pressure range of 0 ~300 kpa. Phosphate buffered saline (PBS) solution was pumped through the samples using a 4 MPa pressure limit pump (Pump-P 500, Pharmacia Biotech) at 4 different flow rates (v): 10, 20, 30 and 40 mL/hr. For each flow rate, Δp, the pressure difference of the upstream fluid and the downstream fluid, which is atmosphere, was measured with a pressure gauge (Ashcroft Cat # 25D1005PS 02L 100). The thickness (L) of samples was measured with digital calipers (0.1 mm accuracy) at three different sites along the scaffold materials. Fluid flow was assessed through a circular area (A) of 5 mm in diameter. And μ is the viscosity of PBS solution ($\mu = 1cp$). Permeability (P) was then calculated using Darcy's Law shown in Equation (1) below:

$$P \ = \ \frac{\mu \, Lv}{A \, \Delta p} \, (1)$$

.

3.2.6 Optimizing the scaffold surface for bone cell adhesion, growth and osteogenic differentiation

All following steps were performed sterilely.

1. Scaffold preparation

1. a. Collagen gel coating process:
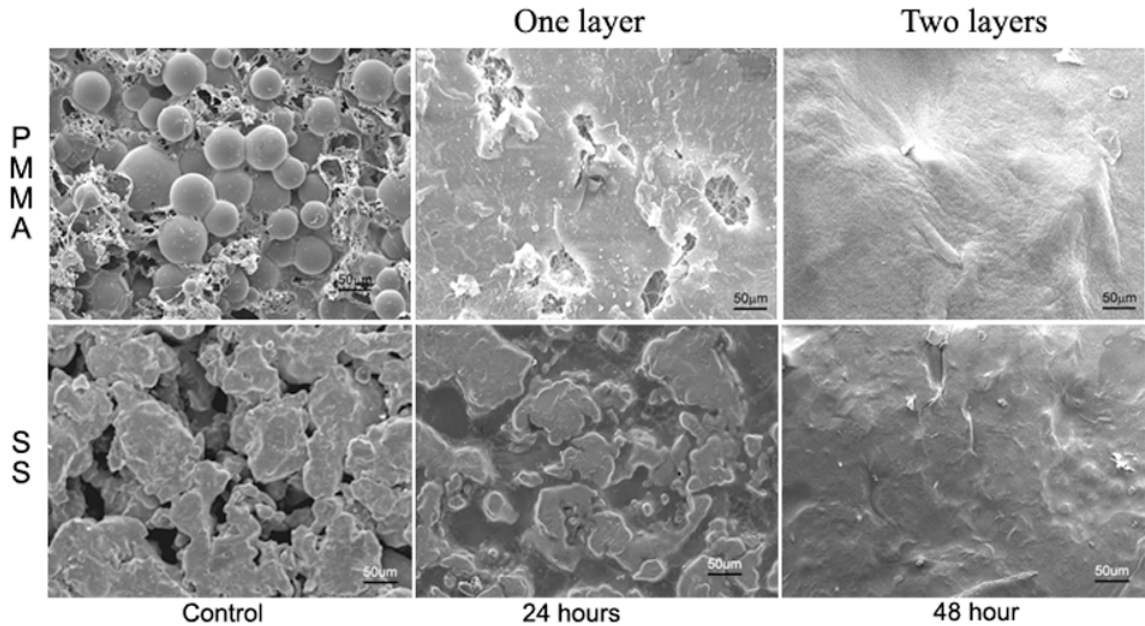
Figure 3-3 SEM images of the surface structure of scaffold after collagen gel coating. the top layer was PMMA scaffold, the bottom layer was stainless steel (SS)
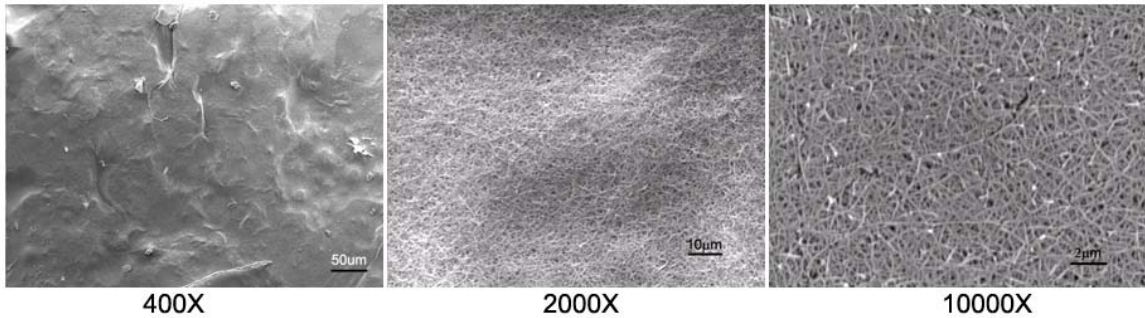
Figure 3-4 SEM images of the surface structure of stainless steel scaffold after 48 hr 2 layer collagen gel coating

A 2 mg/mL rat tail type I collagen solution was prepared from a stock of native type I collagen solution (3.56 mg/mL, Gibco). A 250 μL aliquot of the 2 mg/mL collagen

solution was placed onto PMMA and stainless steel scaffolds in a 12-well plate sitting on ice. Half an hour later; the plate was put into a 37^0 C incubator for 24 hr. Any excess collagen gel was trimmed off with a surgical blade. For second layer coating, a second collagen gel layer was coated onto the first layer, and the plate was put into a 37^0 C incubator for another 24 hr (total 48 hr).

The surface structure of the scaffold after collagen gel coating was shown in Figure 3-3. Comparing to 24 hr one layer coating, 48 hr 2 layer coating generated the smoothest surface structure. Also, high magnification SEM images of the surface structure of stainless steel scaffold after 48 hr 2 layer collagen gel coating are shown in Figure 3-4. It shows that this collagen fiber dimensions are similar as *in vivo* collagen fiber dimensions. Therefore, for our biocompatibility test, the 48 hr 2 layer collagen coating process was applied.

1. b. Fibronectin film coating

A 2 μg/mL fibronectin solution was prepared from a stock fibronectin solution (1 mg/mL in PBS (Sigma)). The scaffold coated with collagen gel layers was put into a new 12-well plate, and a 250 μL aliquot of the 2 μg/mL fibronectin solution was placed directly onto the collagen layer on the scaffold surface. The plate was put into a 37^0 C incubator, and after 2 hr incubation, the scaffold was washed with 500 μL PBS for ten times at room temperature.

2. Short term biocompatibility test

The osteoblast cell line, UMR106-01 BSP, was used to test the short-term biocompatibility of the PMMA and stainless steel scaffolds. A coverslip, a conventional culture material, was used as a positive control. Specifically, 1000 cells /mm^2 cells were seeded onto the collagen and fibronectin coated PMMA, stainless steel scaffold and coverslip in a 12 well plate. Half a milliliter of growth medium (MEM (Cellgro) supplemented with 10% fetal bovine serum (FBS)) was put into each culture well. Cultures were incubated for 14 days and the medium was changed every other day. At 2 hours, three cultures from each group were taken for cell attachment analysis. At day 2, 4, 6, 8, 10, 12, 14, three cultures from each group were taken for cell number counting. The cell number per culture was quantified based on double stranded DNA content using the PicoGreen assay kit from the Molecular Probes. PicoGreen is a dye that binds to the major grooves in dsDNA, and the resulting fluorescence activity corresponds to the dsDNA concentration in solution and represents a surrogate measure of cell number. Specifically, for one culture well, half mL PBS solution was used to wash the well; then 250 μL Lysis buffer (10 M Formamide (Fisher Scientific), 50mM Na acetate (Sigma), 1% SDS (ICN) solution at pH 6) was added into each well; then the well was incubated at 60 ^{0}C for 2 hours; after the culture was cooled down; the cells were scraped into a tube; the tube was sonicated for 30s, now the sample was ready for DNA analysis with PicoGreen assay kit.

At day 14, two cultures was fixed with 2% paraformaldehyde in PBS at 4^0 C overnight, and then stained with 4',6-diamidino-2-phenylindole (DAPI), a fluorescent

DNA dye that stains cell nuclei, and Rhodamine-Phalloidin, a high-affinity probe for F-actin; Then confocal images were taken for morphology analysis with Leica TCS-SP spectral laser scanning confocal microscopes. Then the images were processed with Improvision Volocity software to generate 3D images.

3. Long term biocompatibility test

MC-4 pre-osteoblast cell line (a cell line exhibiting oteogenesis *in vitro*) (a gift from R. Franceschi, Univ. of Michigan) and periosteum cells (primary bone cells) obtained from the tibial diaphyses of 30 day old Sprague Dawley male rats were used for long-term biocompatibility tests of stainless steel scaffolds. Cells were seeded onto the stainless steel scaffolds double coated with collagen and fibronectin at a density of 200 cells/mm^2. Half a milliliter of growth medium (α-MEM (Cellgro) supplemented with 10% fetal bovine serum (FBS)) was put into each culture well. After 4 days, this growth medium was changed to a differentiation osteogenic medium (α-MEM supplemented with 10% FBS and 50 μg/mL L-ascorbic acid 2-phosphate (Sigma), 50 μg/mL L-ascorbic acid (Sigma) and 10 mM β-glycerophosphate (Sigma)). Cultures were incubated for an additional 21 days with changing the medium every day. Cells cultured on a 3-D hydrogel made of collagen and fibronectin and 2-D tissue culture plastic served as controls. Triplicate cultures were done for each culture condition.

At the end of the culture period, cell layers (including collagen and fibronectin layer) were peeled off from stainless steel or culture plates and then fixed with 2% paraformaldehyde in PBS at 4^0 C overnight. After fixation, samples were embedded in

paraffin and oriented in order to cut cross-sectional slices, which would represent the top and bottom of each culture. Seven micron slices were cut from each tissue block. Hematoxylin and eosin (H&E) and DAPI were used to examine cell morphology and nuclei numbers. Three slides were examined from each block.

3.2.7 Statistic analysis

Analysis of variance (ANOVA) caculations with post-hoc multiple comparison tests (Dunn Method) were used for statistical analysis (SigmaStat software v3.5). Quantitative results are reported as the mean ± standard deviation. Unless stated otherwise, statistical significance was set at a p value of less than 0.05.

3.3 Results

3.3.1 Porosity of PMMA and Stainless steel scaffold
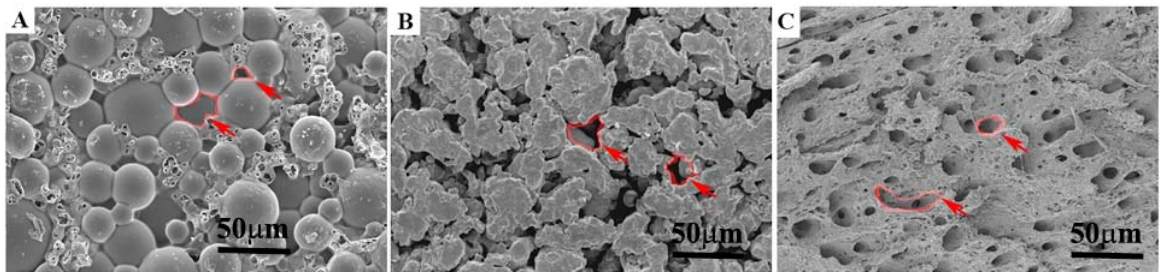
Figure 3-5 Scanning electron microscopy images of PMMA, stainless steel and cortical bone after collagenase treatment. A: PMMA, B: stainless steel, C: cortical bone. The red arrow points to the pores.

A semi-quantitative analysis of the SEM images of PMMA and stainless steel as compared to rat cortical bone (lipids and collagen removed from porous part) showed that PMMA and stainless steel had similar pore sizes (Figure 3-5). From these images, the pore sizes of these three materials were generated: PMMA (21 ± 12 μm), stainless steel

(18 ± 13 μm) and cortical bone (11 ± 10 μm). Based on one way ANOVA analysis (Duncan's method), the differences in the mean value among the groups were not great enough to exclude the possibility that the difference was due to random sampling variability (n=3); there was no significant difference between the pore size of these three materials (p=0.592). A limitation of this analysis in the power of the performed test (0.050) is below the desired power of 0.800. Despite this limitation, this analysis suggests that both stainless steel and PMMA have roughly comparable pore size as cortical bone.

3.3.2 Stiffness of PMMA and Stainless steel

The elastic modulus of PMMA, stainless steel and cortical bone are shown in Figure 3-6. Comparing elastic modulus of these three groups with one way ANOVA (Duncan's method), the difference in the mean value among the groups are greater than would be expected by chance, there was a statistically significant difference
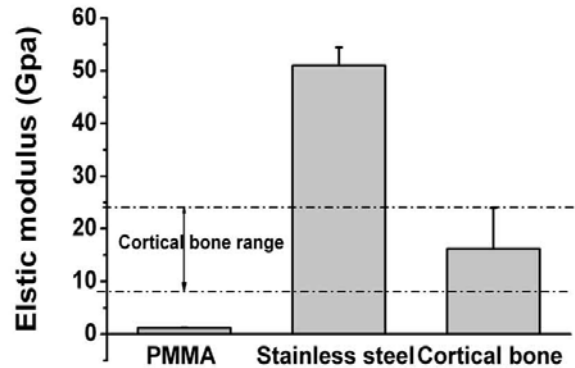
Figure 3-6 Elastic modulus of PMMA, stainless steel with mean pore size of 0.5 μm and cortical bone. Mean ± SD, n = 3

(P<0.001). Specifically, the elastic modulus of PMMA (1.19 GPa) was significant smaller (10 fold) than that of cortical bone (17 GPa) (P < 0.01), and the elastic modulus of stainless steel with mean pore size 0.5 μm (51 GPa) was significant larger (3 fold) than cortical bone (P < 0.01). From this aspect, neither stainless steel nor PMMA exactly

match the elastic modulus of cortical bone.

The ultimate tensile strength of PMMA, stainless steel and cortical bone are shown in Fig 3-7. Comparing the ultimate tensile strength of these three groups with one way ANOVA (Duncan's method), the differences in the mean value between PMMA (21 Mpa) and cortical bone (152 MPa), were greater than would be expected by chance; there was a statistically significant difference (P < 0.001). Specifically, the ultimate tensile strength of PMMA was significantly lower (7 fold) than that of cortical bone. The differences in the mean value between stainless steel (160 Mpa) and cortical bone (152 MPa),

Figure 3-7 Ultimate tensile strength of PMMA, stainless steel with mean pore size of 0.5 μm and cortical bone. Mean ± SD, n = 3

was not great enough to reject the possibility that the difference might be due to random sampling variability. There was not a statistically significant difference between these two groups (P = 0.197). The power of the performed test (0.148) is below the desired power of 0.800. Despite this limitation, the ultimate tensile strength of stainless steel can be considered to be roughly similar to that of cortical bone. From this aspect, stainless steel matched theultimate tensile strength of cortical bone, while PMMA did not.

3.3.3 Permeability of stainless steel and PMMA

Hydraulic permeability value for PMMA, stainless steel and cortical bone are shown in Figure 3-8. Comparing the permeability values of these three groups with one way ANOVA (Duncan's method), the differences in the mean values among all the groups (PMMA (8.2×10^{-14} m^2), stainless steel (5.9×10^{-14} m^2) and cortical bone (3.05×10^{-14} m^2)) were not great enough to exclude the possibility that the difference was due to random sampling variability; there was no statistically significant difference (P=0.057). The power of the performed test (0.462) was below the desired power of 0.800. Nevertheless, the permeability of PMMA and stainless steel were similar to that of cortical bone. Accordingly, PMMA and stainless steel can be considered to be roughly similar to the hydraulic permeability of cortical bone.
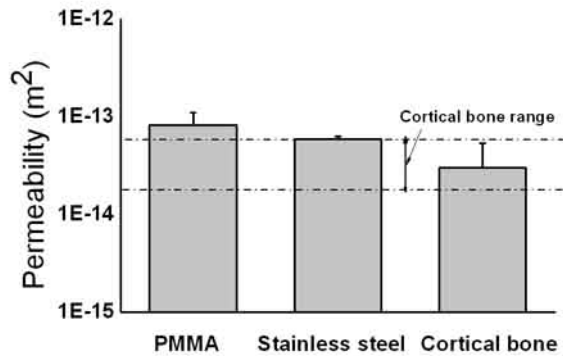
Figure 3-8 Permeability of PMMA, stainless steel with mean pore size of 0.5 μm, cortical bone. Mean ± SD, n = 3
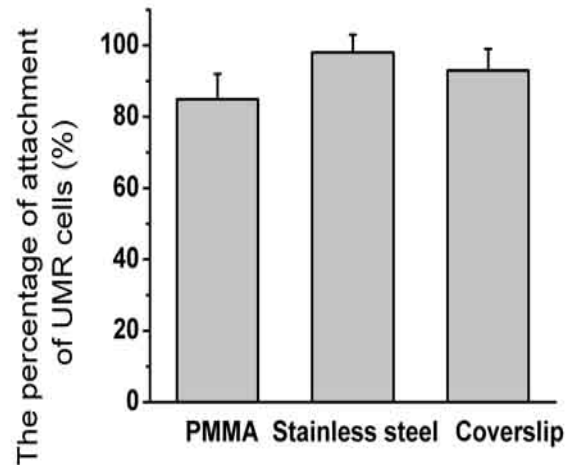
Figure 3-9 The percentage of attachment of UMR cells on PMMA and stainless steel scaffold after 2 hr, coverslip as a control. Mean ± SD, n = 3

3.3.4 Short term biocompatibility of PMMA and stainless steel
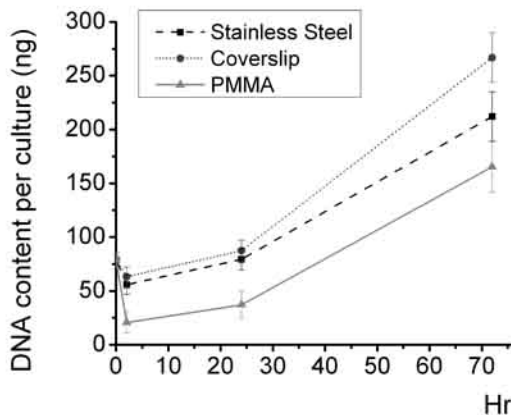
Figure 3-10 The growth curve of UMR cells cultured on PMMA and stainless steel scaffold for 72 hr. Coverslip as control. Mean ± SD, n = 3

Cell attachment percentages of UMR osteoblastic cells on PMMA, stainless steel and coverslip scaffolds are shown in Figure 3-9. Comparing the cell attachment percentage of these three groups with one way ANOVA (Duncan's method), the differences in the mean value among all the groups (PMMA (86%), stainless steel (98%) and cortical bone (94%)) were not great enough to exclude the possibility that the difference was due to random sampling variability; there was not statistically significant difference (P = 0.228). The power of the performed test (0.142) is below the desired power of 0.800. Specifically, there was no significant difference among osteoblastic cell attachment percentages on PMMA, stainless steel and that on coverslip.

Growth of UMR cells on PMMA, stainless steel and glass coverslip
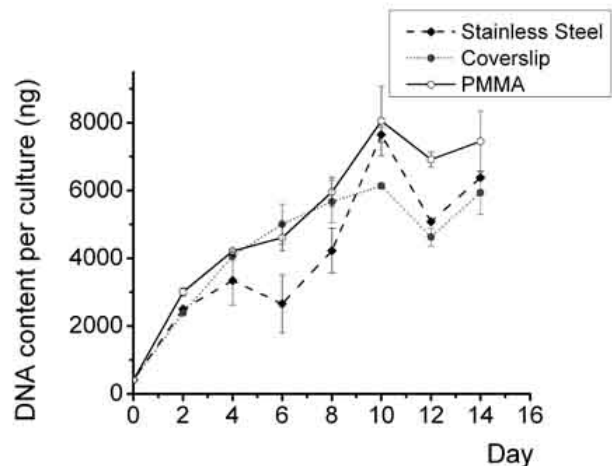
Figure 3-11 The growth curve of UMR cells cultured on PMMA and stainless steel scaffold for 14 days. Coverslip as control. Mean ± SD, n = 3

scaffolds over three day culture is shown in Figure 3-10. Comparing the DNA content per culture at the end point, with one way ANOVA (Duncan's method), the differences in the mean value among all the groups were not great enough to exclude the possibility that the difference was due to random sampling variability; there was not statistically significant difference ($P = 0.591$). The power of the performed test (0.050) was below the desired power of 0.800. Thus, to the limits of our analysis no significant difference was among cell proliferation over three day culture period on PMMA, stainless steel scaffold and coverslip.

The growth curve of UMR cells on PMMA and stainless steel scaffold for 14 days is shown in Figure 3-11. A 2-way ANOVA analysis (means comparison using Tukey Test (factor 1: time point, factor 2: culture material)) was run to compare DNA content per culture, as culture material was concerned, the differences in the mean value among all the groups were not great enough to exclude the possibility that the difference was due to random sampling variability; there was not statistically significant difference ($P=0.174$). The power of the performed test was 0.99. Specifically, there is no difference between the cell proliferation of 14 days culture on PMMA, stainless steel scaffold and that on coverslip.

Moreover, since biocompatibility is defined as 'ability of a biomaterial to perform its desired function with respect to a medical therapy, without eliciting any undesirable local or systemic effects in the recipient or beneficiary of that therapy, but generating the most appropriate beneficial cellular or tissue response in that specific situation, and optimizing

the clinically relevant performance of that therapy', there it is important to compare the cell morphology and osteogenesis of osteoblastic on these material scaffold. Therefore the confocal images of UMR cell cultures on stainless steel and coverslip scaffold were taken (Figure 3-12). It showed that the cultures on both stainless steel and coverslip have been multilayer; the cell nuclei and F-actin staining patterns were similar, which suggested the similarity of the cell morphology of cultures on these two scaffolds.
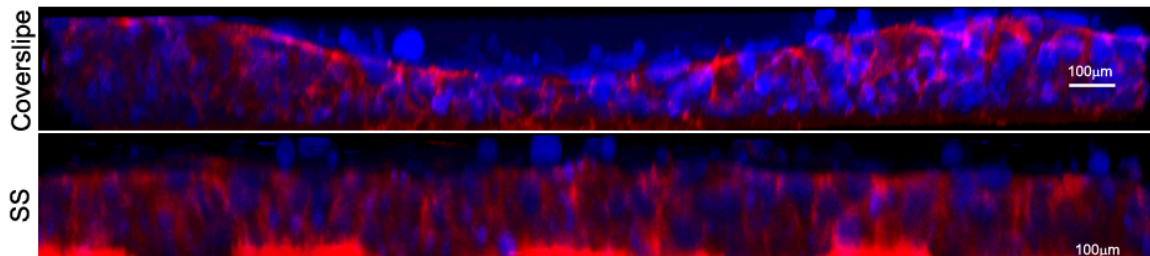
Figure 3-12 Snapshot of confocal image of UMR cell cultured on stainless steel scaffold and coverslip. DAPI staining (nuclei) is blue color, Rhodamine-Phalloidin staining (F-actin) is red color.

In all, from the short-term cell growth tests, with limitation of that no data about the osteogenesis of osteoblastic cells on these two scaffolds, the PMMA and stainless steel scaffolds have roughly similar outcomes (cell proliferation (growth curve) nuclei morphology (growth curve)) as glass coverslip, which is conventional used biomaterial and exhibit good biocompatibility. Therefore, PMMA and stainless steel are considered to be biocompatible for short-term osteoblast cultures.

3.3.5 Long term biocompatibility of stainless steel scaffold

Representative H&E staining images of sections from MC-4 and periosteum cells cultured on collagen-fibronectin coated stainless steel, 3D hydrogels made of type I collagen and fibronectin and 2D conventional tissue culture plastic are shown in Fig 3-13.

These images showed that, for both MC-4 and perisoteum derived bone cells, there were no substantial difference in the thickness of the resultant cell layer, though qualitative difference were noted in staining intensities between cultures on collagen gel, plastic and stainless steel scaffolds. To quantify cell numbers, DAPI staining was used to stain cell nuclei and nuclear numbers were counted.
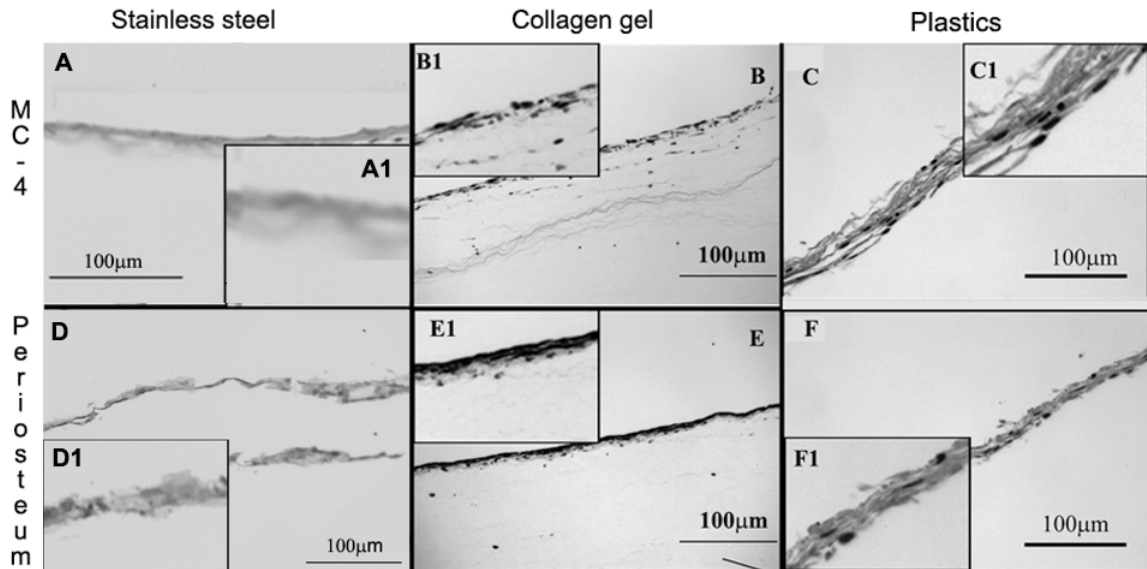
Figure 3-13 H&E staining of cultures on stainless steel, collagen-fibronectin hydrogel and plastic. A-C: MC-4 cells cultured on stainless steel, collagen-fibronectin hydrogel and plastic respectively. D-E: Periosteum cells cultured on stainless steel, collagen-fibronectin hydrogel and plastic respectively. A1-F1: the 2 x enlarged image of A-F respectively.

Representative DAPI staining images of sections from MC-4 or periosteum cells cultured on collagen-fibronectin coated stainless steel, 3D hydrogels made of type I collagen and fibronectin and 2D conventional tissue culture plastic are shown in Fig 3-14. These images showed that, for both MC-4 and perisoteum cells, no significant differences between nuclear numbers on collagen gel, plastics and stainless steel scaffold.
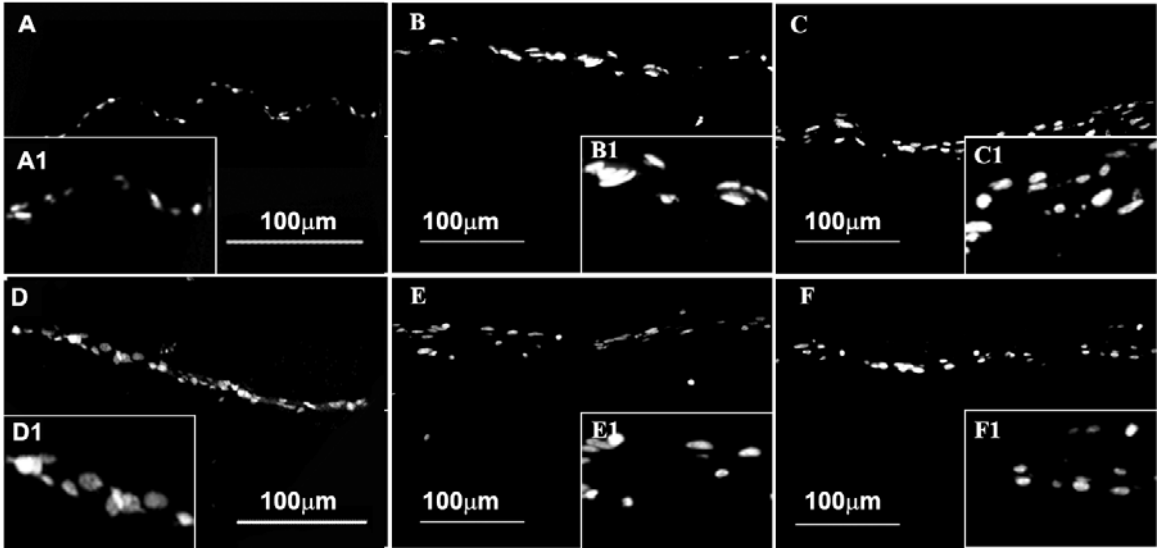
Figure 3-14 DAPI staining of cultures on stainless steel, collagen-fibronectin hydrogel and plastic. A-C: MC-4 cells cultured on stainless steel, collagen-fibronectin hydrogel and plastic respectively. D-E: Periosteum cells cultured on stainless steel, collagen-fibronectin hydrogel and plastic respectively. A1-F1: the 2 x enlarged image of A-F respectively.

One way ANOVA (Duncan's method) was used to compare nuclei number on collagen gel (3.11 $\pm$ 0.56 x 10^3 nuclei /mm^2) (n = 3), plastics (3.01 $\pm$ 0.78 x 10^3 nuclei /mm^2) (n = 3) and stainless steel scaffolds (2.33 $\pm$ 0.33 x 10^3 nuclei /mm^2) (n = 3). This analysis showed that the differences in the mean values among all the groups were not great enough to exclude the possibility that the difference was due to random sampling variability; there was no statistically significant differences (P = 0.342). The power of the performed test (0.078) was below the desired power of 0.800. Despite this limitation, it is reasonable to conclude that cultures on stainless steel scaffolds, glass coverslip or collagen- fibronectin gels yielded similar numbers of osteoblastic cells often extended culture incubation. This suggest that 316 L stainless steel scaffolds are biocompatible for long term bone cell culture.

3.4 Discussion

The gold standard for selecting an optimal scaffold to be used in bone reconstruction surgery is autograft. It then stands to reason that the selection of an appropriate scaffold for bone tissue engineering should meet the key attributes of an autograft [66]. Generally speaking, the key criteria for selecting a bone scaffold includes: (1) biocompatibility, (2) osteoconductivity – permitting cells to attach, proliferate and migrate and allowing nutrient-waste exchange and vessel penetration, (3) osteoinductivity – inducing osteoprogenitors to differentiate into osteoblasts, and (4) osteogenicity – producing mineralized tissue matrix[39, 66, 95]. In addition, there are two more important issues to be considered: (1) having similar mechanical properties as bone; and (2) having similar permeability as bone to promote proper nutrient/waste product exchange rates. Our overall results are shown in table 3-2. It indicated that 316 L stainless steel and PMMA could be manufactured to exhibit roughly similar pore size and permeability properties as cortical bone. From a mechanical properties aspect, stainless steel partially matched with cortical bone (elastic modulus) while PMMA did not match up with cortical bone.

Moreover, our results showed that a 316L stainless steel scaffold exhibited appropriate biocompatibility both short term and long term bone cell culture. PMMA exhibited appropriate biocompatibility for short term culture; and its long term biocompatibility needs to be investigated in the future. Therefore, we can conclude that both PMMA and 316L stainless steel have reasonable well matched properties with cortical bone, thus

enabling them to be used in tissue engineering systems. Based on our data, our first choice would be 316L stainless steel, and the second choice would be PMMA.

Still there are some limitations in this study that should be addressed in future study: (1) the long term biocompatibility of PMMA was not tested; (2) an extensive growth curve of long term cultures; (3) extracellular matrix was not immuno- stained to investigate if there were qualitative differences between cultures on stainless steel, collagen fibernectin hydrogel and plastic by 25 days I culture culture; (4) Osteogensis (suck as alkaline phosphatase activity staining, bone matrix protein, and/ or calcium mineral staining) needs to be evaluated to determine the full biocompatibility of the materials for bone cells; (5) the power test showed that the power was below the designed power and in the future study the sample number should be increased to be able to exclude random variability.

Properties	PMMA	Stainless steel	Cortical bone
Pore size	√	√	√
Elastic modulus	x	x	√
Ultimate tensile strength	x	√	√
Permeability	√	√	√
Short term biocompatibility	√	√	√
Long term biocompatibility	n/a	√	√

Table 3-2 The properties of PMMA and stainless steel scaffold

CHAPTER IV

LIPIDS AND FIBRILLAR COLLAGEN MATRIX RESTRICT THE HYDRAULIC PERMEABILITY WITHIN THE POROUS COMPARTMENT OF ADULT CORTICAL BONE

4.1 Introduction

Hydraulic permeability of cortical bone is the measurement of the ease of fluid flow through cortical bone. Fluid flow inside cortical bone is critically important for nutrient and waste product transport, which is important to maintain osteocyte viability and regulate the physiological processes of bone remodeling and homoestasis [7, 98]. Therefore hydraulic permeability may be a key attributor that needs to be mimicked in bone tissue engineering. Thus a study of hydraulic permeability of cortical bone and the bone components that regulate it need to be further investigated.

Adult cortical bone tissue is a biocomposite material which is composed of 67% mineral salts and 33% organic matrix by dry weight containing 62% type I collagen, 26% minor collagens and non-collagenous proteins, 6% lipids and 6% complex carbohydrates [19, 60]. Based on fluid accessibility, bone tissue is separated into two generalized compartments: a non-porous compartment and a porous compartment comprising 90~95% and 5~10% of its volume, respectively [14]. The porous compartment contains vascular channels (Haversian and Volkman's canals) interconnected by a lacuna-canalicular system filled with osteocytes, their filipodial extensions and a surrounding pericellular matrix [9, 10, 15, 88]. Biological fluids flow within this porous compartment of cortical bone thereby providing a system to exchange nutrients and metabolic waste products [18, 52]. Since permeability of cortical bone is a measure of fluid flow through this porous compartment, it should be affected by the tissue composition within this compartment.

To date, few studies have experimentally measured the hydraulic permeability of cortical bone in part because of the engineering challenges in measuring extreamly low permeabilities. These devices require high pressure tolerances in both the bone tissue holding chamber and other upstream components of the permeability device in order to accurately measure the permeability of cortical bone. Li et al. measured the permeability of adult canine versus puppy cortical bone [46]. They reported that the radial permeability of adult canine tibial cortex was $5 \times 10^{-17}\,\mathrm{m}^2$ and that the radial permeability of puppy bone was 6-fold higher than that of adult canines. In addition, they suggested

that the periosteal portion of cortical bone was relatively impermeable as compared to the endosteal portion of cortical bone. Though this prior study provided fairly accurate estimations of the radial permeability of adult cortical bone, there have been no prior reports addressing what chemical components within the porous compartment of cortical bone are the primary contributors to these low permeability values. To select a bone tissue engineering scaffold with similar permeability properties as cortical bone, we need to first measure the permeability of cortical bone. Also, investigating the contributions of select components to bone permeability will help us to modify existing scaffold to obtain similar permeability level. Therefore, in this Chapter we designed a device to assess radial hydraulic permeability of cortical bone that enabled us to make repeated measures on the same bone tissue wafers before and after sequential chemical or enzymatic treatments. This enabled us to test two hypotheses: (1) the presence of hydrophobic molecules within the porous compartment of cortical bone would reduce its permeability, and that removal of such hydrophobic materials would increase its permeability; and (2) the presence of a densely packed pericellular matrix (mostly type I collagen) within the porous compartment of cortical bone would reduce its permeability, and digestion of the collagen fibers would increase its overall permeability. To test the first hypothesis, acetone-methanol (or zwitterionic detergent) was used to remove lipids from the porous compartment of cortical bone and assess contribution of lipids to the hydraulic permeability of cortical bone. Bacterial collagenase and dispase were used to digest

48

fibrillar collagens in the porous compartment of cortical bone and assess the contribution of collagen matrix to the hydraulic permeability of cortical bone.

4.2 Material and Methods

All bone tissues were obtained from animals that had been sacrificed in the course of IACUC approved research investigations conducted elsewhere at this institution. Mid-diaphyseal portions of tibia were harvested from adult outbred canines (~25-30 kg body weight). Periosteal tissue layers, including most of the basal cambium cell layer, were stripped off the bone by dissection. Bone marrow was flushed out of the bone with phosphate buffer saline (PBS) (Cellgro). These tibial diaphyses were then stored in PBS with 0.05% sodium azide (Sigma) at 4° C and used within a 2 week period from collection. Thin sections were cut from these tibial diaphyses in a cross-sectional plane and stained with basic fuchsin to reveal the patterns and orientation of Haversian and Volkman's canals. Such histological analysis revealed that the presence and orientation of Haversian and Volkman's canals were different in the periosteal versus the endosteal halves of the canine cortical bone (Fig 4.1A). In the periosteal half there appeared to be fewer Volkman's canals compared to the endosteal half. In the endosteal half, some of these channels traversed radially throughout its entire width. Thus, in agreement with the assessments by literature [51], the endosteal halves seemed to be more amendable for radial hydraulic permeability measurements than their corresponding periosteal halves.

49
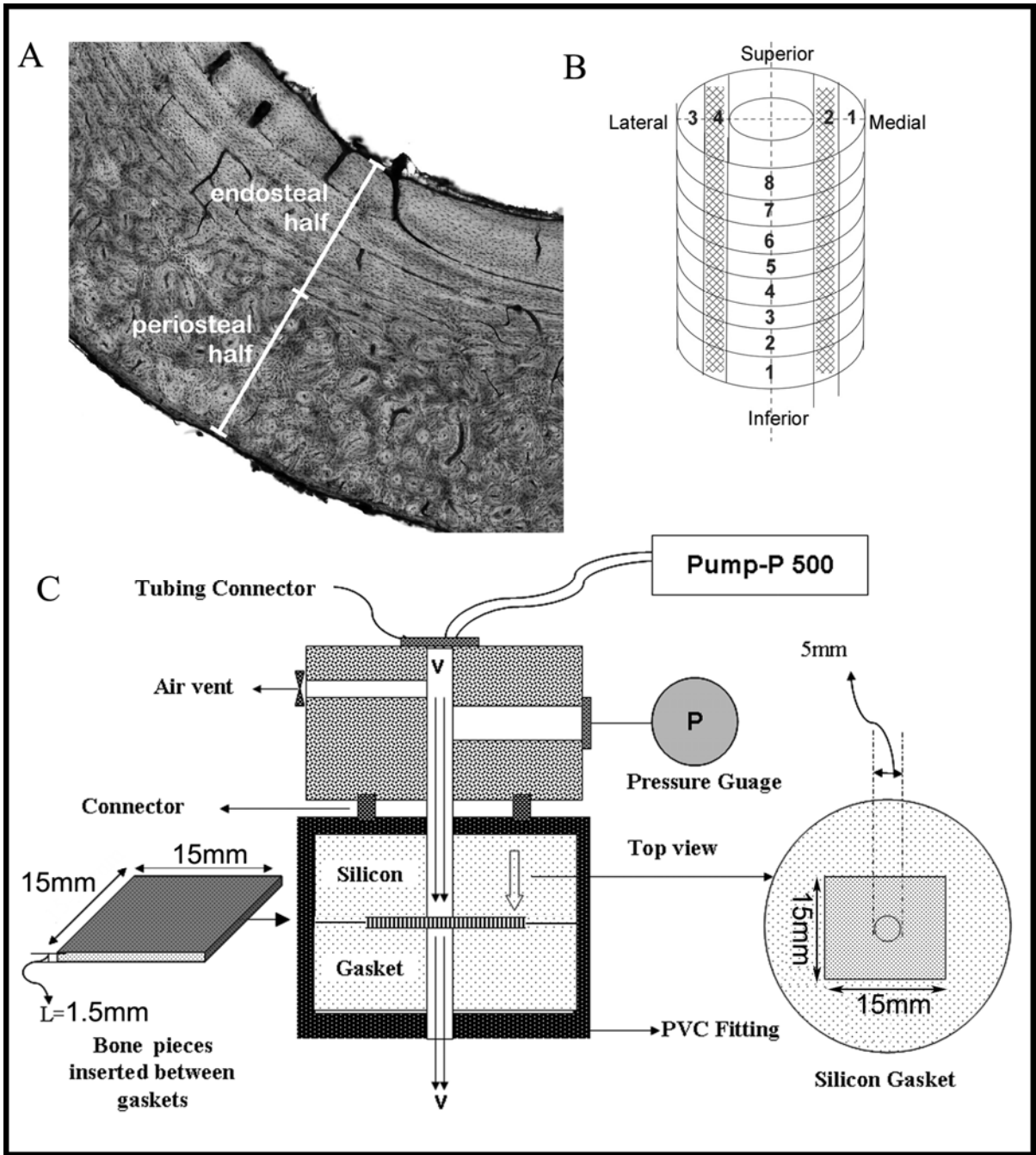
Figure 4-1 Selection of bone tissue regions and the means to measure hydraulic permeability of cortical bone. Panel A shows a representative histology image of a cross section of canine tibial diaphysis. Panel B illustrates the sampling of cortical bone specimens along the tibial diaphysis length. Shaded areas represent the bone wafer tested. Panel C: The schematic of the device used for measuring permeability (dimensions of this device refer to appendix 1).
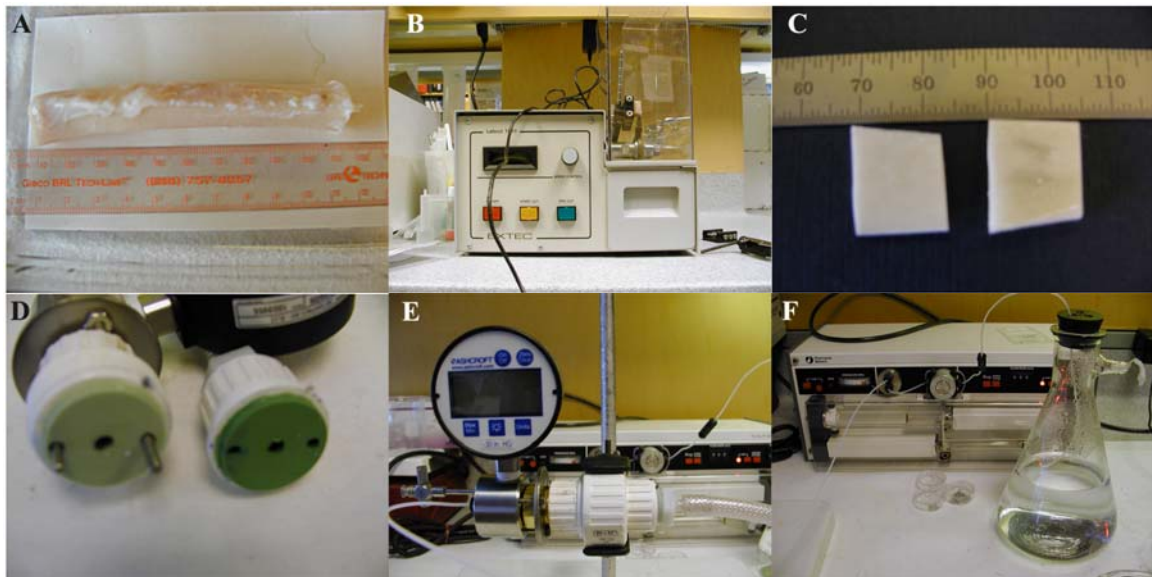
Figure 4-2 Images of the devices for cutting bone and measuring bone permeability. A: Canine tibia. B. EXTEC ® Labcut 1010 Low Speed Diamond Saw (EXTEC Corp). C. Bone wafers. D. Bone holder. E. Overview of the permeability device. F. Pump-P 500

Based on the above histological findings, this study focused on measuring radial hydraulic permeability of bone wafers from the endosteal halves of these adult canine tibial diaphyses. Endosteal bone wafers from the medial and lateral aspects of the diaphyseal cortex (over the entire superior to inferior axis, see shaded regions in Fig 4.1B) were separately collected and, if not analyzed immediately, then they were stored in PBS with 0.05% sodium azide in pre-weighed glass bottles. Bone wafers with dimensions of ~20 mm length, ~15 mm width, and 1.5 mm thick were cut from the diaphyseal portions of tibial cortices with an EXTEC ® Labcut 1010 Low Speed Diamond Saw (EXTEC Corp) (Fig 4.2A-C). The permeability of each fresh bone wafer was measured three

independent times in a radial direction using a customized device (Fig. 4.1C (dimensions of this devices in appendix 1), Fig 4.2D-F). The bone holder device was modified from Standard-Wall (Schedule 40) White PVC Pipe Fitting (1/2" Pipe Size, Female Union, pressure limit 150 PSI (1033 kpa). Device construction was completed in the Prototype and Polymer Labs in the Department of Biomedical Engineering at the Cleveland Clinic. Firstly, bone wafers were sealed in the bone holder. Then PBS solution was pumped through the bone wafers using a pump (Pump-P 500, Pharmacia Biotech), at four different flow rates (v): 10, 20, 30 and 40 mL/hr. For each flow rate, Δp, the pressure difference between the upstream fluid and the downstream fluid (atmosphere) was measured with a pressure gauge (pressure limit 100 PSI (690 kpa)) (Ashcroft Cat # 25D1005PS 02L 100). The thickness (L) of each bone wafer was measured with digital calipers (TRESNA, 111-102B; 0.1 mm accuracy) at three different sites along the bone wafer surface. Fluid flowed through a circular area (A) (5 mm diameter) of the bone

wafer. Permeability (P) was then calculated based on Darcy's Law: $$P = \frac{\mu L v}{A \Delta p}.$$

Here, P: permeability (m^2), μ: the viscosity of PBS solution (1 cp = 0.001 kg/(m·s)), L: the average thickness of bone wafer (mm), v: the flow rate of the flow through bone wafers (mL/h), A: the area of flow through bone wafers, ΔP: the pressure difference between the upstream and downstream of flow (kpa).

Based on Darcy's law, there is a linear relationship between flow rate (*v*) and Δp, the pressure difference between the upstream fluid and the downstream fluid. The relationship between the flow rate and pressure difference measured by our device (for one representative sample) is shown in Fig 4.3. It shows that a linear relationship
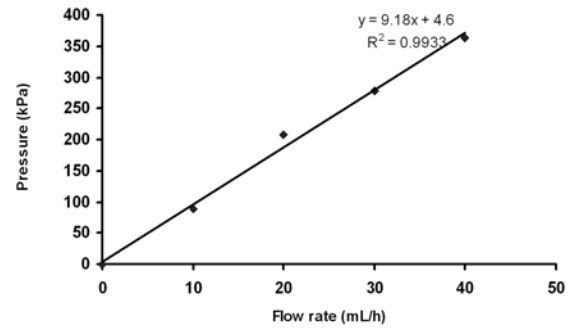
Figure 4-3 Relationship of flow rate and pressure difference

(R^2 = 0.9933) between these two parameters indicating it can be used to measure hydraulic permeability of cortical bone wafers. A visible inspection of the bone provided documentation indicating holder device at every test run lack of leakage, and in the case of fresh or unprocessed bone wafers, no fluid flow up to 100 psi pressure.

After permeability measurements of unprocessed bone wafers were completed, wafers were treated with 10 ml of a 1:1 (v/v) acetone-methanol (AM) (Sigma) solution at 4° C for three days (or a limited number of wafers treated with 2% (w/v) chaps [80] in PBS solution at 4° C for 7 days) in pre-weighed glass bottles. This volume ratio of AM solution to sample volume is estimated to be 20~30-fold volume excess. After such treatments the bone wafers were put into new bottles and washed with 10 mL PBS solution three times for 2 hr each time. Permeability of each AM-treated bone wafer was measured three times independently. Proof that the AM treatments of the bone wafers extracted lipids was sought as follows. The AM solutions in their respective sample

53

bottles were placed under a nitrogen stream to evaporate the organic solvents and obtain dried waxy residues. After evaporation, the sample bottles were weighed again and the dry weight of lipids was obtained by taking the difference between the weight of each bottle before and after evaporation. Lipid residues were analyzed for specific lipid contents by gas chromatography-mass spectroscopy performed at the Kansas Lipidomics Research Center (Manhattan, KS). Cholesterol was measured spectrophotometrically as previously published [67].

After measuring permeability of AM-treated specimens, each bone wafer was then treated with 5 mL of a 100 U/mL bacterial collagenase (type XI, Sigma C-9407) solution in PBS supplemented with 10 μM 4-(2-Aminoethyl) benzenesulfonyl fluoride hydrochloride (AEBSF) (Sigma) overnight at 37° C. AEBSF was added to inhibit the activities of other serine proteases potentially contaminating the collagenase preps. Following collagenase digestion, all bone wafers were washed with 10 mL PBS solution three times for 1 hr each time. Permeability of each collagenase-treated bone wafer was measured three times independently. Proof of collagenase activity was sought by measuring the amounts of hydroxyl-proline released from the bone wafers into the collagenase solution. Briefly, a 0.5 mL aliquot from each collagenase digestion reaction was placed into Reacti –Vials (Pierce) and frozen overnight at -20° C. The frozen solutions were vacuum dried in a Speed Vac SC110 Concentrator (Savant) for 2 hrs. The dried residues were resuspended in 0.3 mL 6 N hydrochloric acid (Constant boiling purity for amino acid analysis, Pierce). These vials were placed into a Reacti-Therm III heating

module (Pierce) and heated at 105° C for 16 hrs to quantitatively release free amino acids. After acid hydrolysis, a nitrogen gas stream was used to remove the HCl from each sample at 37° C. Each sample was then rehydrated in 0.5 mL of Mill-Q water (Millipore), and their hydroxyl-proline contents were measured by a spectrophotometric method [8, 81].

After measuring the permeability of collagenase-treated bone wafers, they were treated with 5 mL of a 1.2 U/mL bacterial Dispase (Sigma) solution overnight at 37° C. Following dispase digestion, all bone wafers were washed with 10 mL PBS solution three times for 1 hr each time. Permeability of each dispase-treated bone wafer was measured three times independently. Proof of dispase activity was sought by measuring the amounts of hydroxyl-proline released from the bone wafers into the dispase solution in a manner similar to that described above for the collagenase solution.

After measuring the permeability of dispase-treated specimens, bone wafers were then treated with 20 mL of a 400 mM EDTA (pH 8) solution at 4° C until all of the mineral content was removed (~2-3 weeks). Confirmation of a complete removal of the mineral content of each specimen was obtained by X-ray micro-computed tomography (micro-CT) imaging at an isotropic voxel resolution of 26 μm. Following EDTA decalcification, all specimens were washed with 10 mL PBS solution three times, 30 min each time. Permeability of each EDTA-treated bone wafer was measured three times independently. The remaining insoluble bone organic matrix was hydrolyzed with 6N hydrochloric acid and the total amount of hydroxyl-proline in the remaining insoluble

tissue matrix after EDTA treatment was measured by a spectrophotometric method as described above, and served as a measure of total insoluble collagen in each sample.

In addition, the porosity of fresh or unprocessed bone wafers was measured. Bone wafers with dimensions of 20 mm length, ~15 mm width, and 1 mm thick were cut from the diaphyseal portions of tibial cortices with an EXTEC ® Labcut 1010 Low Speed Diamond Saw (EXTEC Corp). Micro-CT volumes of bone wafers (Sample size N = 6) were acquired using a SkyScan 1172 (3 μm voxel resolution) *ex vivo* imaging system. Porosity analysis was performed using Matlab R2008a (MathWorks), Image Pro-Plus v6.1 (Media Cybernetics), VolSuite (Ohio Supercomputer Center, Columbus, OH), and MicroView v2.2 (GE Healthcare). Bone volumes (~1800 x 1000 x 1000 voxels) were rotated and cropped using VolSuite, and imported into Image-Pro as individual image stacks. In each plane of a particular stack, holes were filled using a morphological "closing" filter and bone outgrowths from the endosteal surface were removed using a watershed filter. The resulting contiguous, "filled" bone volumes were then multiplied by an inverted and thresholded version of their corresponding original volume to reveal porous content that was further filtered in Matlab to remove pores below a given volumetric threshold (connected components algorithm). Subsequently, total pore volume and porous volumes in both the axial and radial directions were calculated (identified by ellipitical orientation of each pore -25 to 155 degrees from vertical in the xy plane with permeability measured along the x-axis, indicating the radial direction). The total porosity of cortical bone was calculated as the total pore volume divided by the total

cortical bone volume, the axial porosity was calculated as the axial porous volume divided by total cortical bone volume, and the radial porosity was calculated as the radial porous volume divided by total cortical bone volume. Segmented pore volumes were then imported into MicroView for anisotropy analysis that utilized a mean intercept length approach in which intersections of a test grid composed of lines separated by 3 pixels were passed through each volume at 200 different angles to generate a fabric ellipsoid whose long axis was aligned in the direction of the most prominent structural orientation. Lastly, Euler's number for both the axial and radial components of the segmented porous content of each sample was calculated and divided by total bone ("filled") volume to determine connectivity density (mm^{-3}).

Repeat measures for Analysis of variance (ANOVA) (Friedman Repeated Measures of ANOVA) were used for statistical analysis (SigmaStat software v3.5). Quantitative results are reported as the mean ± standard deviation. Unless stated otherwise, statistical significance was set at a p value of less than 0.05.

4. 3 Results

4.3.1 Structure and Porosity of cortical bone

The structural properties of cortical bone wafers cut from adult canine tibial diaphyses were assessed after removing bone marrow and periosteum soft tissues. Gross observations of each bone wafer showed that the endosteal surface contained large ridges and valleys as compared to the cut surface (Fig 4.4A and B, ES versus CS panels). Environmental scanning electron microscopy images of each bone wafer showed that the

57

natural endosteal surface (ES) exhibited numerous large pores (50 – 100 μm width) and

intermediate-sized pores (10 - 50 μm width) (Fig 4.4C).   Similar imaging of the

opposing cut surface (CS) of these bone wafers revealed fewer intermediate-sized pores
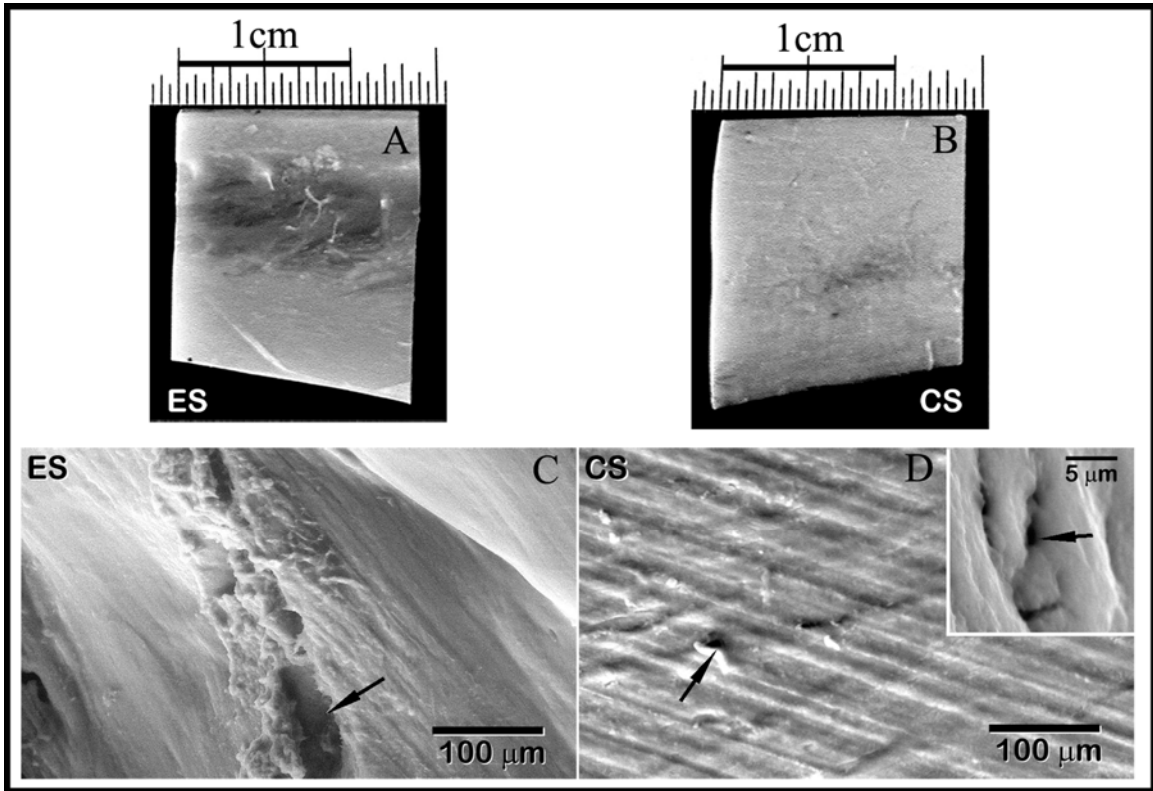
Figure 4-4 Images of cortical bone wafers prior to permeability measurement. Panel A shows a representative gross view of a natural endosteal surface (ES) from a bone wafer. Panel B shows a representative gross view of the opposing cut surface (CS) from the bone wafer shown in panel A. Panel C shows an environmental scanning electron microscope image of the natural endosteal surface from a bone wafer. Panel D shows an environmental scanning electron microscope image of the opposing cut surface from the same bone wafer shown in panel C; the roughly parallel ridges apparent in the image are generated by the rotary cutting blade. Inset image in panel D is a higher magnification view revealing the presence of small pores along the cut surface of a bone wafer. Arrow points to the pores.

and numerous small pores (1 – 5 μm width), but no large pores (Fig. 4.4D and inset).
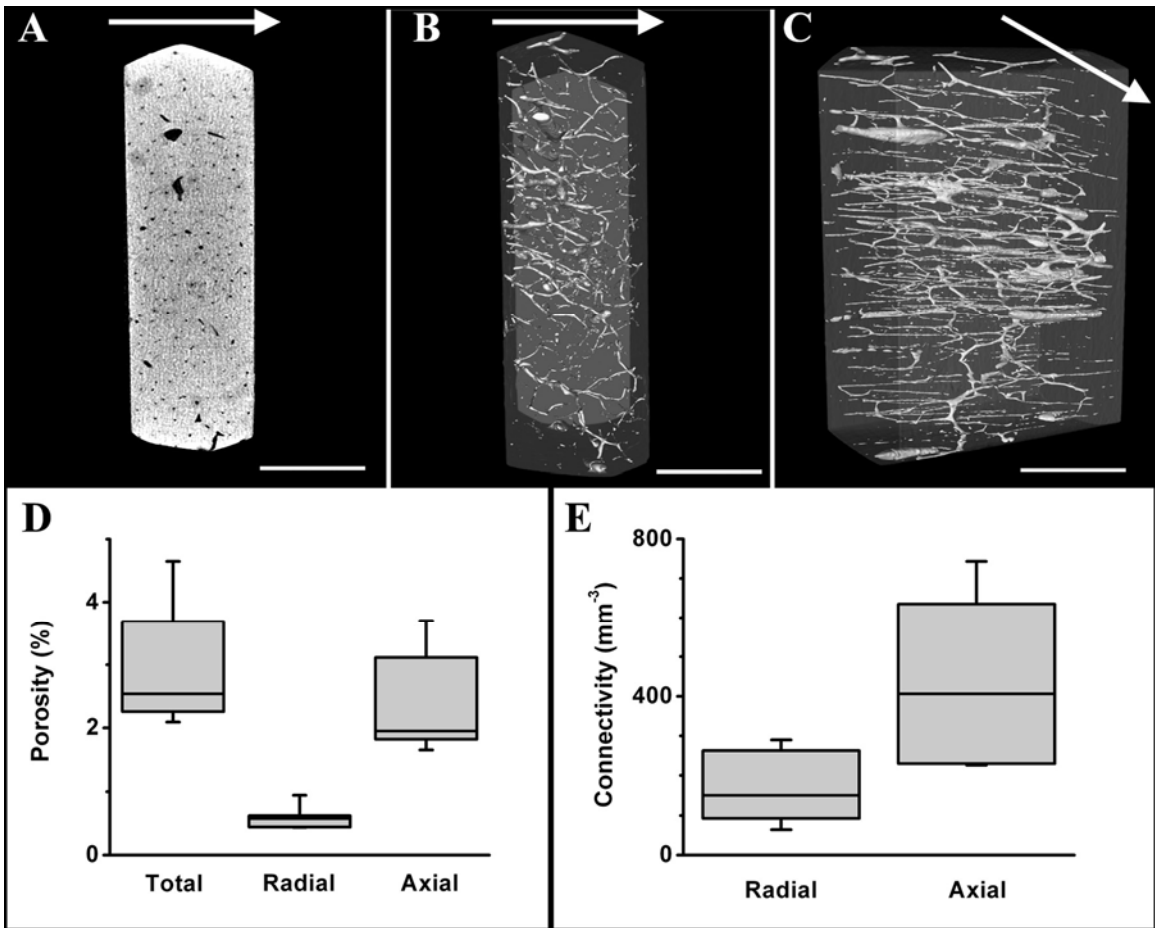
Figure 4-5 Porosity and connectivity measurement of cortical bone wafers. Panel A shows a representative 3D micro-CT scanning image at 3 μm resolution. Panel B shows a representative inverted 3D micro-CT image in the radial direction. Panel C shows a representative inverted 3D micro-CT image in the axial direction. Panel D shows the total, radial and axial porosity of cortical bone. Panel E shows the radial and axial connectivity of the porous compartment in cortical bone. Shown are box and whisker plots exhibiting median (line within the box) and percentiles of the data. The ends of the boxes define 25th and 75th percentiles, and the two bars outside the box define 10th and 90th percentiles. Scale bars in panel A-C are 200 μm.

Presence of pores on both sides of the bone wafers suggested that some of these pores may interconnect across the wafer thickness and provide channels for fluid flow.

Three dimensional, micro-CT imaging was used to assess the validity of this suggestion (Fig. 4.5). Micro-CT imaging (at 3 μm resolution) showed that the pores on both sides of the cortical bone wafers were interconnected across the wafer thickness both radially and axially (Fig. 4.5 B, C). Our calculations showed that the total porosity of adult canine cortical bone wafers was 2.95 ± 0.91%, the radial porosity was 0.60 ± 0.17%, and axial porosity was 2.36 ± 0.71% (Fig. 4.5D). Connectivity density calculations revealed a value for radial connectivity of $175 \pm 87 mm^{-3}$ and axial connectivity of 438 ± 204 mm^{-3} (Fig. 4.5 E).

4.3.2   Radial   hydraulic permeability of cortical bone

<u>1.   The   Permeability   of unprocessed cortical bone</u>

Figure 4.6 shows that the radial hydraulic permeability of fresh cortical bone wafers (1.5-mm thick) was below the detection limit of our customized system (4.0 x 10^{-17} m^2). We set
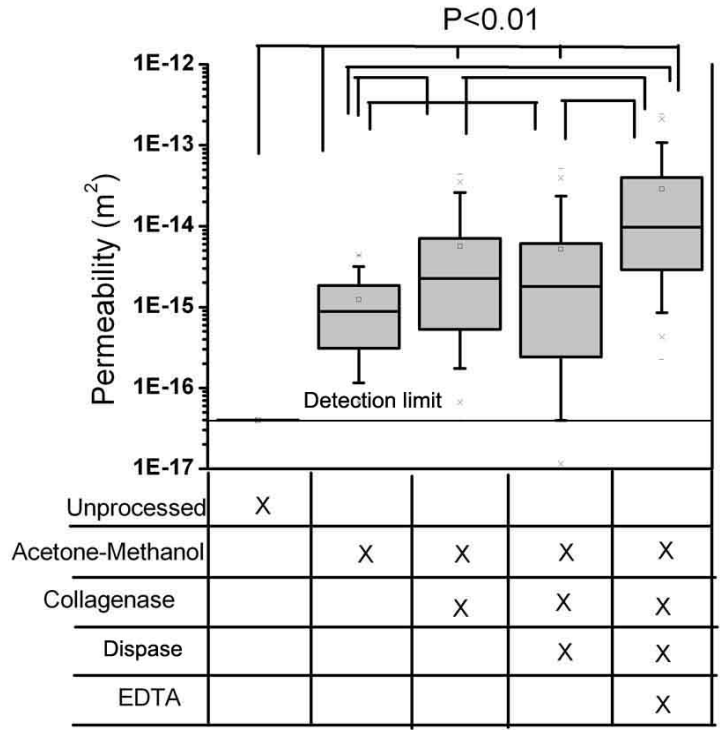
Figure 4-6 The permeability of cortical bone.

unprocessed bone at this limit value because prior evidence by Li et al [46] indicated the

radial hydraulic permeability of adult canine cortical bone to be 5 x 10^{-17} m^2.

2. Contribution of lipids to the permeability of cortical bone

Figure 4.6 shows that after acetone-methanol (AM) treatment, the permeability of bone wafers (1.5-mm thick) increased to 1.2 x 10^{-15} ± 1.1 x 10^{-15} m^2. Thus, the increase in permeability after AM treatment suggests that lipids in the porous compartment of cortical bone restricted its radial hydraulic permeability.

3. Contribution of collagen to the permeability of cortical bone

After AM treatment, cortical bone wafers were then digested with high purity bacterial collagenase. Comparing the permeability of cortical bone before and after collagenase treatment with one way ANOVA, the differences in the mean value between these two groups

Figure 4-7 Lipids extracted from cortical bone wafers by acetone-methanol (AM) treatment. Panel A shows the absolute amount of lipids recovered from the AM solutions normalized to the wet weight of each bone wafer. Panel B shows the percentage composition of extracted lipids recovered from the AM solutions. FFA: Free fatty acids. PL: Polar lipids. TAG: Triacylglycerols. Chol: cholesterol
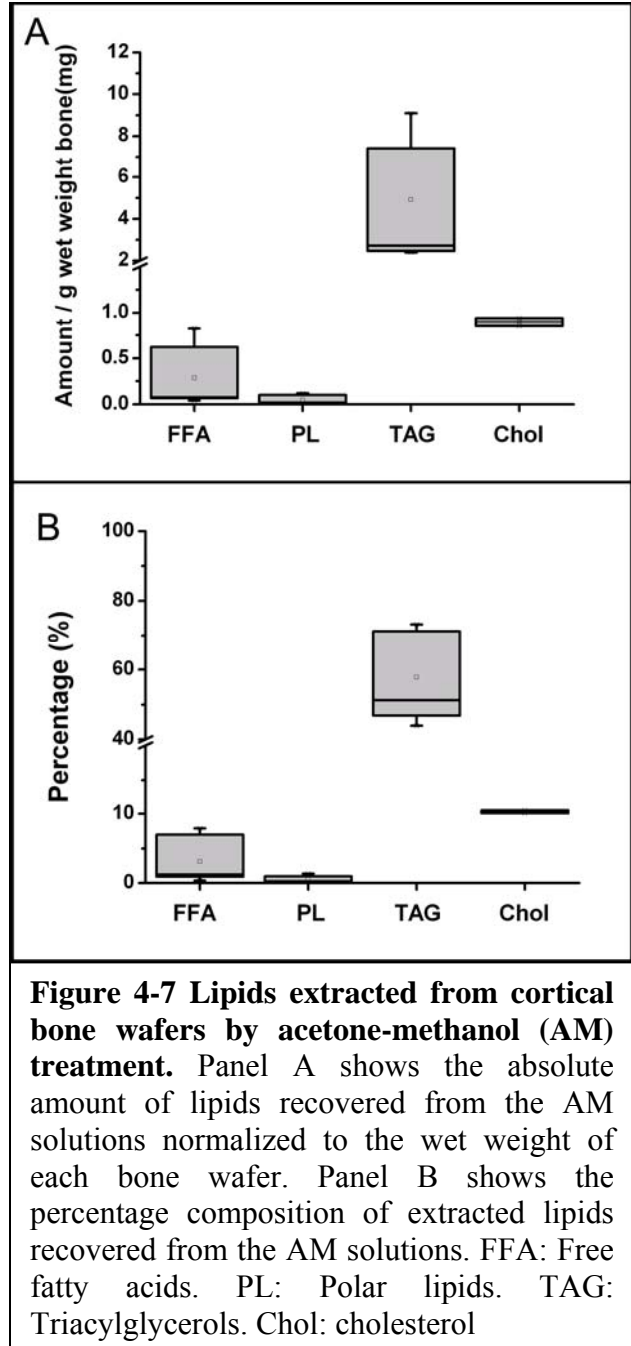
were greater than would be expected by chance (P < 0.001). Specifically Figure 4.6 shows that the permeability of 1.5-mm thick specimens significantly increased to 5.6 x $10^{-15} \pm 8.3$ x 10^{-15} m^2 after collagenase digestion, which suggested that the densely packed collagen matrix also restricted radial hydraulic permeability of cortical bone. After collagenase treatment, cortical bone wafers were then digested with bacterial dispase solution. Comparing the permeability of cortical bone before and after dispase treatment with one way ANOVA, the difference in the mean value between these two groups was not great enough to reject the possibility that the difference might be due to random sampling (p = 0.197). Specifically, there was no significance between the permeability of bone wafers before and after dispase treatment, which suggested that bulk removal of the organic matrix is not necessary to elevate its permeability.

4. Contribution of mineral to the permeability of cortical bone

The contribution of the non-porous compartment to the permeability of cortical bone can only be accessed by removing its calcium mineral salts, here by using EDTA treatment. After dispase treatment, cortical bone wafers were then treated with EDTA solution. Comparing the permeability of cortical bone before and after EDTA decalcification with one way ANOVA, the differences in the mean value between these two groups were greater than would be expected by chance (P < 0.001). Specifically, Fig 4.6 shows that after EDTA decalcification, the radial hydraulic permeability of the bone wafers was increased to 2.9 x $10^{-14} \pm 4.1$ x 10^{-14} m^2. No surprisingly, this suggested that the mineral content of bone restricts its permeability.

5. Lipids in the porous compartment of cortical bone

To confirm that lipids were removed from these cortical bone wafers by AM treatment, the organic solvent phase of the recovered AM extracts was evaporated and the dried waxy residue was submitted to gas chromatography separation and mass spectrometry detection of free fatty acids, phospholipids and triacylglycerols and cholesterol was measured with a colorimetric method [67]. In total, these four types of lipids comprised ~76 % of the residue's dry weight and accounted for ~9 mg/g wet weight of cortical bone. Triacylglycerols comprised the largest class of lipids (60%), followed by cholesterol (11%), free fatty acids (~4%) and phospholipids (~0.5%).

6. Collagen in the porous compartment of cortical bone

To confirm digestion of fibrillar collagen from these bone wafers, the amounts of hydroxyl-proline released into the collagenase digestion solution were measured (Fig 4.8, CS) and found to be 63 ± 37 μg hydroxyl-proline/g wet bone.
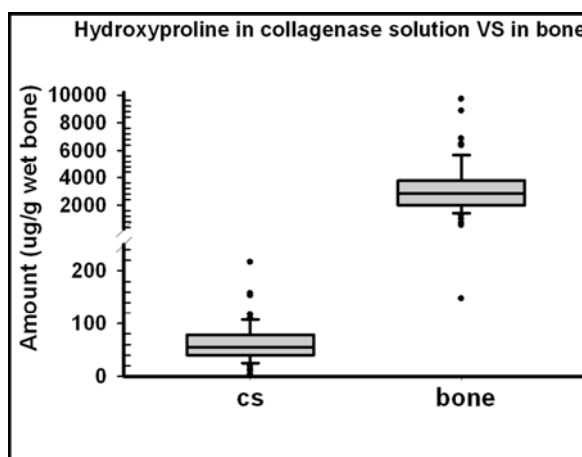
Figure 4-8 Amounts of hydroxyl-proline released from cortical bone wafers by collagenase digestion. *CS* represents the amount of hydroxyl-proline released into solution from the porous compartment of bone wafers by bacterial collagenase digestion. *Bone*, represents the amount of hydroxyl-proline released into solution from the collagenous matrix within the non-porous compartment after complete decalcification of bone wafers using EDTA.

Additional digestion of these bone wafers after collagenase with dispase released an

additional 90 ± 110 μg hydroxyl-proline/g wet bone. This observation suggested that collagenase digestion did not remove all the fibrillar collagen content from the porous compartment of these bone wafers. After EDTA treatment, the insoluble matrix from the decalcified bone wafers was totally hydrolyzed to measure its total amount of hydroxyl-proline. The hydroxyl-proline content in the insoluble matrix of decalcified bone wafers was 3100 ± 1800 μg/g wet bone (Fig. 4.8, bone). Using the values of hydroxyl-proline released by collagenase and dispase digestions mentioned above, the relative proportion of the porous to non-porous collagen content was calculated to be 4.9% (= [63 + 90]/3100 x 100%). This relative proportion of hydroxyl-proline content is close to the average porosity value (~3%) calculated from micro-CT imaging in Fig 4.5.

4.4 Discussion

In living bone tissue, interstitial fluids flow through a porous compartment containing vascular channels referred to as Haversian and Volkmann's canals [9, 88]. Fluid flow is important for the transport of nutrients, growth factors, and waste products inside bone. The permeability of cortical bone is the measurement of the ease of the fluid flow through the cortical bone [69]. The objective in this chapter was to identify some of the components in the porous compartment of cortical bone that regulate its radial hydraulic permeability. Two hypotheses were tested in this chapter: (1) the presence of hydrophobic molecules within the porous compartment of cortical bone restricts its hydraulic permeability; and (2) the presence of a densely packed pericellular matrix

64

(containing collagen fibers) will reduce the hydraulic permeability within the porous compartment of cortical bone.

Until now, few studies have experimentally measured the permeability of cortical bone. The earliest work was done by Johnson et al. [39] and they determined that the radial permeability of cortical bone containing large vascular channels was 2.5 x 10^{-14} m^2. Li et al. [46] measured the radial permeability of fresh cortical bone devoid of large vascular channels and after removing 0.5-1.0 mm of bone from the periosteal surface. Their results revealed that the average radial permeability of cortical bone from adult canine tibiae was 5 x 10^{-17} m^2. Beno et al. [7] estimated the permeability within cortical bone based on finite elemental analysis using microstructural measurements strictly of the lacuna-canalicular system. They predicted that the permeability of cortical bone at the lacuna-canalicular level was in the range of 10^{-18}~10^{-20} m^2. They concluded that the permeability of actual cortical bone tissue should be higher than this value given that bone tissue contains both a lacuna-canalicular system and larger inter-connecting channels. We could not measure the permeability of unprocessed bone wafers (1.5 mm) since the detection limit of our device is 4 x 10^{-17} m^2. However, based on the Darcy's law, if we decreased the thickness of the bone wafers, we can lower the detection limit of the device. Moreover, the pressure limit of the bone holder is 150 PSI, increasing the pressure limit of the bone holder can also lower the detect limit of the device. Still, we were able to measure the permeability of bone wafers with 200 μm thickness, and found its permeability is in the range of 4.0 x 10^{-16} m^2 to 1.0 x 10^{-17} m^2, consistent with these

previous determinations. The limitation here is that there may be difference between the permeability of the thinner and thicker bone wafers since the pore space of cortical bone has a hierarchical structure.

The porous compartment of bone is mainly composed of type I collagen fibers, non-collagenous proteins, lipids and cells [9]. The contributions exerted on bone's hydraulic permeability by these various organic components within the porous compartment of cortical bone have not been determined until now. This knowledge should help to better understand the regulation of fluid flow inside bone tissue. In turns, this may help *in vitro* bone tissue engineering approaches to improve the design of new bone scaffolds to better mimic *in vivo* properties.

Our finding that removing lipids from the porous compartment of cortical bone increased its radial hydraulic permeability indicates that the presence of lipids in the porous compartment of cortical bone reduces its permeability and suggests that the presence of such lipids is a factor restricting fluid flow in cortical bone. Our lipid composition results are consistent with those reported by Dirksen and Marinetti [19] and Leach [45] who measured the lipid contents of human and ox cortical bone and found high levels of triacylglycerols and low levels of phospholipids.

The lipid composition results suggest that osteocyte cell membranes and any vesicles that bleb off from these membranes are not likely to be the major source of lipids located in the non-porous compartment of bone since they both have a high content of phospholipids[9]. Instead, triacylglycerols comprise the major source of lipids in this

bone compartment, and this observation raises an intriguing hypothesis for the source of this hydrophobic material. Triacylglycerols are produced inside most vertebrate cells including those in the osteogenic lineage and stored within lipid droplets [82]. Takahashi [82]et al. have shown that osteogenic cells can secrete lipid droplets into their extracellular matrix. Thus, the source of these triacylgycerols extracted from fresh cortical bone might originate from secretion by its resident bone cell populations (osteoblasts lining Haversian and Volkman canals and osteocytes embedded within the lacuna-canalicular system). It is unclear at present what would regulate this secretion process and why such hydrophobic materials are deposited within the porous compartment of cortical bone tissue.

In addition to lipids reducing the radial permeability of cortical bone, we determined that the densely packed pericellular matrix [67] within the porous compartment of cortical bone also reduced its permeability. Removal and/or loosening of the collagen-rich matrix in the porous compartment of cortical bone with collagenase digestion substantially increased its permeability. This indicates that the pericellular matrix in the porous compartment of cortical restricts fluid flow and represents another factor regulating its permeability.

There were some limitations that should be addressed in future. Studies includes: (1) the hydraulic permeability of cortical bone needs to be measured. To do this there are two methods can be used: (a) with current device, the bone wafers can be cut into several pieces of thinner wafers with same thickness and the hydraulic permeability of these

wafers will be measured at same conditions; then the hydraulic permeability of bone wafers will be average of all these measurements; (b) a new device with lower detection limit needs to be made. Right now the detect limit of the present device results from the pressure limit of the holder made of PVC. Therefore, the bone holder made from stainless steel with same design as proposed in this chapter will increase the pressure limit of the bone holder thereby lower the detection limit. Compare to method (a) the advantage of this method is that the hydraulic permeability can be measured directly and the disadvantage is that some cost will be applied on the new device. (2) Hydraulic permeability of the cortical bone from periosteum side and the contribution of bone components to its permeability need to be studied to understand the mechanism of the nutrient and waste transport underneath periosteum layer, which is critical important for bone formation *in vivo*. To do this, a new device with much lower detect limit needed. (3) Changes in ultrastructure of the remaining pericellular matrix after removing lipids and / or collagen may have effect on the changes on the permeability. To determine whether there is the change of ultrastructure, transmission electron microscopy (TEM) images of the wafers after collagenase and or acetone methonal treatment need to be compared with that of the wafers before treatments.

Altogether, our results from this study showed that the presence of lipids and collagen-rich pericellular matrix within the porous compartment of canine cortical bone reduced permeability in a radial direction and thereby restricted fluid flow through this bone tissue compartment. The findings in this study may have bearing on investigations

attempting to promote bone formation *in vitro* via tissue engineering approaches. Perhaps the presence and distribution of lipids and densely packed collagen matrix applied to appropriate scaffolds may help promote osteogenic differentiation of progenitor cells and produce a more bone-like tissue construct in bone bioreactor designs.

CHAPTER V

EXPERIMENTAL MEASUREMENT AND MATHEMATICAL MODEL OF

GLUCOSE DIFFUSION IN CORTICAL BONE SCAFFOLD

5.1 Introduction

Glucose supply always needs to be considered in bone tissue engineering since it is essential to maintain cell viability [66]. Several studies have attempted to improve glucose supply, such as using rotating flasks instead of conventional immobile flasks [79]. In our proposed bone tissue engineering system, the 3D scaffold will consist of a cortical bone under layment and a type I collagen- fibronectin hydrogel interface to promote bone cell attachment this scaffold. In this 3D scaffold design, glucose will be supplied from both top and bottom of the 3D scaffold. Under static culture conditions, glucose transport is only mediated by diffusion. Over extended culture time under these conditions, nutrient supply may become limited for the metabolism of bone cells. To determine when glucose

becomes limited in our system, the glucose concentration profile will be calculated by a mathematical model. Mathematically, to calculate the glucose concentration profile, the diffusion coefficient of glucose needs to be known. Up to now, few studies have measured a glucose diffusion coefficient in cortical bone [35, 43]. Jackson et al. reported that the glucose diffusivity in bovine annulus fibrous was $1.38 \times 10^{-10} \, m^2 /s$ [35]. Lang et al showed that the glucose diffusivity in bone was in the magnitude of $3 \times 10^{-13} \, m^2/s$ [43]. Therefore in this chapter: (1) the diffusion coefficient of glucose in cortical bone in a radial direction was measured with diffusion cell; and (2) a mathematical model was established to generate the glucose diffusion profile in our system.

5.2 Experimental measurement of glucose diffusion in cortical bone

5.2.1 Materials and methods

<u>1. Bone wafer preparation:</u>

All bone tissues were obtained from animals that had been sacrificed in the course of IACUC approved research investigations conducted elsewhere at this institution. Mid-diaphyseal portions of tibia were harvested from outbred adult canines (~25-30 kg body weight). Periosteal tissue layers, including most of the basal cambium cell layer, were stripped off the bone by dissection. Bone marrow was flushed out of the bone with phosphate buffer saline (PBS) (Cellgro). These tibial diaphyses were then stored in PBS with 0.05% sodium azide (Sigma) at 4° C and used within a 2 week period from collection. Cortical bone wafers from the endosteal side of tibial diaphyses with dimensions of 15 mm length, 15 mm width, and 200 μm thick were cut with an EXTEC

® Labcut 1010 Low Speed Diamond Saw (EXTEC Corp). Six bone wafers were submitted for glucose diffusion measurements. These wafers were selected from the same tibial for which permeability values were determined.

2. Diffusion measurements with a diffusion cell system

Solute diffusion coefficients can be measured using a diffusion cell system as shown in Figure 5-1 (Crown Glass, Somerville, NJ). A schematic of the diffusion cell system is shown in Fig 5-2. The cell consists of two well- stirred compartments that contain known volumes of a solute of interest (here glucose), separated by a thin membrane (here a 200 μm thin cortical bone wafer). Initially, each compartment is filled with differing solute concentrations; typically a zero concentration on the receiver side and some specific initial concentration on the donor side. In our experiments we chose a glucose concentration of 2 mg/mL which is in the high physiological range. The flux of solute (glucose) across the membrane (bone wafer) can be determined by the measurement of the solute concentration in both donor and receiver sides over increasing time. Experiments ran for 10 days each. The concentration of glucose was determined using glucose assay kit based on hexokinase activity (Sigma). The glucose detection limit is 50μg / mL with this method.

3. Calculation of diffusion coefficients

We assume that these experiments are in pseudo-steady state (volume change can be omitted in both donor and receiver sides). The solute concentrations in the donor and receiver sides were assigned as C_D (mg/mL) and C_R (mg/mL) respectively, the volumes

72

of solution in donor and receiver sides as V_D (mL) and V_R (mL), the fluid transport area as A (mm^2), and the flux rate of glucose as J. Therefore, the mass transfer equation (1) for the donor side is:

$$V_D \frac{dC_D}{dt} = -AJ \quad (1)$$

The mass transfer equation (2) for the receiver side is:

$$V_R \frac{dC_R}{dt} = AJ \quad (2)$$

According to Fick's law, the flux rate is:

$$J = \frac{D}{L}(C_D - C_R) \quad (3)$$

Here, D is the diffusion coefficient of the solute and L is the thickness of the cortical bone. Since the volumes in the donor and receiver sides are equal, then we can set: $V_D = V_R = V$.

Solving for D (the diffusion coefficient) using these three equations (1) ~ (3), we generate the following equation (4):

$$D = -\frac{LV}{2At}(Ln\frac{C_D - C_R}{C_{D0} - C_{R0}}) \quad (4)$$

Therefore, upon measuring the concentrations of glucose in both the donor and receiver sides at different time points, we can calculate the slope between time t and $Ln\frac{C_D - C_R}{C_{D0} - C_{R0}}$, and then input the thickness of cortical bone (L), the area of fluid

73
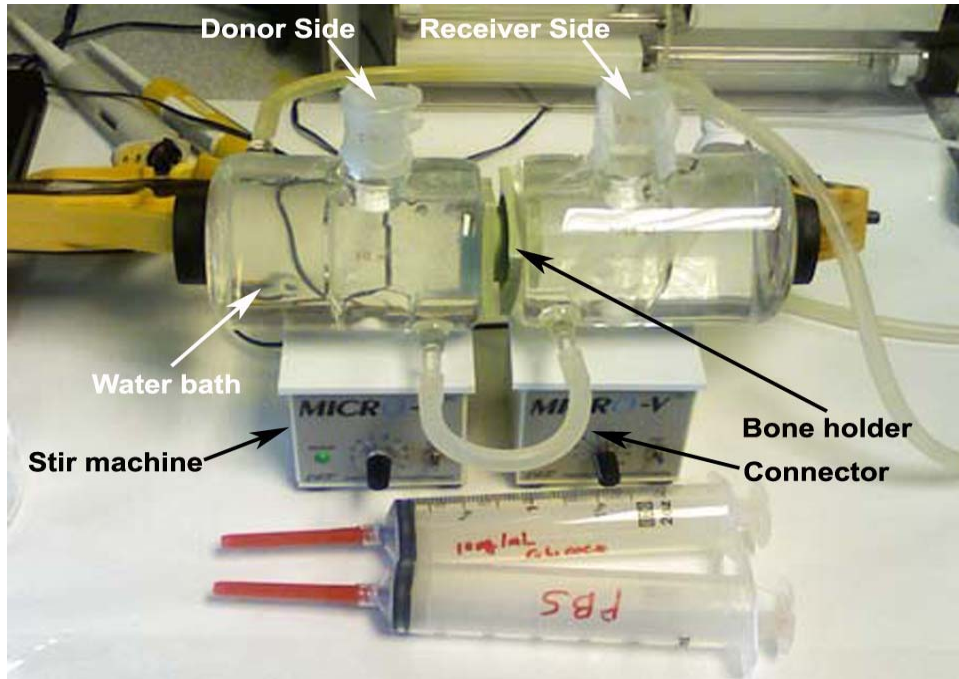
Figure 5-1 Picture of diffusion cell system
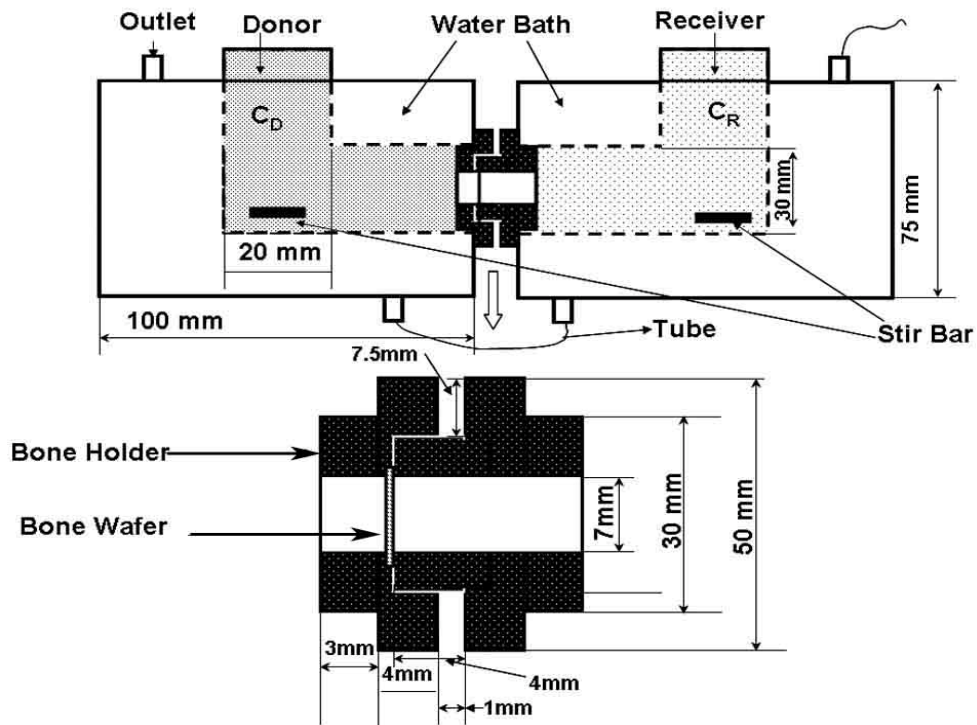
Figure 5-2 Schematic of diffusion cell system transport

74

area (A) and the volume of solution in donor and receiver side (V) therefore we can solve for the diffusion coefficient (D).
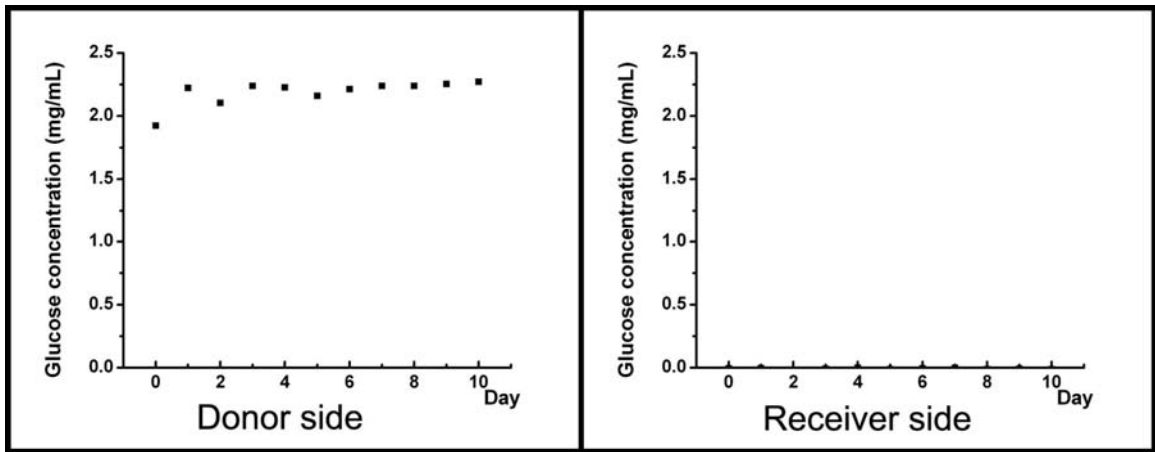
Figure 5-3 Glucose concentration profile in both donor and receiver

5.2.2 Results

Figure 5-3 shows the glucose concentration profiles in both donor and receiver sides. It showed that there is no change of glucose concentration in either side, suggesting that the diffusion coefficient of glucose in cortical bone is very low and can not be measured using the current diffusion cell system.

5.2.3 Discussion and conclusions

1. Limitation of the diffusion cell system:

In our system, the thickness of the cortical bone wafer is 200 μm, the fluid transport area is a 7 mm diameter circle, the original glucose concentration in the donor side is 2 mg/mL, and the lowest concentration of glucose that can be detected in the receiver side with our assay is 50 μg/mL. Given that each experiment ran for 10 days, we can input all

these parameters in equation (4), and then back-calculate the lowest diffusion coefficient that could be detected by this device (3.9×10^{-8} cm^2 /s). Based on these calculations, we conclude that the diffusion coefficient of glucose in cortical bone must be less than the detect limit by this device. For future reference, in order to obtain an accurate measure of the diffusion coefficient of glucose in cortical bone, a more sensitive assay method (such as radio-labelled glucose), a thinner bone piece and / or extended experiment time can be applied in new experiments.

2. Diffusion coefficient of glucose in cortical bone calculated from porosity and tortuosity

Diffusion coefficients of solutes in porous materials are influenced by its porosity and tortuosity [2, 73]. Several studies have been done to correlate the diffusion coefficient of solutes in porous materials with respect to material porosity and tortuosity [2, 73]. Since we were not able to accurately measure the diffusion coefficient of glucose in adult cortical bone, we can calculate the diffusion coefficient of glucose in adult cortical bone using an already established relationship between the diffusion coefficient of a solute in a porous material and its porosity (ε) and tortuosity (τ) based on porosity measurement of cortical bone (Chapter 4, 0.6% porosity in radial direction). Baron [2] et al. reported the relationship between the effective diffusion coefficient in a porous glass matrix and its porosity and toruosity as Equation (5):

$$D_{eff} = D\frac{\varepsilon}{\tau} \ (5)$$

Here D_{eff} is the diffusion coefficient in a porous glass matrix, D is the diffusion coefficient in collagen, ε is porosity, and τ is tortuosity. Since cortical bone is composed of disc-shaped mineral crystals and the packed pattern of the porous glass approximates that of bone, we can apply this equation to calculate the diffusion coefficient of glucose in cortical bone from its (1) porosity (ε), (2) tortuosity (τ), and (3) the diffusion coefficient of glucose in a collagen matrix (D).

Since the mineral is disc-shaped in cortical bone, we can calculate its tortuosity from its porosity based on equation

$$\tau^2 = 1 - Ln(\varepsilon) \ [73]$$

$\varepsilon = 0.006$ (Data from Chapter 4, the axial porosity of cortical bone 0.6%) then $\tau = 2.47$. The diffusion coefficient of glucose in collagen gel (D) is 1.3 x 10^{-6} cm^2 /s [96]. Input all parameters into equation 5, we calculate the diffusion coefficient of glucose in cortical bone (D_{eff}) to be 3.15 x 10^{-9} cm^2/s. This value is consistent with the low end estimates of glucose diffusion in cortical bone. It also explains why we were unable to accurately measure the diffusion coefficient of glucose in our current diffusion cell system.

Therefore, we conclude that the glucose diffusion coefficient in cortical bone less is than 3.9 x 10^{-8} cm^2/s and maybe around 3.15 x 10^{-9} cm^2/s.

5.3 Mathematical model of predicting a nutrient concentration profile in a 3D scaffold made of cortical bone and a type I collagen-fibronectin hydrogel

5.3.1 Model establishment

A concentration profile for small molecular weight nutrients inside a 3D scaffold used for cortical bone tissue engineering can be calculated using a mass balance analysis. This 3D scaffold includes bone cells on top of a type I collagen hydrogel layer (mimicking an osteoid layer) and a porous cortical bone layer underneath the collagen layer that has had its cellular contents removed by NaOH treatment. Assumptions were made to calculate this concentration profile: (1) the diffusion process is at steady state, (2) a nutrient is transported only by molecular diffusion and not by convection, (3) nutrient consumption occurs only within the collagen gel layer and is consumed uniformly, and (4) non-metabolic consumption of a nutrient is negligible within the 3D scaffold because the nutrient content is well above the saturable limit for non-specific adsorption in the 3D scaffold. This concentration profile represents the relationship between the distance from the top surface of the collagen gel and the nutrient concentration at that site. The following variables are defined: (1) the distance from the top surface of the collagen gel is y, (2) the thickness of collagen gel is L_c, (3) the thickness of cortical bone is L_B, (4) the starting concentration of the nutrient in the medium is C_0 and represents the concentration at both the top surface of the collagen gel and the bottom surface of the cortical bone, (5) the metabolic consumption rate in the collagen gel is r_{max}, and (6) the diffusion coefficients of the nutrient in collagen gel and cortical bone layers are D_c and D_B respectively. A schematic of the concentration profile is shown in Figure 5.4.

The mass balance equation (6) in the collagen gel layer can be expressed as:

$$D_c \frac{d^2C_c}{dy^2} = r_{max} \quad (6)$$

The mass balance equation (7) in the cortical bone layer can be expressed as:

$$D_B \frac{d^2C_B}{dy^2} = 0 \quad (7)$$

The concentration of
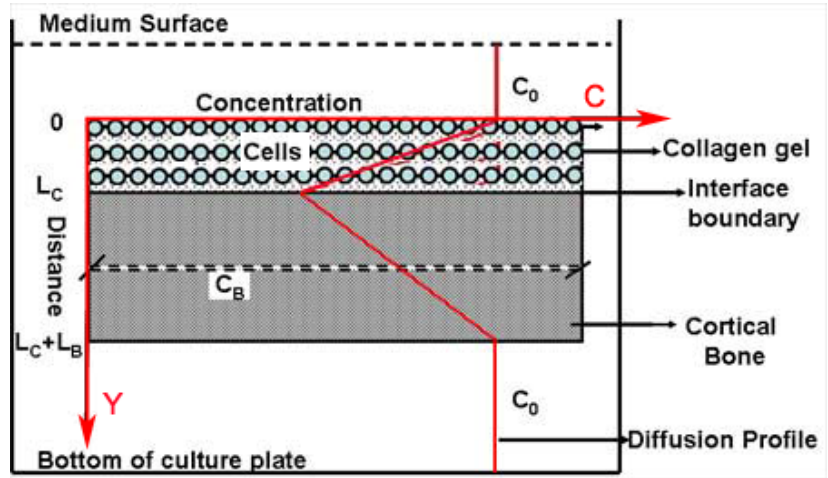
Figure 5-4 The schematic of concentration profile of the nutrient in 3D scaffold

nutrient at both the top surface of the collagen gel and bottom surface of the cortical bone is C_0. We can set boundary equations (8) and (9) as:

$$y = 0, C_c = C_0 \quad (8)$$

$$y = L_c + L_B, C_B = C_0 \quad (9)$$

At the boundary between the collagen gel and cortical bone, since they refer to the same interfacial surface, their concentrations and transport rates are the same. We can set boundary equations (10) and (11) respectively:

$$y = L_c, C_c = C_B \quad (10)$$

$$y = L_{c,} D_c \frac{dC_c}{dy} = D_B \frac{dC_B}{dy} \quad (11)$$

Intergrating equations (6) and (7) and applying the boundary equations (8)-(11) into these two equations, the nutrient concentration profile equations for both the collagen gel

layer and the cortical bone layer can be derived to yield equation (12) as the profile in the collagen layer and equation (13) as the profile in the cortical bone layer.

$$C_c = \frac{r_{max}}{2D_c}y^2 + (\frac{r_{max}D_B L_c^2}{2D_c(L_B + D_B L_c)} - \frac{r_{max}}{D_c}L_c)y + C_0 \quad (12)$$

$$C_B = \frac{r_{max}L_c^2}{2D_c(L_B + D_B L_c)}y - \frac{r_{max}L_c^2(L_c + L_B)}{2D_c(D_B L_C + L_B)} + C_0 \quad (13)$$

5.3.2 Discussion

1. Application of this model

Based on our assumption, this model can only be applied to predict the nutrient concentration when the transport process is (1) at steady state, (2) only through molecular diffusion, (3) uniform consumption in the upper layer and (4) no consumption in the lower layer. Therefore, it can be used to predict the concentration of any nutrient or waste product molecules in the scaffold (composed of 2 layers) in static culture. It can not be used to predict a nutrient concentration in cortical bone *in vivo* since there is nutrient consumption in cortical bone. To be able to predict a nutrient concentration *in vivo*, a consumption factor needs to be added in equation (7) and diffusion coefficient (D) needs to be modified to incorporate any convection influence.

2. Glucose concentration profiles in a 3-D scaffold design for bone tissue engineering *in vitro*

Using the above equations, we can calculate glucose concentration profiles in a 3-D scaffold made of a cortical bone wafer and a type I collagen hydrogel (Fig 5.4). Values

for the following variables were obtained from the literature: (1) our analysis suggested that the diffusion coefficient of glucose in cortical bone (D_B) is in the range of 3.9 x 10^{-8} ~ 3.15 x 10^{-9} cm^2/s, and here we assume a value within this range D_B= 1x 10^{-8} cm^2/s; (2) the diffusion coefficient of glucose in a collagen gel (Dc) is 1.3 x 10^{-6} cm^2/s, and (3) the specific glucose consumption rate of 1 x 10^6 osteoblasts in bone is assumed to be 320 nmol/h [97]. In our system, the thickness of the cortical bone scaffold would be 300 μm thick and the cells plus artificial osteoid layer yield a combined 30 μm thickness. We assume the maxium cell density in collagen gel layer is 5000 cells /mm^2 (based on the average cell density in the cultures with collagen-fibronectin hydrogel, Chaper 6, Figure 6-14), making the consumption rate of glucose in the collagen gel layer r_{max} = 320 nmol/h x 5000 cells/mm^2 / (1 x 10^6 cells) [70]. We set the starting glucose concentration C_0 as 1 mg/mL as this is the physiological concentration of glucose in the growth medium. Putting all these parameters into equations (12) and (13), we can calculate the glucose concentration profile for the collagen gel and cortical bone layers respectively (Figure 5-5). These profiles can be expressed as equations (14) and (15) respectively.

Equations:

$$y = 0.0004x^2 - 0.0239x + 1 \text{ (14)}$$

$$y = 1.1963x - 0.6052 \text{ (15)}$$
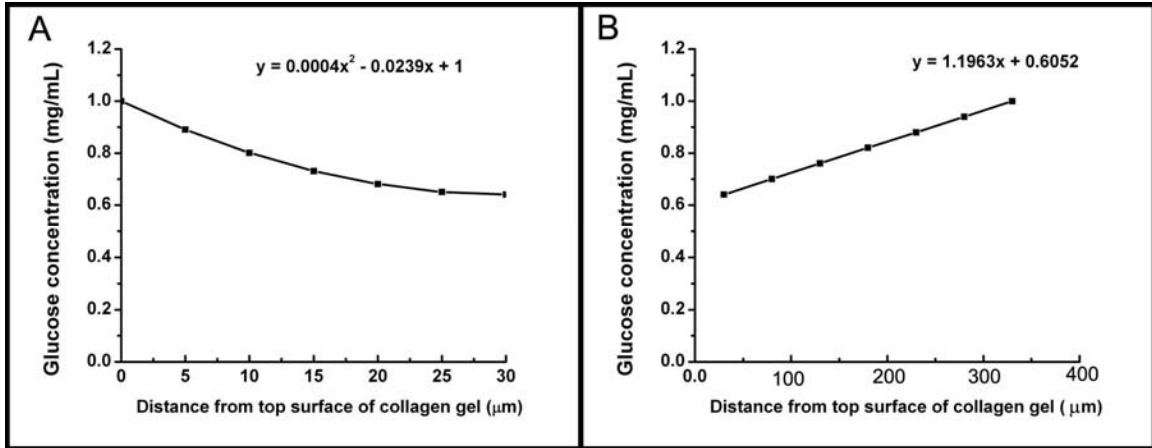
Figure 5-5 Glucose concentration profile in the culture on the scaffold. A: in the collagen gel layer; B: in scaffold layer

These profiles show that the glucose concentration in the collagen gel layer decreased from 1 mg/mL to 0.64 mg/mL from its top to bottom surface. The glucose concentration in the cortical bone layer decreased from 1 mg/mL to 0.64 mg/mL from its bottom to top surface. This suggests that there is no limitation of glucose supply for bone cells to grow up to 30 μm thick on this type of cortical bone scaffold.

3. The thickness of a bone cell layer growing on a 300 μm cortical bone scaffold without nutrient limitation.

When the glucose concentration on the bottom surface of the collagen gel becomes 0, the glucose supply would become limiting for cell survival, proliferation and/ or differentiation. During culture it is anticipated that new bone tissue would be deposited beneath the cell layer and in the collagen matrix over incubation time. If we set the concentration on the bottom of the collagen gel as 0, we can re-calculate the accumulated thickness of new matrix beneath the cell layer by equation (12) and (13) and it is 50 μm

on the scaffold. These calculations suggest that the highest amount of new bone tissue that can be deposited in this system is 50 μm. To grow more tissue in this static system, we would need to improve nutrient (glucose) transport, which could be accomplished by applying dynamic mechanical loads to introduce convection to promote nutrient transport.

4. Glucose transport in cortical bone *in vivo*

Glucose transport is considered important in cortical bone in order to maintain the viability of its constituent bone cells. Transport can be accomplished via diffusion, convection force and carrier diffusion. Here, we empirically measured the diffusion of glucose in cortical bone with a diffusion chamber. Our results showed that the diffusion coefficient of glucose in cortical bone was very low. After 10 days, few amount of glucose diffused through a 200 μm bone wafer. Given that osteocytes remain viable in bone tissue *in vivo* then it is more likely the transport of glucose in cortical bone is achieved by convection forces that move fluids (caused by dynamic mechanical load and blood pressure). Alternatively, perhaps there is another metabolic nutrient source to meet the needs of bone cells' consumption. For example, extracellular lipids, may be internalized and degraded to carbon units that might meet the metabolic needs of osteocytes.

There were some limitations that should be addressed in future. Studies includes: (1) the glucose diffusion coefficient in cortical bone could not be measured in current diffusion cell system. The detect limit of current system results from the method used to measure the glucose concentration. Therefore in future a more sensitive detection method

needs to apply this system, such as using radiolabel chemicals. (2) Oxygen transport is another important issue to be considered in bioreactor system. Diffusion coefficient of oxygen needs to be studied to generate the oxygen concentration profile with this model system [66]. (2) Based on my lipids data from Chapter IV, there were considerable amount of lipids in porous compartment of cortical bone. Therefore the diffusion coefficient of hydrophobic molecules (such as prostaglandin [64]) in cortical bone needs to be studied to better understand the nutrient transport inside the bone. (3) Fluid flow caused by mechanical load increases the nutrient and waste product transport inside the bone [18]. Therefore, the diffusion coefficient of glucose in cortical bone under mechanical load needs to be studied to better understand the nutrient transport inside the bone. (4) This mathematical model system can only be applied to the static system since only molecular diffusion was considered for glucose transport in this system. Therefore, in future convection factors needed to be included in the model system to predict the glucose concentration profile in the system with mechanical load.

CHAPTER VI

BASOLATERAL MINERAL DEPOSITION BY VARIOUS OSTEOBLAST SOURCES CULTURED ON 3D COLLAGEN FIBRONECTIN HYDROGEL SCAFFOLDS

6. 1 Introduction

Cell source and scaffold material are two key components in bone tissue engineering [39, 66]. Until now, sources of cells used in bone tissue engineering have included mesenchymal stem cells derived from different tissues, such as bone marrow, periosteum, human umbilical cord blood [5, 6, 13, 29, 30, 33, 39, 42, 50, 51, 76-79, 89], and mature osteoblasts, such as primary cells from human trabecular bone obtained during iliac crest biopsies [60]. Bone marrow is the highly cellular tissue found in the medullary cavity of long bones (see Figure 2-1). Cells from bone marrow comprise a heterogeneous group of phenotypes including hematopoietic stem cells, mesenchymal stem cells and endothelial stem cells [9, 66]. Mesenchymal stem cells, a source of primary cells used in bone tissue

engineering, can be separated from the other two stem cell populations by a colony forming adhesion assay [66]. In vitro, studies have shown the osteogeneic potential of bone marrow cells. For example, Barralet et al. cultured bone marrow cells on type I collagen gels for 21-28 days and showed new osteoid-like tissue formation by these cells [6]. Sikavitsas et al. cultured bone marrow cells in a flow perfusion bioreactor and showed that such a fluid-flow bioreactor culture system minimized diffusion constraints and provided mechanical stimulation to the bone marrow cells, leading to the accumulation of a cancellous bone-like mineralized tissue [78].

Osteo-progenitor cells also reside within the periosteal cambium layer and can develop into osteoblasts, which are responsible for increasing the width of a long bone and the overall size of axial and craniofacial bone types [48]. These osteo-progenitor cells can be isolated, which provides another source of primary osteoblastic cells for bone tissue engineering [48]. Several studies have reported on the osteogenic properties of periosteal cells. Wiesmann et al. cultured periosteal derived osteoblasts on Petri dishes as well as within 3D collagen constructs. They showed that these cells can form 'bone like' mineral deposits in both 2- and 3-D environments and formed an extracellular matrix containing osteocalcin, SPARC (osteonectin), and newly synthesized collagen type I in both environments [89]. Koshihara et al. showed that periosteum cells are osteoblastic cells that could differentiate into osteocytes and deposited calcified mineral in response to 1, 25 dihydroxyvitamin D_3 [48].
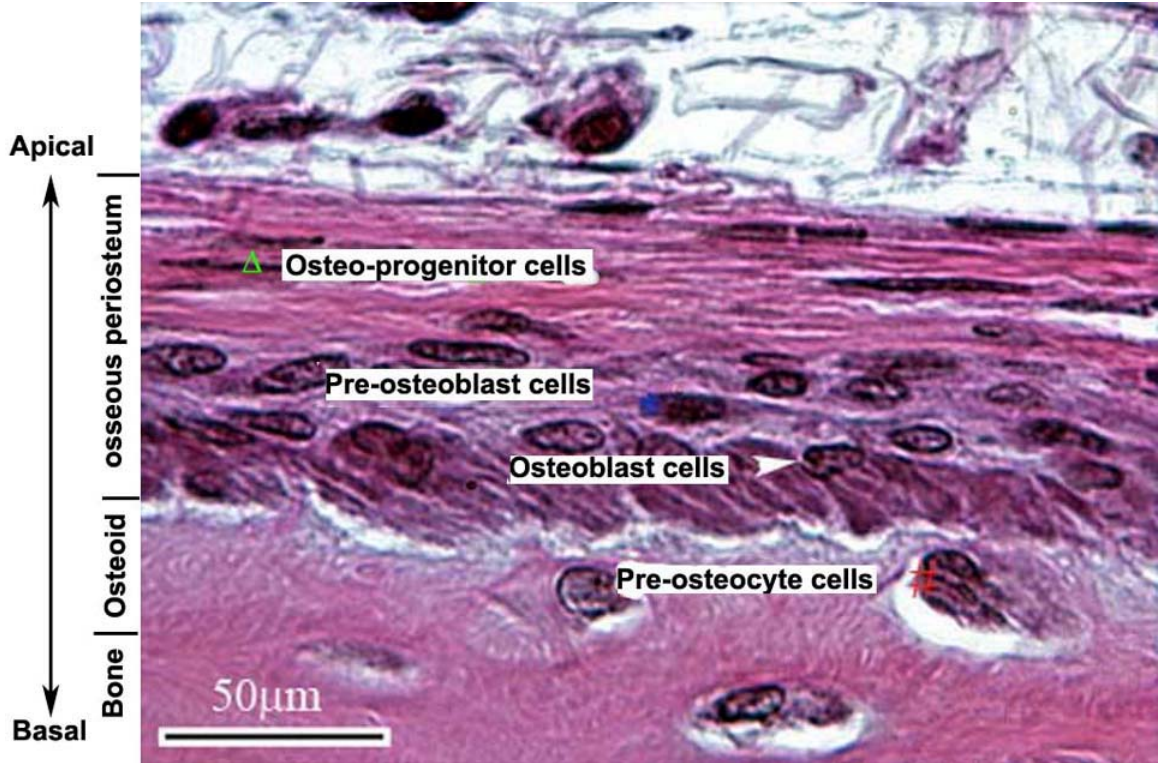
Figure 6-1 The morphology of cells in the periosteum. Done in Midura lab

In vivo periosteum, (Figure 6-1) is composed of 6~7 cell layers; three different cell types are located in periosteum tissue: osteo-progenitor cells, pre-osteoblasts and osteoblasts. Pre-osteocytes are located within the osteoid layer-- the densely packed type I collagen rich organic matrix secreted by mature surface osteoblasts that eventually becomes mineralized and forms bone tissue [9]. All these cells are responsible for increasing the width of a long bone's diaphysis and the overall thickness of bone types [9]. The morphology of these cells is different: from spindle shaped osteo-progenitors with a nuclear length/ width aspect ratio of 8- 9 at top cell layer (apical) to round/ cuboidal

shaped osteoblasts with an aspect ratio of 1- 2 at the bottom cell layer (basal). Moreover the space between nuclei in each layer from top to bottom is different, suggesting that different cell layers may contain different densities of cells. All of these observations indicate a polar distribution of cells and extracellular matrix along the bone formation front, whereby apical cells are more flattened than basal cells, and extracellular matrix accumulates beneath the basal cells. This kind of cell and matrix distribution may be important for continual bone formation*in vivo*.

To mimic the periosteum tissue structure *in vitro*, osteo-progenitors derived from bone marrow or periosteum could be used to form bone cell layers on a 3D collagen-fibronectin hydrogel (artificial osteoid layer) intended to represent a bioartificial osteoid layer. In this system we hypothesized that: (1) extracellular matrix protein and mineral deposition in bone marrow and periosteum 3D collagen fibronectin hydrogel cell cultures will be higher comparing to on conventional 2D tissue plastic; (2) cell density, extracellular matrix protein and mineral deposition in bone marrow and periosteum 3D collagen fibronectin hydrogel cell cultures will exhibit a basal lateral deposition pattern while not on 2D conventional tissue plastic; (3) cell nuclear morphology at different stages of osteogenesis would exhibit different aspect ratio; (4)osteo-progenitors derived from bone marrow and periosteum cells exhibit equivalent osteogenic capacity.

In order to test these hypotheses, bone marrow and periosteum cells were isolated from tibial diaphyses of juvenile rats because they are two conventional normal osteoblast models. A bio-artificial osteoid matrix was constructed using matrix type I

collagen gelled into 3D hydrogels coated with fibronectin because the components of osteoid layer is type I collagen (mainly) and some other extracellular protein (such as fibronectin); and studies showed that fibronectin and collagen scaffold promoted osteogenesis of osteoblasts *in vitro*. The experimental design used in this study employed a direct comparison of the same bone cell type cultured on the 3D bio- artificial osteoid matrix versus on conventional 2D tissue culture plastic surfaces. 3-4 weeks (25 days) culture period was selected based on prior knowledge that this is first time period to reliably assess mineral content *in vitro* [6, 30, 48]. The outcomes included the amount and distribution of cell nuclei density, extracellular matrix (bone sialoprotein (BSP [9, 26]) and sereted protein acid rich with cysteines (SPARC [9, 38])) and calcium mineral [9, 68] deposited in the cultures. SPARC and BSP were selected as indicators of ostoegenesis because they are both bone matrix molecules that exhibit calcium binding properties and are deposited by osteoblast cells at different stage of osteogenic differentiation. The expression of SPARC occurs when osteoblasts stop proliferating and begin terminal differentiation. It is considered to be an early to intermediate marker of osteoblast differentiation [9, 38]. The expression of BSP occurs at a later stage of osteogenic differentiation coinciding with the ability to deposit calcium mineral [9, 26]. Ultimately, the unique attribute of osteoblast activity is the ability to deposit hydroxyapaptite crystals (calcium mineral) [9, 68] in a collagenous tissue matrix.

Specifically, osteo- progenitor cells derived from two different cell sources (bone marrow and periosteum) were cultured on two culture modality (3D collagen-fibronectin

hydrogels and 2D conventional tissue plastic) for 25 days respectively in two culture conditions (growth medium and differentiation medium) (three cultures were done for each group (n=3)) for a total of 8 groups. At 25 days, the cultures were cultures were fixed and underwent standard paraffin histological processing. H&E staining was used to provide gross observation of the culture. 4',6-diamidino-2-phenylindole (DAPI) staining was used for nuclei morphology and nuclei number analysis. Immunohistochemistry staining of BSP and SPARC was used for the analysis of BSP and SPARC deposition. Alizarin red S staining was used for the analysis of calcium mineral deposition confirmed by decalcification in serial sections. Three slides were stained for each staining. 25 ~30 images were taken for each slide for each staining and the image-Pro software was used for quantification analysis. The amount (quantity) of extracellular matrix (BSP, SPARC) and mineral deposited on the cultures was defined as the average positive stained area per layer within each image. The distribution of extracellular matrix and mineral was defined as the spreading of positive stained area in each layer within image.

6. 2 Methods and procedures

6. 2.1 Preparation of type I collagen Gel

A 2 mg/mL type I collagen solution was prepared from a stock of native rat tail type I collagen solution (3.56 mg/mL, Gibco). 250 μL aliquot of the 2 mg/mL collagen solution was placed into each well of 12-well plate sitting on ice. The plate was placed into a 37^0 C incubator overnight to let the collagen gel solidify. A 2 μg/mL fibronectin solution was prepared from a stock of fibronectin powder (1mg stock stored in - 20 ^{0}C,

90

Sigma). A 200 µL aliquot of the 2 µg/mL fibronectin solution was placed onto each collagen gel. The plate was incubated at 37^0 C for 2 hours to coat the collagen gel with fibronectin because fibronectin has collagen binding domains. Each well was washed with 500 µL of phosphate buffered saline solution (PBS) for 10 times to remove any unbound fibronectin. An aliquot of 500 µL growth medium was put in each well and the plate was incubated at 37^0 C for overnight to equilibrate the collagen-fibronectin gel with culture medium. The collagen-fibronectin gel was ready for use in cell culture experiments.

6.2.2 Cell culture

1. Isolation of periosteum and bone marrow cells from rat tibia

All of the animal procedures used in this study were reviewed and approved by the Institutional Animal Care and Use Committee. The periosteum and bone tissue were harvested according to a previously published protocol [48]. Briefly 12 Harlan-Sprague-Dawley male rats of one month age (40~ 45g body weight) were euthanized by asphyxiation with CO_2. A 7-mm-long segment from the middle diaphysis of each tibia was obtained from the rats using aseptic techniques. Periosteal tissue layers, including most of the basal cambium cell layer were stripped off the bone by dissection, and bone marrow tissue was flushed out of the medullary cavity. Recovered periosteum tissues were placed into a 50 mL tube containing 3 mL Dulbecco's Modified Eagle's Medium (DMEM) (Sigma) solution supplemented with 0.6 Unit/mL Dispase (Gibco) and 100 Unit/mL bacterial Collagenase (Sigma). Cells were released from the periosteum matrix

by incubation in this digestion solution at 37^0 C for 2 hours at which time all the tissue matrix was completed dissolved. Cells were recovered from the digestion solution by centrifugation at 100g for 5 min, and re-suspended in 2 mL growth medium (α-minimal essential medium (MEM, Cellgro) supplemented with 10% FBS (Hyclone), 20 mM HEPES (Cellgro), 20 μg/ml gentamycin (Sigma), and 0.25 μg/ml Amphoterin B (Sigma)). This cell suspension solution was placed into a 35 mm culture dish and incubated at 37° C in a 5% CO_2 humidified incubator. After 48 hr incubation, the medium was replaced and adherent cells were cultured for 5~6 more days to reach confluence with medium exchanges every 2 days. At this time, periosteum cells were ready for culture experiments.

Bone marrow tissue was placed into a 100 mm dish containing 10 mL of growth medium. Cells were released by repeated pipeting through 18 gage needles and transferred into a 50 mL tube. Cells were recovered by centrifugation at 100g for 5 min and re-suspended in 2 mL growth medium. This cell suspension solution was placed into a 35 mm culture dish and incubated at 37° C in a 5% CO_2 humidified incubator. After 48 hr of incubation, the medium was replaced and adherent cells were cultured for 5~6 more days to reach confluence with medium exchanges every 2 days. At this time bone marrow cells were ready for culture experiments.

2. Cell culture
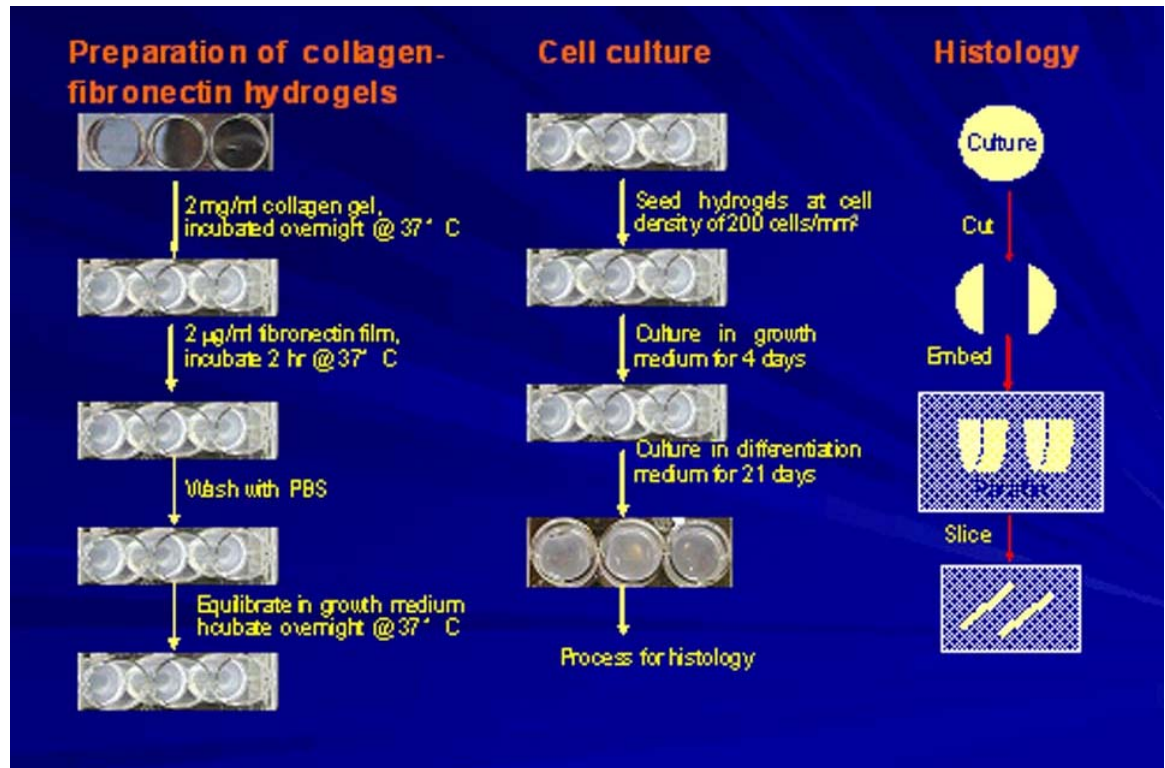
Figure 6-2 cell culture and histology.

For both cell types, cells were typsinized, counted and then seeded onto conventional 2D tissue culture plastic or 3D collagen-fibronectin hydrogels in a 12 well plate at an initial density of 200 cells/mm^2, a density at which cells became confluent in 4 days (Figure 6-2). For the first four days of incubation, cells were cultured with 250 µL of growth medium. At this time point, for each cell type and each culture modality (2D and 3D), cells were separated into two sub-groups. One sub-group was maintained in growth medium (250 µL/ well) for another 21 days with media exchanges every other day. The second sub-group was switched to an osteogenic differentiation medium (250 µL/ well) for another 21 days with media exchanges every other day. Growth medium was α-MEM

(Cellgro) supplemented with 10% FBS (Hyclone), 20 mM HEPES (Cellgro), 20 ug/ml gentamycin (Sigma) and 0.25 μg/ml Amphoterin B (Sigma). Differentiation medium consisted of growth medium supplemented with 50 μg/mL L-ascorbic acid 2-phosphate (Sigma), 50 μg/mL L-ascorbic acid (Sigma) and 10 mM β-glycerophosphate (Sigma).

6. 2.3 Histological processing

1. Fixation and embedding

At the end of the 25 day culture period, cultures were fixed with 2% paraformaldehyde in PBS at 4^0 C overnight. Intact tissues were peeled off from the culture well, dehydrated with an increasing series of ethanol concentrations, and embedded in paraffin maintaining an orientation, that yielded cross-sections of each tissue in order to locate the top and bottom of each culture (Figure 6-2).

2. H & E staining

An overall histological assessment of each culture was determined by H&E staining. It was done by the histology lab in Biomedical Engineering Department in Cleveland Clinic. Specifically, three slices were de-paraffinized subsequently rinsed in running tap water for 5 minutes to re-hydrate, then stained in Haematoxylin for 20-30 seconds, rinsed in the running tap water until stain dissipated. To remove excess stain, the slices were treated with 1% ammonium hydroxide for 10 seconds. This step was repeated to remove excess bluing reagent. Then the slices were stained with Alcoholic Eosin for 1 minute and the dehydration begin immediately by dipping sequentially for 10 seconds in each of Ethanol

70%, 70%, 95%, 95%, Absolute Ethanol, Absolute Ethanol, Xylene, Xylene. Then the slices were mounted in Cytoseal-XL, dried and stored in dust-free box until evaluated.

3. BSP and SPARC Staining

The presence of extracellular proteins BSP and SPARC in the cell and matrix layer of each culture was determined with immunohistochemistry. Antibodies specific for BSP (LF-100) and SPARC (Bon-1) were kindly provided by Dr. Larry Fisher [N. I. D. C. R, NIH]. Three slides were deparaffinized and re-hydrated for 15 min with 50 mM Tris-HCL buffer solution containing 150 mM sodium chloride (NaCl) (pH=7.5) (TBS), and then incubated with 5% ovalbumin in TBS for 1 hr at room temperature to reduce non-specific antibody binding. After ovalbumin blocking, the slides were incubated with primary antibody solution in TBS with 0.1% ovalbumin (1:200 dilution) (LF100 or Bon-1) for overnight at 4 $^{\circ}$C. After primary antibody exposure, the slides were washed with TBS three times for 10 min each time, and then incubated with Alexa-Fluor 488 (Invitrogen) anti-rabbit secondary antibody solution in TBS with 0.1% ovalbumin (1:200 dilution) at room temperature for 2 hours. Following secondary antibody treatment, the slides were washed with TBS, 3 times for 10 min each time then stained with alizarin red. The serial section for each test section was only incubated with secondary antibody and stained under the same conditions as a control to determine secondary antibody non-specific binding level (negative control).

4. Alizarin Red –S Staining

95

Calcium mineral location in the culture sections was determined with alizarin red S (ARS) staining. After BSP / SPARC staining, the slides were incubated with 0.4 mM alizarin red S (Sigma) in milli-Q water solution (pH 4.52) for 10 min at room temperature and then washed with TBS for 10 min. Slides were then ready for DAPI staining. A serial section was decalcified with 10% trichloroacetic (Sigma, TCA) at 4 $^{\circ}$C for 30 min and stained with alizarin red S under same conditions. This section was set as alizarin red S stain negative control image to determine the non-specific binding level of ARS to collagen gel.

<u>5. DAPI staining</u>

Both ARS and SPARC or BSP stained sections were counter stained with DAPI for cell nuclei identifying. The slides were incubated with 5 μg/mL DAPI in TBS solution for 20 min at room temperature and washed with PBS solution 10 min each for 5 times. Vectashield Mounting Medium (Vector Labs, H-1000) was added to each slide and a glass coverslip was placed over each specimen and sealed with clear nail polish.

6.2.4 Image acquisition

Light or epi-fluorescent images of the samples were obtained using a Leica RXA2 upright wide –field microscope outfitted with a Spot-RT cooled-CCD camera. A total of 25-30 40 X field of view images (each 1520 x 1080 pixels) were imaged per slide. All together, these images constituted ~ 70% of the total area of each tissue section thus providing an accurate representation.

6.2.5 Image Analysis

Nuclei morphology (aspect ratio), SPARC and BSP positive stained areas, as well as alizarin red S (ARS) stained area were analyzed using commercially available image processing software (ImagePro Plus Version 6.2, Media Cybernetics, MA); since this method can enable us to generate both the amounts and distribution of cell nuclei density, extracellular matrix and mineral deposition. Briefly DAPI and Alizarin red S (ARS) images were uploaded into Image-Pro plus 6.2. Then a top boundary was set for both DAPI and ARS images as follows: (1) select ARS image, (2) apply large-spectral filter to equalize grayscales in all images, (3) apply a median filter to remove background noise, (4) segment image to generate a binary mask, (5) apply same process on DAPI image, (6) converge ARS and DAPI masks together, (7) fill in any discontinuous area with a morphological " closing" operation , (8) apply a boundary search algorithm that proceeds along the width of the image looking for top-most pixel with a value >0. After setting the initial boundary conditions, apply area threshold to get a DAPI mask for each DAPI image (The area threshold is set as 5 mm^2, which is based on the apoptotic body size), apply the intensity threshold to get a ARS mask for each ARS image (the intensity threshold is set as the highest intensity of decalcified control slide image). Then input the cell layer thickness (here set as 5 μm based on the average nuclei length) to generate a layer mask. Apply this layer mask to each segmented mask (DAPI, ARS) to calculate nuclear morphometrics (length, width, area, aspect ratio,and orientation) and the total positive staining area within the layer. Repeat applying the layer mask on the segmented mask until the end of the image. Finally, all data are exported to excel spreadsheet with
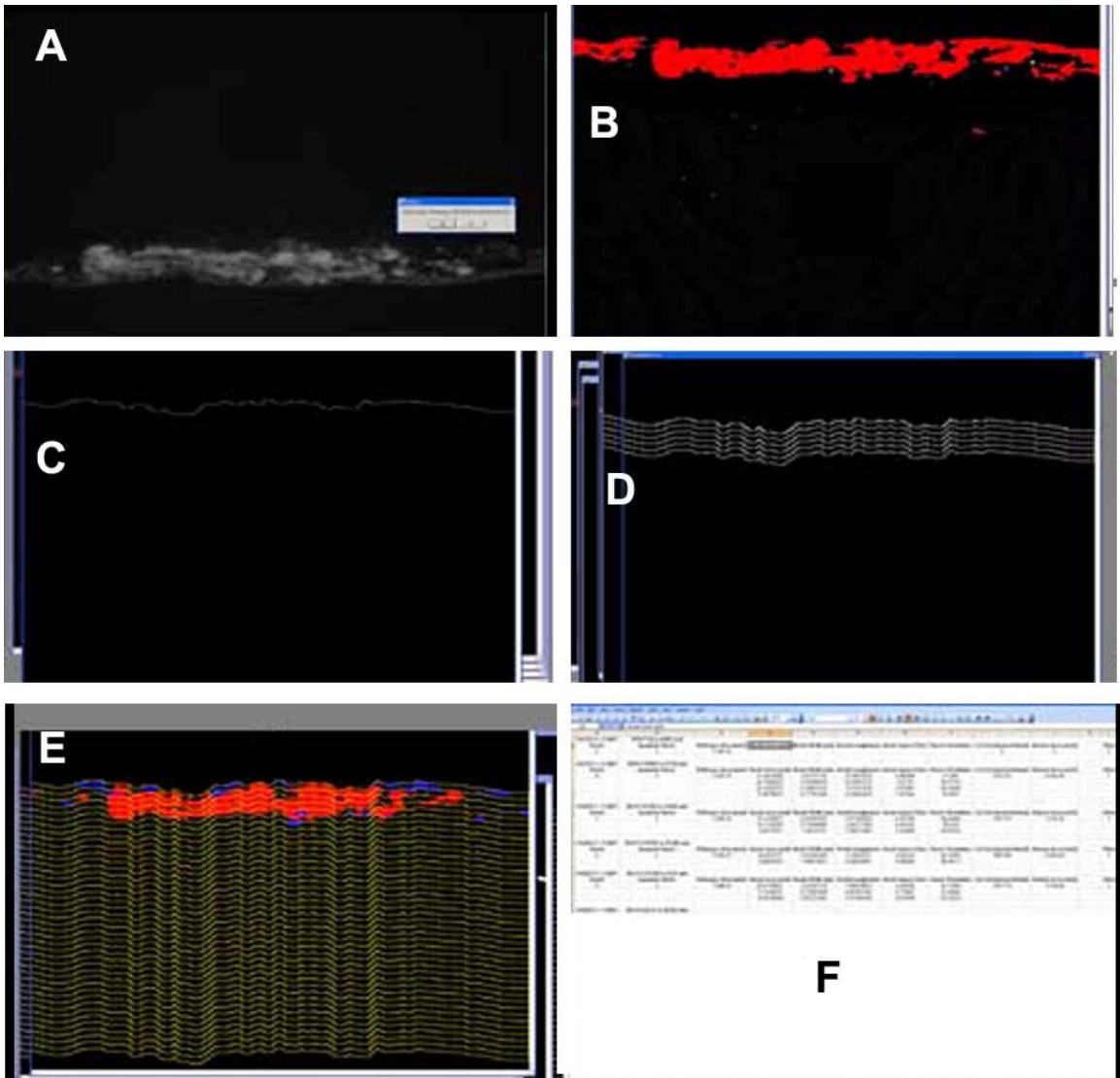
Figure 6-3 Images process. A: original image B: make a mask of image C: set the boundary of the tissue, D: set the layer thickness (5 mm) and continue applying layer mask on the image, E: finish process, F: export the excel sheet

nuclei number, aspect ratio, apoptotic body number, ARS area, layer area and cell density. As for SPARC and BSP images, the similar process was applied except that the intensity threshold set for these images was the highest intensity of the control image and 10% value of the highest intensity of these images (Figure 6-3).

6.2.6 Statistical analysis

Analysis of variance (ANOVA) techniques with mean comparison with turkey test were used for statistical analysis (Sigma-Stat software v3.5). Significance was set as a P value less than 0.05.

6.3 Results

6.3.1 Osteogenesis of bone marrow and periosteum derived cells

1. H&E staining of bone marrow and periosteum cultures on 2D plastic and 3D hydrogel

H&E staining was used to make gross visual observations regarding cells and extracellular matrix accumulation for 2D plastic and 3D hydrogel cell cultures. Comparing the cultures of bone marrow and periosteum cells on both 2D plastic (top of Figure 6-4 and Figure 6-5) and 3D hydrogel (bottom of 6-4 and 6-5), these two cells showed considerable similarity to each other within the same culture modality (2D VS 3D). Comparing the same cell types across different culture modality, both cell types on both 2D plastic and 3D hydrogels, had multiple cell layers (3~4); their nuclear shape was elongated; their cell / matrix layer thickness was around 15~20 μm; and there appeared to be some extracellular matrix substance surrounding the cells. Differences were noted when comparing cultures on 2D plastic versus similar cultures on 3D collagen-fibronectin hydrogels: 3D cultures exhibited a more intense staining, and had contained a few migrated cells in the underlying gel (Asterisks in Figure 6-4, 6-5).
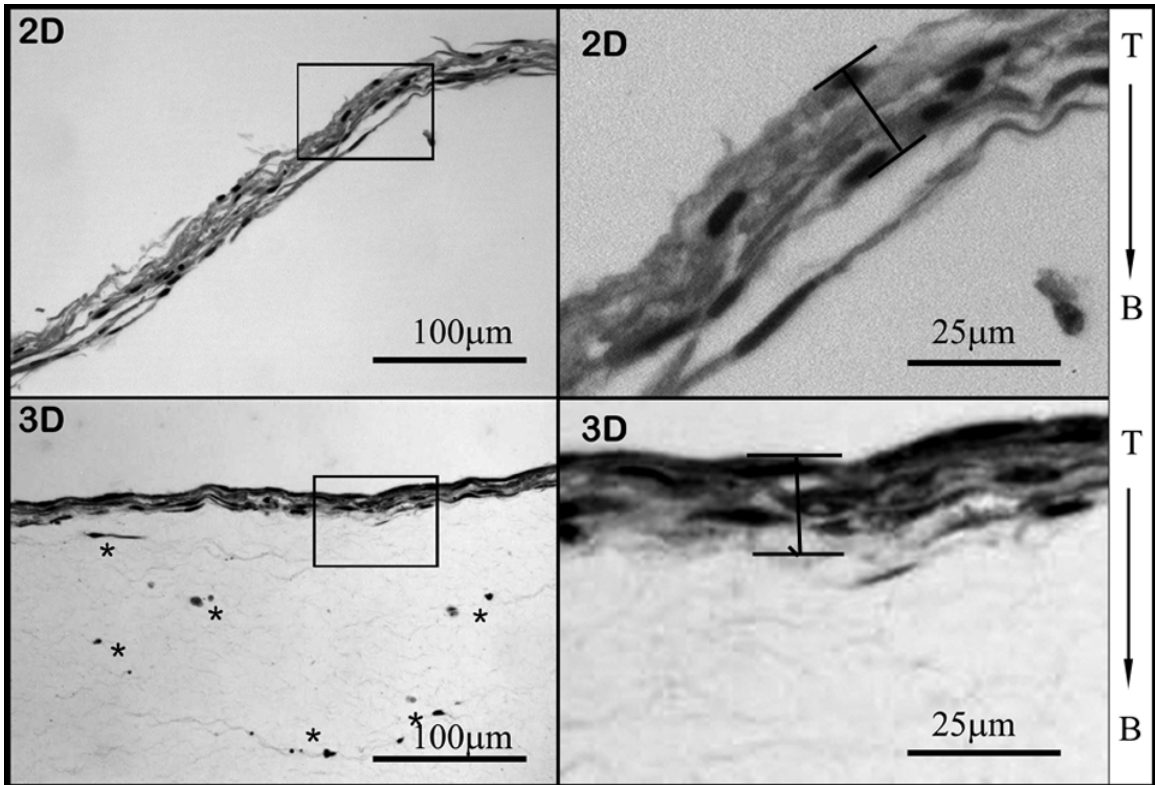
Figure 6-4 Representative images of H&E staining of bone marrow cultures on 2D plastic VS 3D control. T: top of the culture, B: bottom of the culture, Asterisks : point to migrating cells. For both cultures, the bottom refer to the plastic wall of the plate. Bars indicate linear measures used to determine the thickness of major cell/matrix layer.
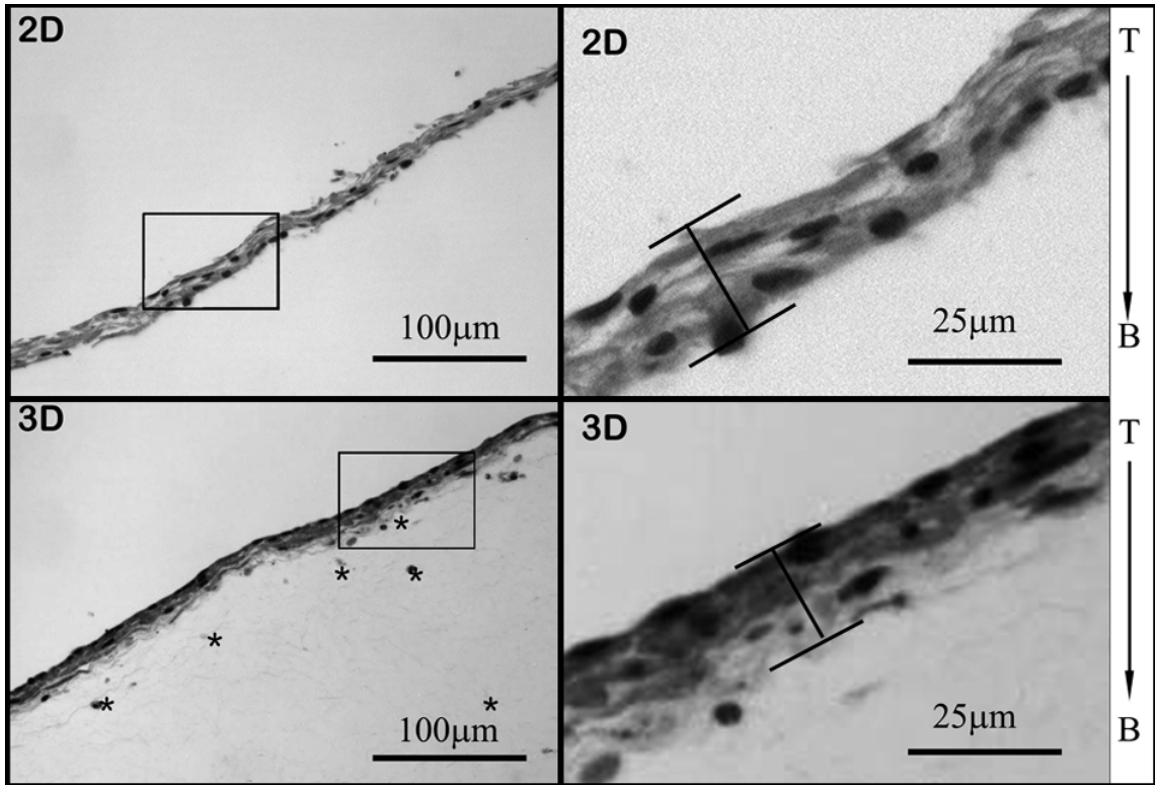
Figure 6-5 Representative images of H&E staining of periosteum cultures on 2D plastic VS 3D control. T: top of the culture, B: bottom of the culture, Asterisks : point to migrating cells. For both cultures, the bottom refer to the plastic wall of the plate. Bars indicate linear measures used to determine the thickness of major cell/matrix layer.

2. Quality of immuno-histochemical staining of BSP and SPARC and chemical staining of minerals of calcium bone marrow and periosteum cells on 2D plastic and 3D hydrogels.

Representative images of DAPI, SPARC and ARS staining of bone marrow cells and periosteum cells in differentiation medium are shown in Figure 6-6 through 6-9. These two cell type showed roughly similar staining patterns on both 2D plastic and 3D hydrogel. When comparing the cultures on 2D plastics versus 3D hydrogels, both cell types had multiple cell layers, and had positive staining areas of SPARC and ARS. Some

differences were noted regarding a little bit more positive SPARC and ARS stained areas on 3D hydrogel than on 2D plastic.

Representative images of DAPI, BSP and ARS staining of bone marrow cells and periosteum cells in differentiation medium are shown in Figure 6-10 through 6-13. Again these two cells showed roughly similar staining patterns on both 2D plastics and 3D hydrogels. When comparing the cultures on 2D plastics and 3D hydrogels, both cell types had multiple cell layers and positive staining area for BSP and ARS. As observed for SPARC staining there seemed to be a little more positive BSP and ARS stained area on 3D hydrogels than on 2D plastics.
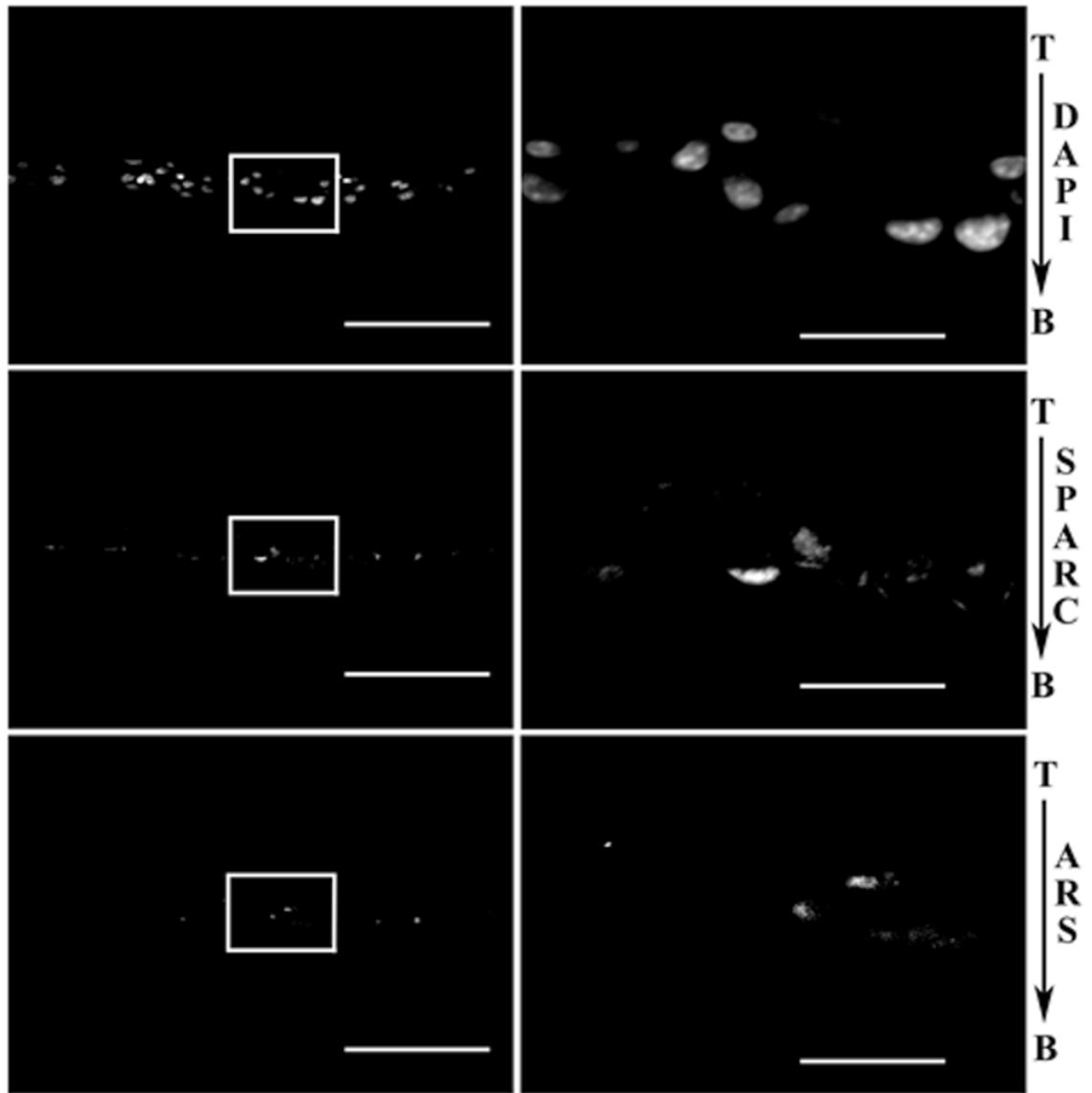
2D Bone Marrow

Figure 6-6 Representative images of SPARC and ARS staining of bone marrow cells cultures on 2D plastic in differentiated medium. T: top of the culture, B: bottom of the culture. Scale bar: 50 μm and 10 μm in low and high magnification images respectively. Low magnification images are in the left column of each group images. High magnification images are in the right column of each group images.
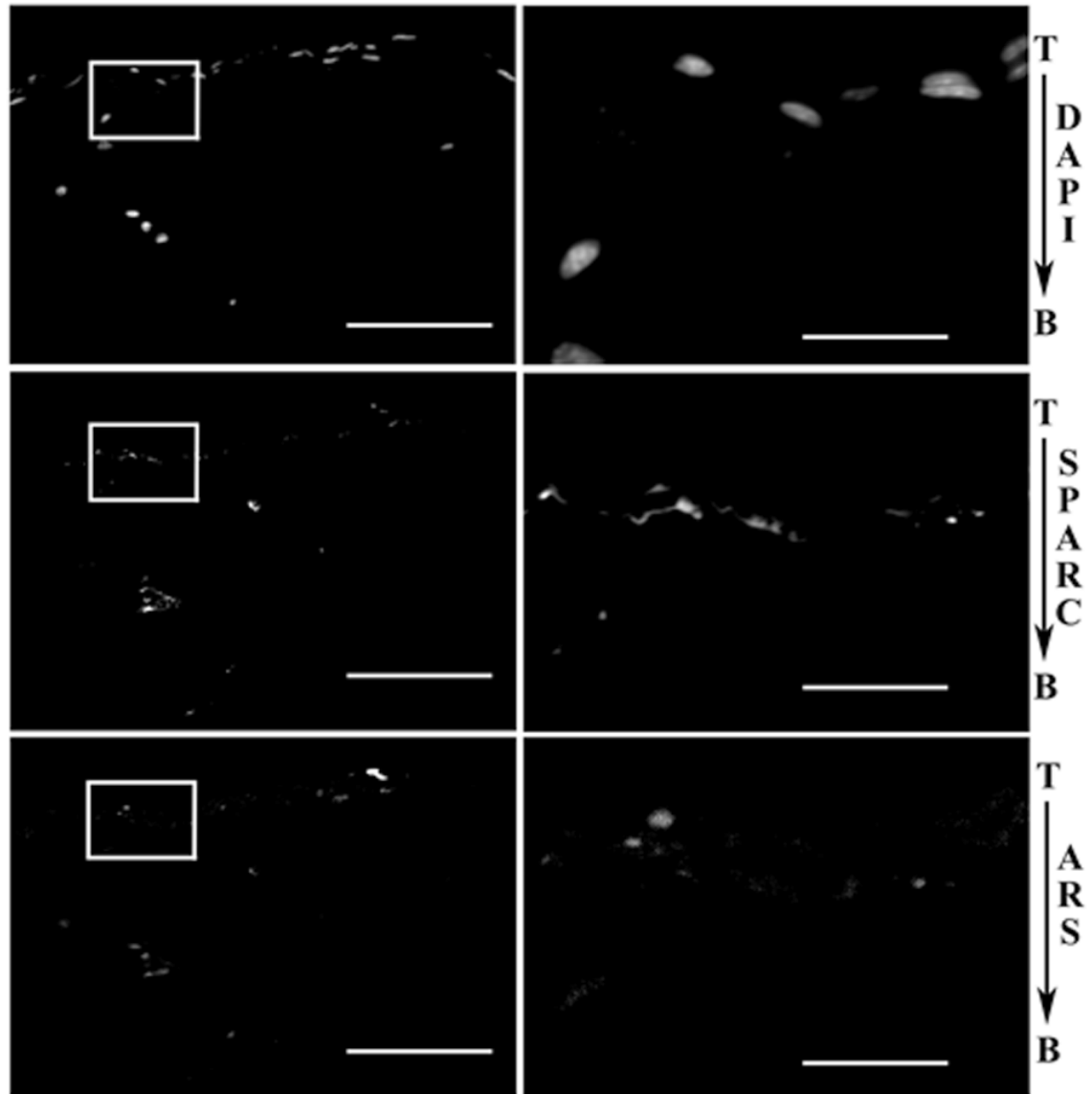
3D Bone Marrow

Figure 6-7 Representative images of SPARC and ARS staining of bone marrow cells cultures on 3D hydrogels in differentiation medium. T: top of the culture, B: bottom of the culture. Scale bar: 50 μm and 10 μm in low and high magnification images respectively. Low magnification images are in the left column of each group images. High magnification images are in the right column of each group images.

Figure 6-8 Representative images of SPARC and ARS staining of periosteum cells cultures on 2D plastic in differentiated medium. T: top of the culture, B: bottom of the culture. Scale bar: 50 μm and 10 μm in low and high magnification images respectively. Low magnification images are in the left column of each group images. High magnification images are in the right column of each group images.
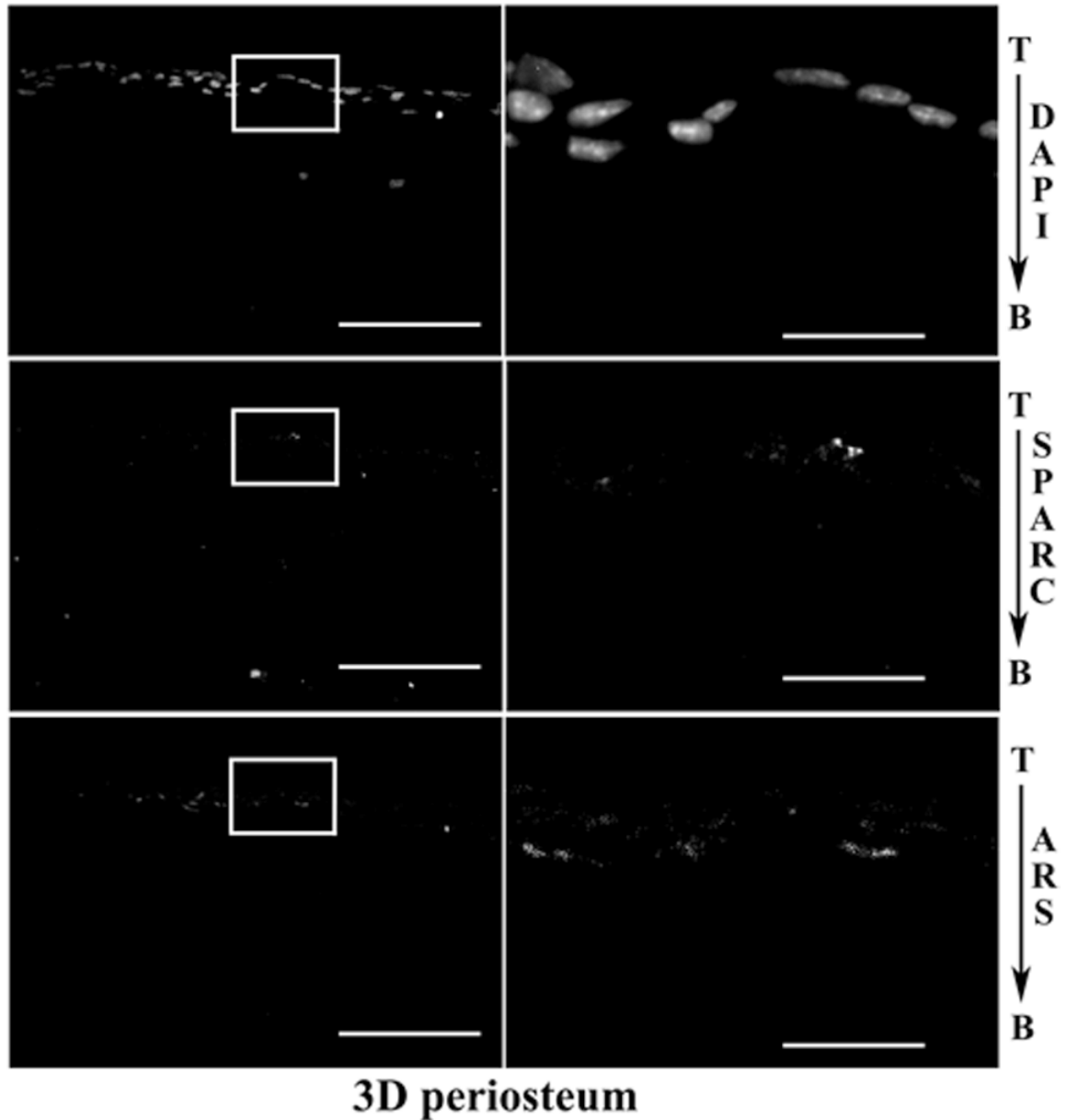
Figure 6-9 Representative images of SPARC and ARS staining of periosteum cells cultures on 3D hydrogel. T: top of the culture, B: bottom of the culture. Scale bar: 50 μm and 10 μm in low and high magnification images respectively. Low magnification images are in the left column of each group images. High magnification images are in the right column of each group images.
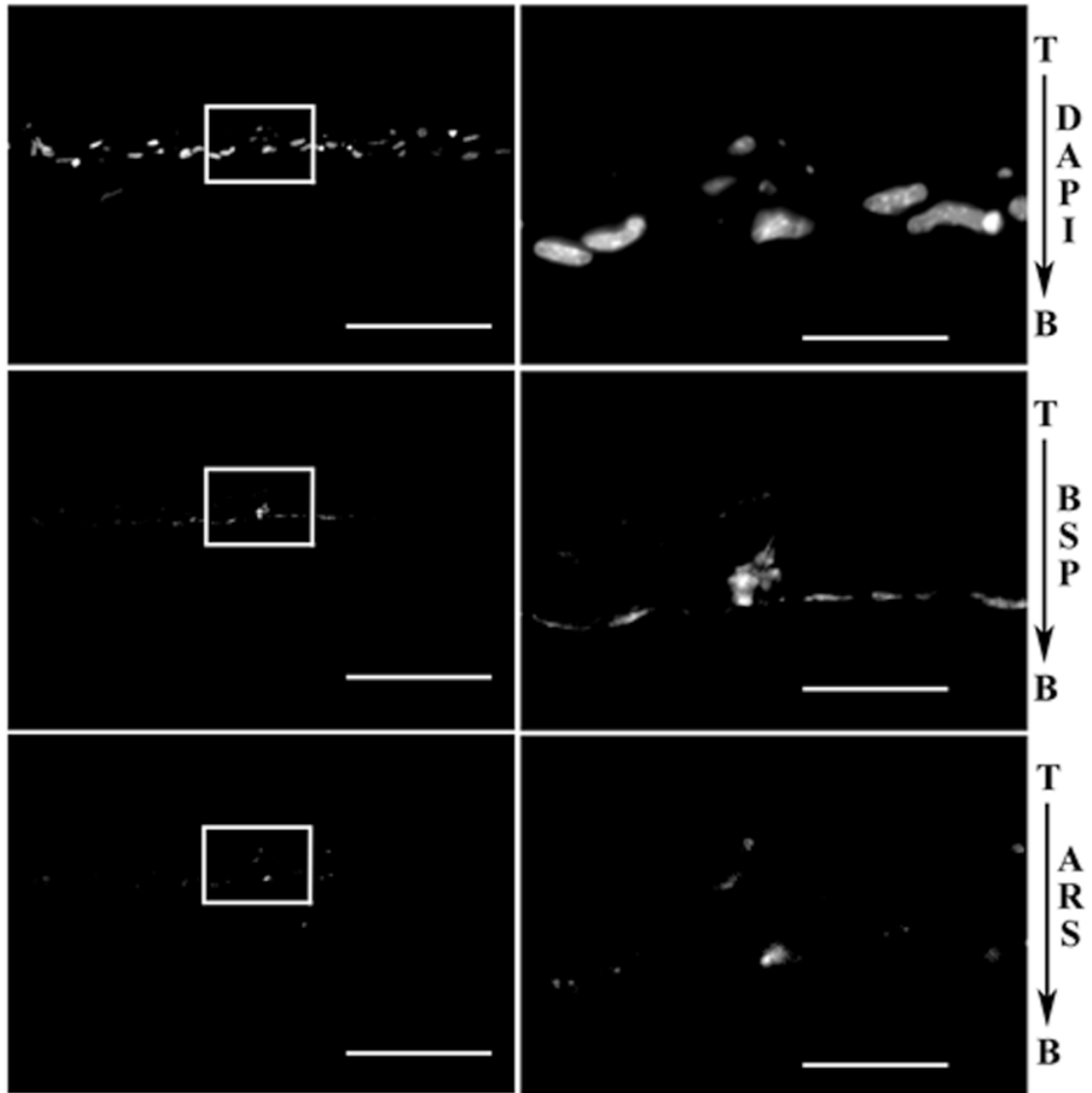
2D Bone Marrow

Figure 6-10 Representative images of BSP and ARS staining of bone marrow cells cultures on 2D plastic in differentiated medium. T: top of the culture, B: bottom of the culture. Scale bar: 50 μm and 10 μm in low and high magnification images respectively. Low magnification images are in the left column of each group images. High magnification images are in the right column of each group images.
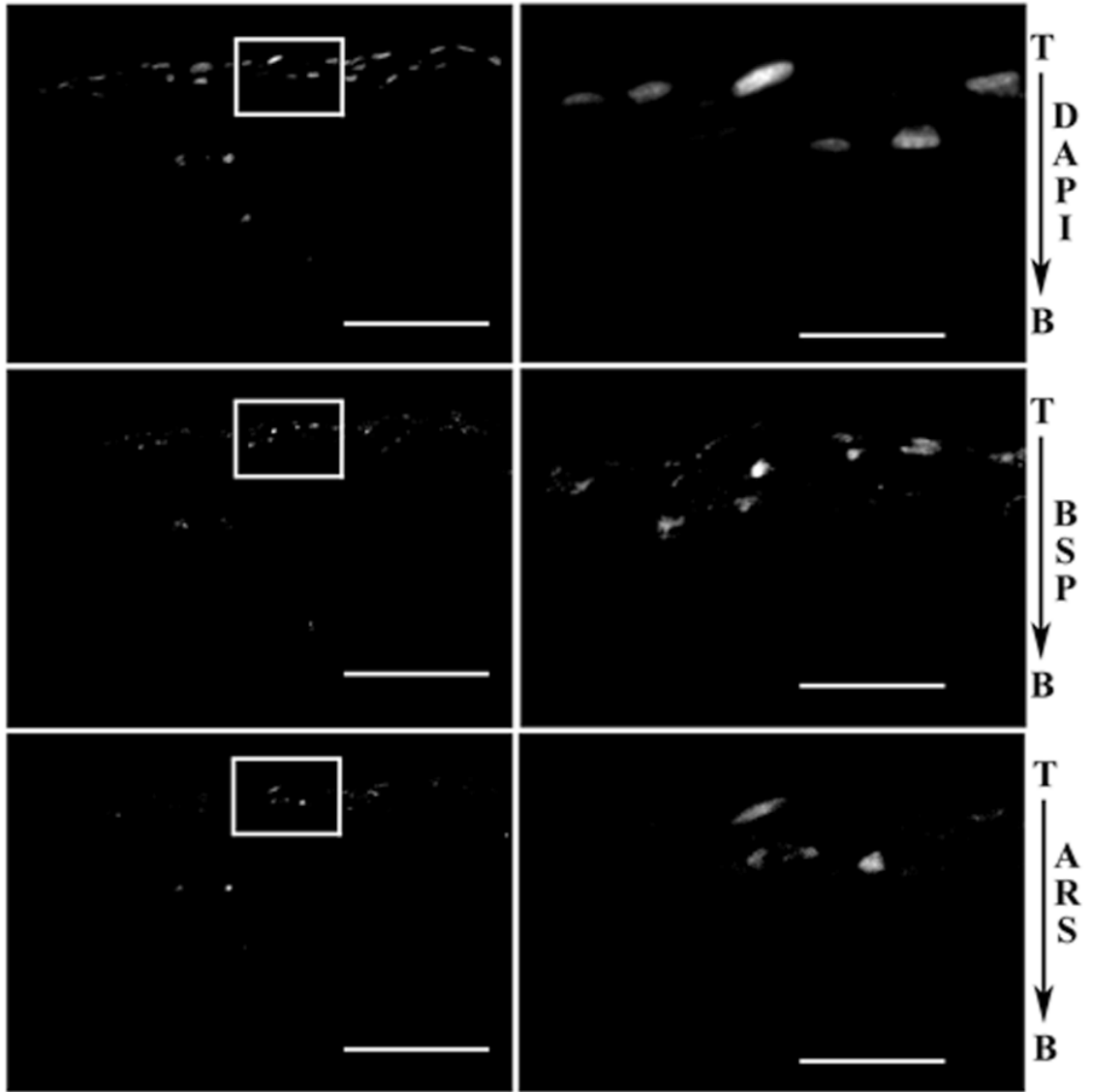
3D Bone Marrow

Figure 6-11 Representative images of BSP and ARS staining of bone marrow cells cultures on 3D hydrogel in differentiation medium. T: top of the culture, B: bottom of the culture. Scale bar: 50 μm and 10 μm in low and high magnification images respectively. Low magnification images are in the left column of each group images. High magnification images are in the right column of each group images.
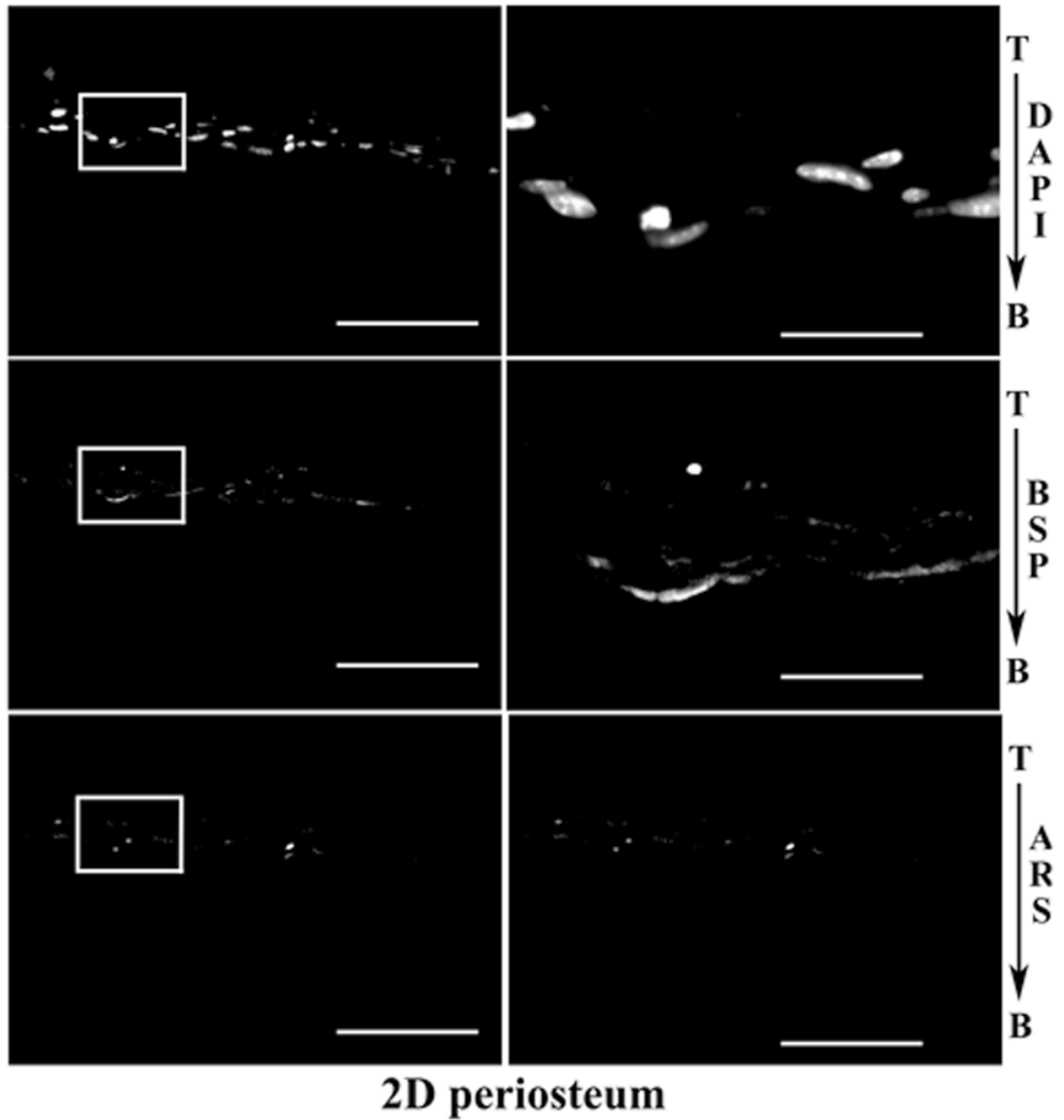
2D periosteum

Figure 6-12 Representative images of BSP and ARS staining of periosteum cells cultures on 2D plastic in differentiated medium. T: top of the culture, B: bottom of the culture. Scale bar: 50 μm and 10 μm in low and high magnification images respectively. Low magnification images are in the left column of each group images. High magnification images are in the right column of each group images.
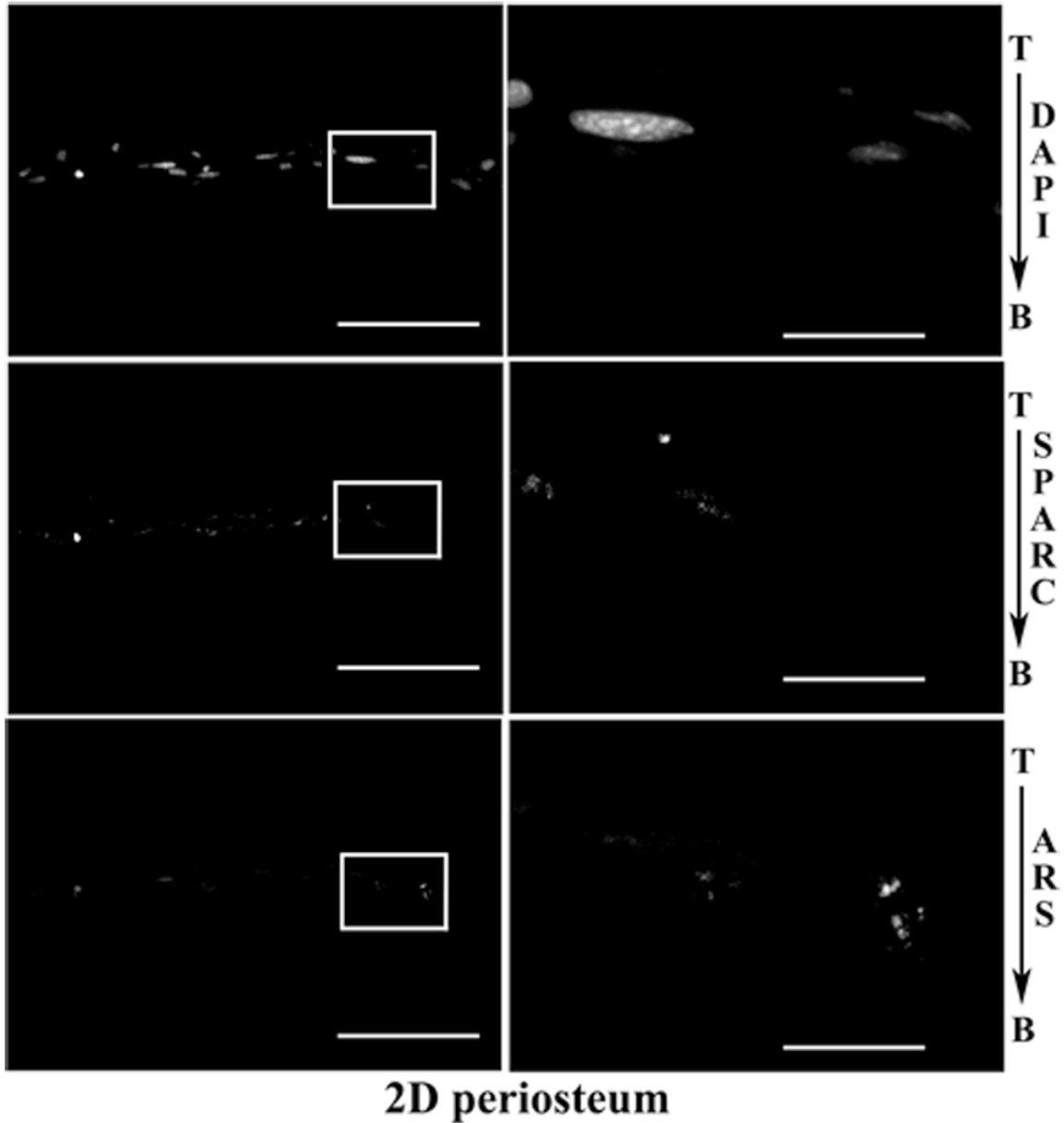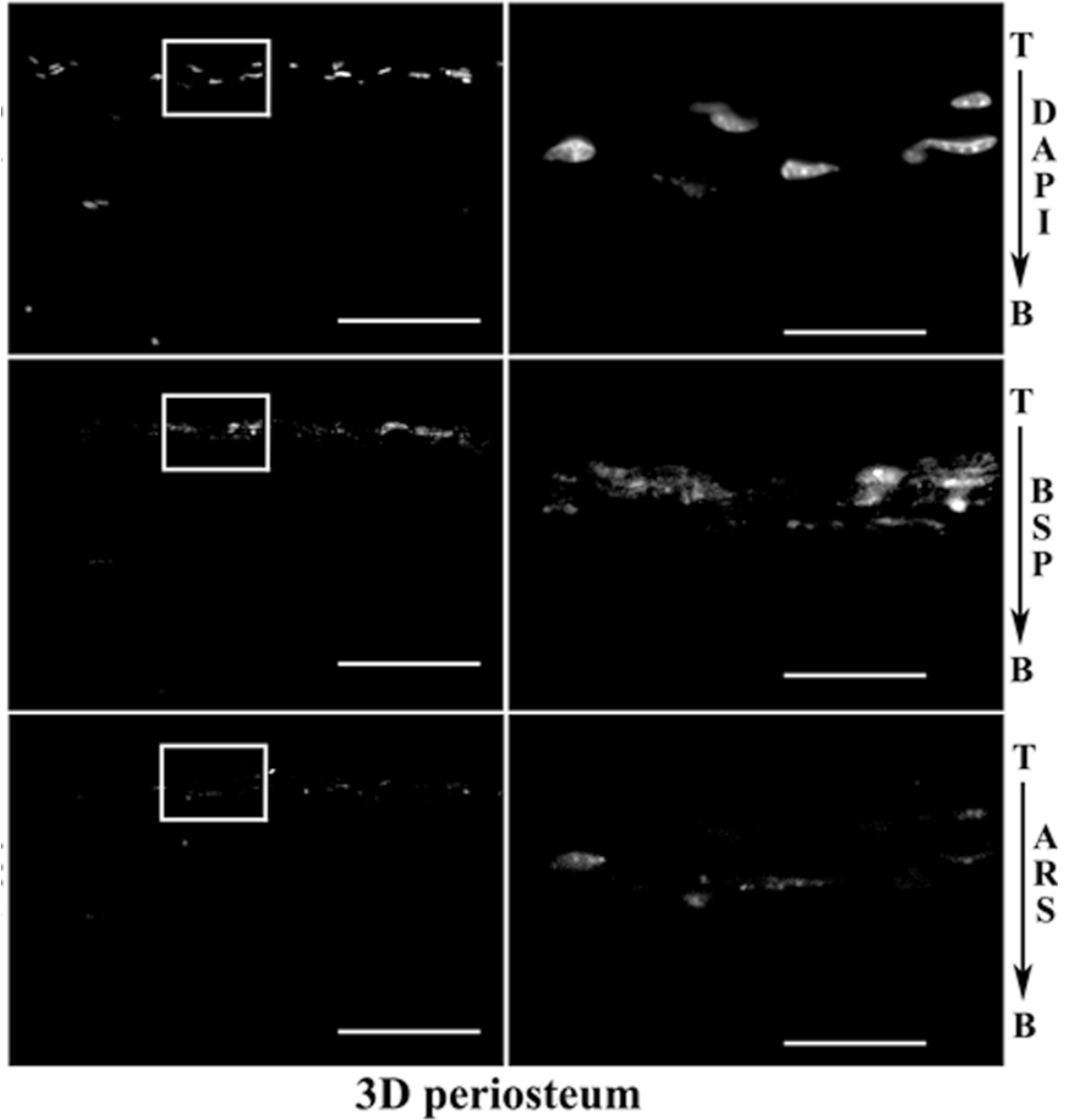
Figure 6-13 Representative images of BSP and ARS staining of periosteum cells cultures on 3D hydrogel in differentiation medium. T: top of the culture, B: bottom of the culture. Scale bar: 50 μm and 10 μm in low and high magnification images respectively. Low magnification images are in the left column of each group images. High magnification images are in the right column of each group images.

3. Quantity of cell density, extracellular matrix and calcium mineral of bone marrow and periosteum cell cultures on 2D plastic and 3D hydrogels.

To quantify cell density, immuno-histochemical staining of SPARC or BSP, chemical staining of calcium mineral and nuclei morphology of bone marrow and periosteum cell cultures on 2D plastic and 3D hydrogels, the top 5 layers were selected as main area of interest since the total cell layer thicknesses on both 2D plastic and 3D hydrogel were no more than 25 µm thick (Figure 6-4, 6-5), which would calculate to 5 layers, each of 5 µm thickness. Figure 6-14 and 6-16 show the quantitative results of cell density (Figure 6-14), extracellular matrix (Figure 6-15) and calcium mineral (Figure 6-16) of bone marrow and periosteum cell cultures. Here, the quantity is defined as the average positive stained area (μm^2) per layer per standard image (around 1800 μm^2).

A. Cell density

For each cell type, there were a total of four different culture conditions: growth medium on 2D plastic, differentiation medium on 2D plastic, growth medium on 3D hydrogel and differentiation medium on 3D hydrogel. Comparing the quantity of cell density of the combined eight groups (bone marrow and periosteum) with three way ANOVA with a means comparison using a tukey test (factor one is cell type, factor two is culture medium, factor three is culture modality (2D VS 3D)) (Figure 6-14), none of these three factors (cell type, culture medium and culture modality) is a factor having significant influence on the cell density. Specifically, there was no significant difference

between the cell density of the bone marrow and periosteum cell cultures, no significant difference between the cell density of the cultures with growth medium and differentiation medium, and no significant difference between the cell density of the cultures on 2D plastics and 3D hydrogel (p values in table 6-1).
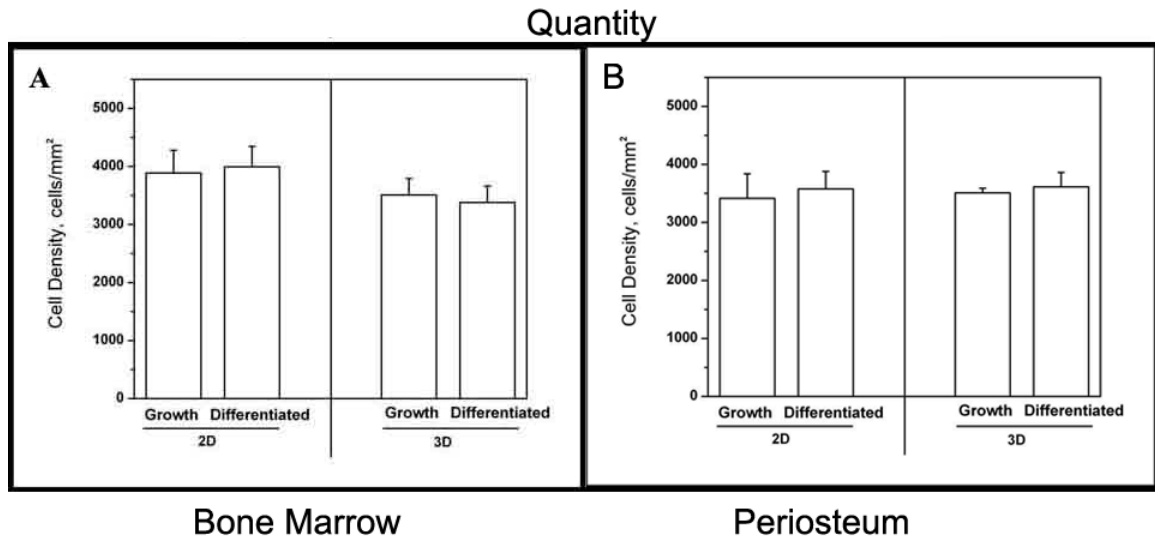
Figure 6-14 The Quantity and distribution of cell density of cells cultures on 2D plastic VS 3D hydrogel.

B. SPARC and BSP

The quantity of immuno-histochemical staining of SPARC in these eight groups was compared with a three way ANOVA with means comparison using a tukey test (factor one is cell type, factor two is culture medium, factor three is culture modality (2D VS 3D)) (Figure 6-15A, Figure 6-15B). Cell type was not a factor having a significant influence on the amount of SPARC staining area. Thus, there was no significant difference found between the SPARC staining areas of the bone marrow vs periosteum cell cultures. Culture medium was found to be a factor having a significant influence on

112

the amount SPARC staining area. Specifically the SPARC staining area in differentiation medium was significantly higher than in growth medium. Culture modality was found to be a factor having a significant influence on the amount of SPARC staining area. Specifically, the SPARC staining area on 3D hydrogels was significantly higher than on 2D plastics (p value in table 6-1).
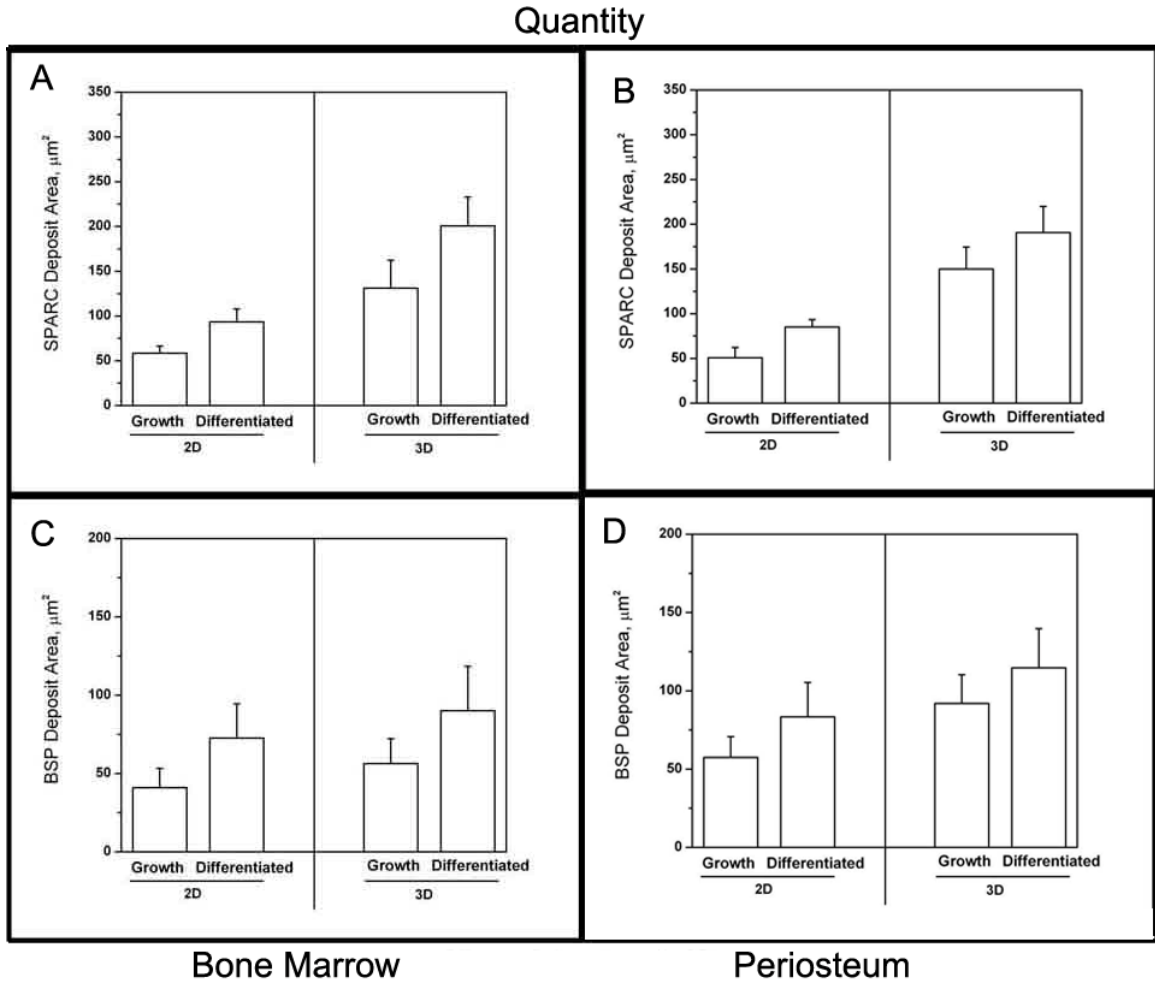
Figure 6-15 The Quantity BSP and SPARC staining area of cells cultures on 2D plastic VS 3D hydrogel.

The quantity of immuno-histochemical staining of BSP in these eight groups was

compared with a three way ANOVA with means comparison using a tukey test (factor one is cell type, factor two is culture medium, factor three is modality (2D VS 3D)) (Figure 6-15C, Figure 6-15D). Cell type was not a factor having a significant influence on the amount of BSP staining area. Thus there was no significant difference found between the BSP staining areas of bone marrow vs periosteum cell cultures. Culture medium was found to be a factor having a significant influence on the amount of BSP staining area. Specifically, BSP staining area in differentiation medium was significantly higher than in growth medium. Culture modality was found to be a factor having significant influence on the BSP staining area. Specifically, the BSP staining area on 3D hydrogels was significantly higher than on 2D plastics (p value in table 6-1).

C. Calcium mineral
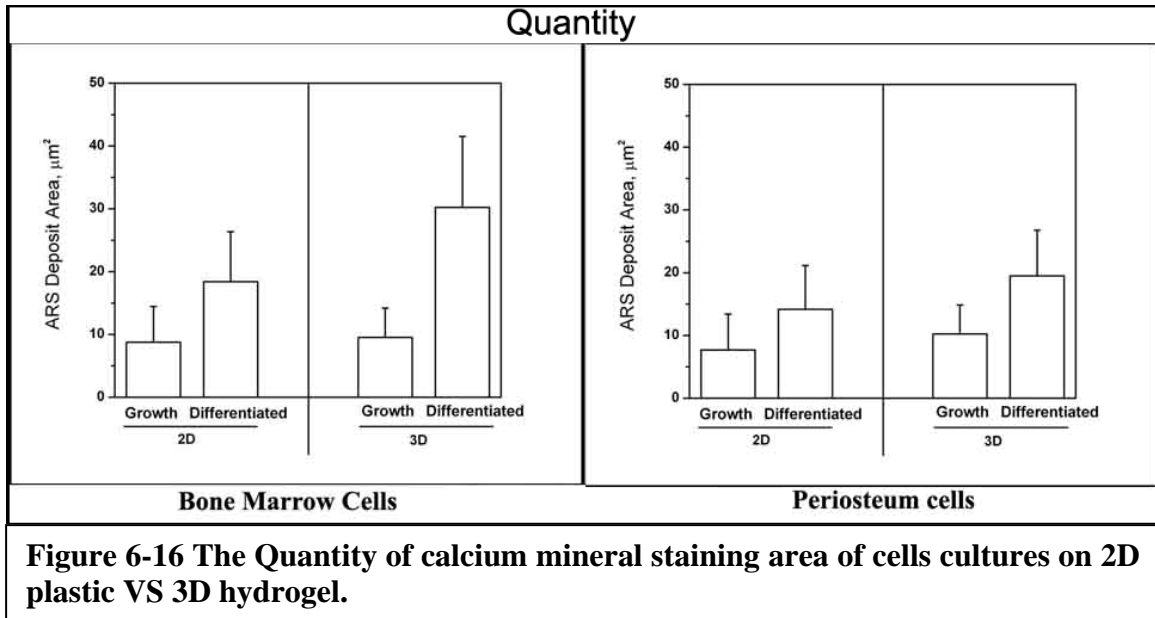
Figure 6-16 The Quantity of calcium mineral staining area of cells cultures on 2D plastic VS 3D hydrogel.

The quantity of calcium mineral staining of these eight groups was compared with a three way ANOVA with means comparison using a tukey test (factor one is cell type,

factor two is culture medium, factor three is culture modality (2D VS 3D)) (Figure 6-16). Cell type was not a factor having significant influence on the mineral staining area. Thus, there was no significant difference between the calcium mineral staining area of bone marrow and periosteum cell cultures. Culture medium was found to be a factor having a significant influence on the amount of calcium mineral staining area. Specifically, calcium mineral staining area in differentiation medium was significantly higher than in growth medium. Culture modality was found to be a factor having a significant influence on the amount of calcium mineral staining area. Specifically, calcium mineral staining area on 3D hydrogels was significantly higher than on 2D plastics (p value in table 6-1).

Factors	Cell density	SPARC	BSP	ARS
Cell type	0.02	0.94	0.29	0.19
Culture medium	0.53	0.008	0.001	0.009
Culture modality	0.03	0.0001	0.0002	0.0001

Table 6-1 p value of quantitative analysis

In all, my results of this part studies showed that for both bone marrow and periosteum there were more SPARC, BSP and mineral staining in the culture on 3D hydrogel than on 2D plastic, which proved my first hypothesis that more extracellular matrix and calcium mineral were deposited in the cultures of both periosteum and bone marrow cells on 3D collagen-fibronectin hydrogel comparing with the culture on 2D conventional tissue plastic.

4. Distribution of cell density, extracellular matrix and calcium mineral of bone marrow and periosteum cell cultures on 2D plastic and 3D hydrogels.
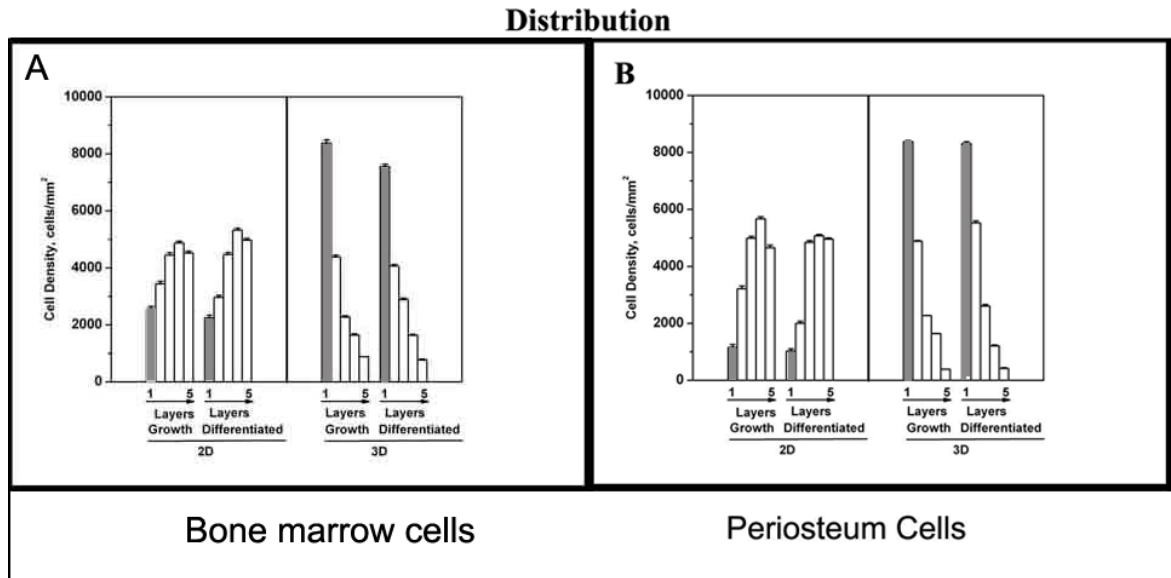
Figure 6-17 The distribution of cell density of cultures on 2D plastic VS 3D hydrogel.

The original distribution of cell density, extracellular matrix and calcium mineral of the cell cultures on 2D plastic vs 3D hydrogel are shown in Figure 6-17 to Figure 6-19. The extracellular matrix and calcium mineral in the first layer can only be deposited by the cells in the first and/or second layers, while in the remaining cell layers they can be deposited by all the layers surrounding them, therefore the first layer is distinguished from all the remaining layers. Thus, percentage of the first layer staining area to the total staining area can be used as a parameter used to compare the distribution pattern of extracellular matrix and calcium mineral on the cultures.

Distribution
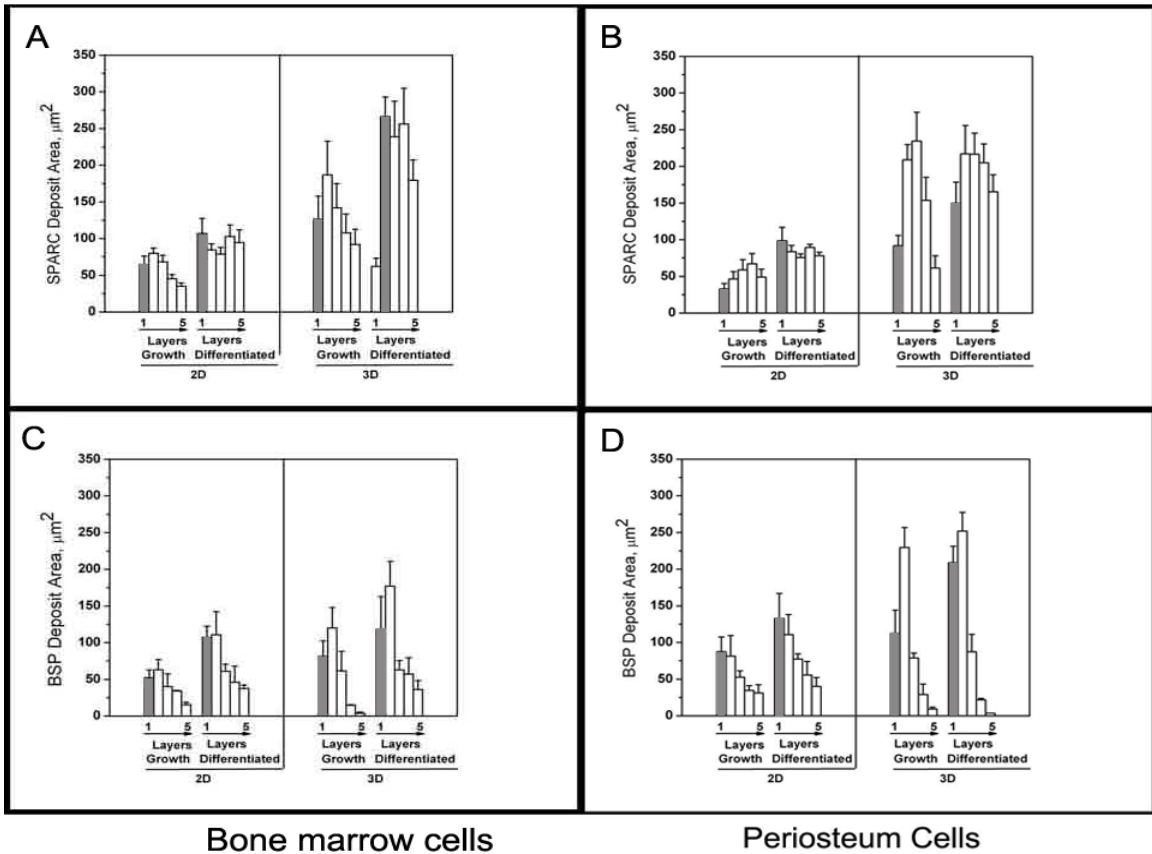
Bone marrow cells

Periosteum Cells

Figure 6-18 The distribution BSP and SPARC staining areas of cells cultures on 2D plastic VS 3D hydrogel.

Distribution
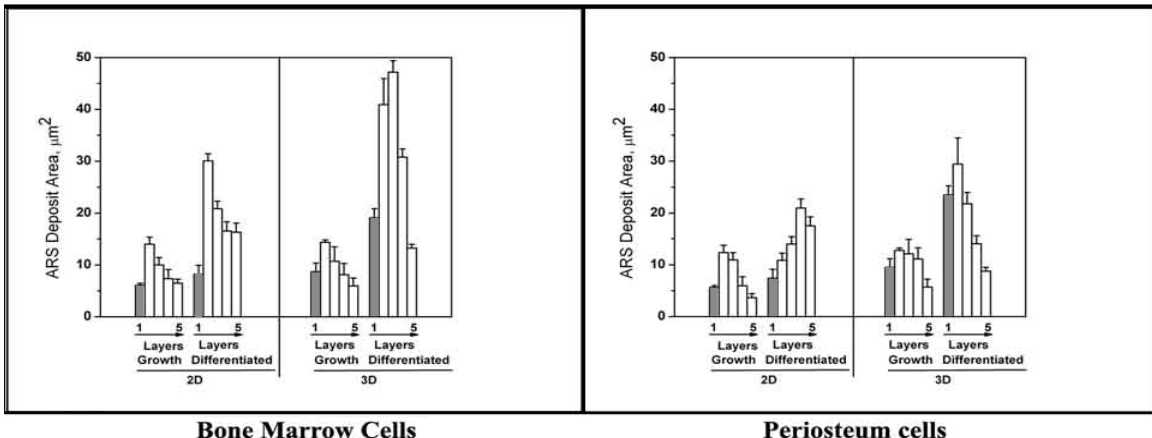
Bone Marrow Cells

Periosteum cells

Figure 6-19 The distribution of calcium mineral staining area of cells cultures on 2D plastic VS 3D hydrogel.

A. Cell density
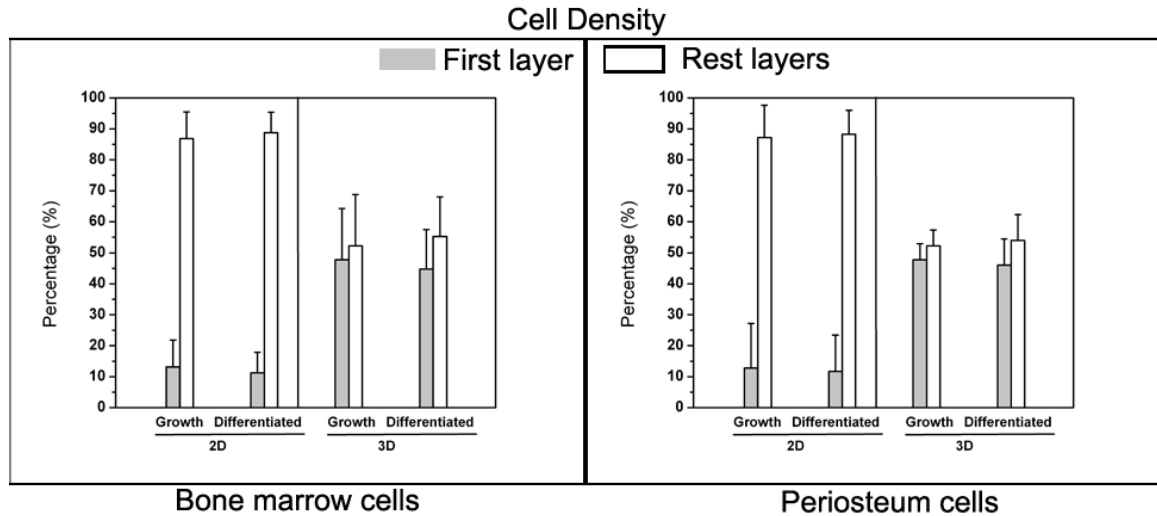
Figure 6-20 The percentage of cell density in first layer VS rest layers.

Comparing the percentage of cell density in first layer of the combined eight groups (bone marrow and periosteum) with three way ANOVA with a means comparison using a tukey test (factor one is cell type, factor two is culture medium, factor three is culture modality (2D VS 3D)) (Figure 6-20), cell types and culture medium were not factors having significant influence on the percentage of cell density in first layer. Specifically, there was no significant difference between the percentage of first layer of the bone marrow and periosteum cell cultures, no significant difference between the percentage of cell density in first layer with growth medium and differentiation medium. Culture modality was found to be a factor having a significant influence on the percentage of cell density. Specifically, the percentage of cell density in first layer on 3D hydrogels was significantly higher than that on 2D plastics (p value in table 6-2). This suggested that the cells density distribution on 3D hydrogel was different from that on 2D plastic.

B. SPARC and BSP

The percentage of immuno-histochemical staining of SPARC in the first layer of these eight group cultures was compared with a three way ANOVA with means comparison using a tukey test (factor one is cell type, factor two is culture medium, factor three is culture modality (2D VS 3D)) (Figure 6-21). None of these three factors (cell type, culture medium and culture modality) was a factor having significant influence on the percentage of immuno-histochemical staining of SPARC in the first layer. Specifically, there was no significant difference between the percentage of immuno-histochemical staining of SPARC in the first layer of the bone marrow and periosteum cell cultures, no significant difference between the percentage of immuno-histochemical staining of SPARC in the first layer of the cultures with growth medium and differentiation medium, and no significant difference between the percentage of immuno-histochemical staining of SPARC in the first layer of the cultures on 2D plastics and 3D hydrogel (p value in table 6-2). In all no difference of SPARC distribution was found between these 8 groups.

The percentage of immuno-histochemical staining of BSP in the first layer of these eight group cultures was compared with a three way ANOVA with means comparison
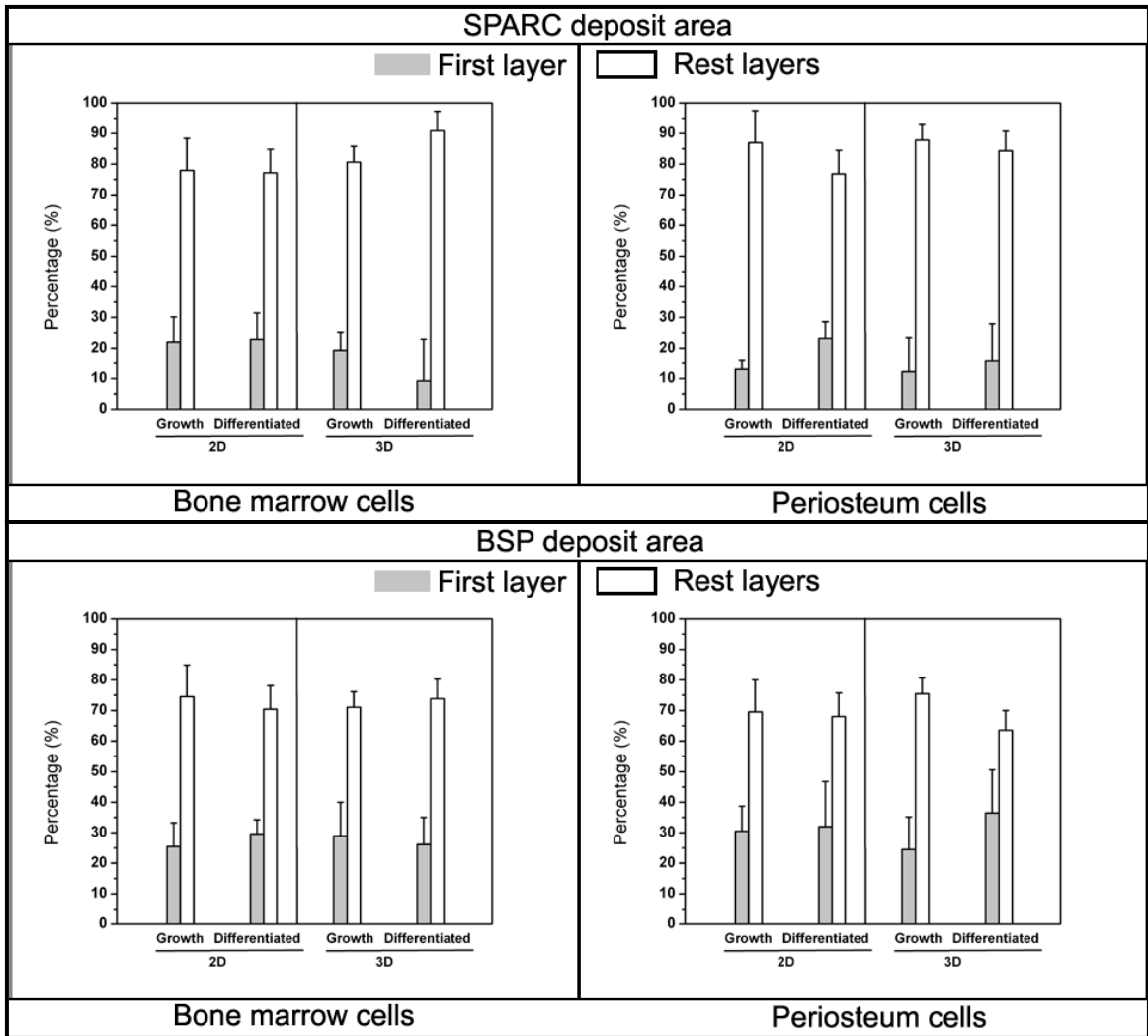
Figure 6-21 The percentage of immuno-histochemical staining SPARC and BSP in first layer VS rest layers.

using a tukey test (factor one is cell type, factor two is culture medium, factor three is culture modality (2D VS 3D)) (Figure 6-21). None of these three factors (cell type, culture medium and culture modality) was a factor having significant influence on the percentage of immuno-histochemical staining of BSP in the first layer. Specifically, there was no significant difference between the percentage of immuno-histochemical staining

of BSP in the first layer of the bone marrow and periosteum cell cultures, no significant difference between the percentage of immuno-histochemical staining of BSP in the first layer of the cultures with growth medium and differentiation medium, and no significant difference between the percentage of immuno-histochemical staining of BSP in the first layer of the cultures on 2D plastics and 3D hydrogel (p value in table 6-2). In all no difference of BSP distribution was found between these 8 groups.

C. Calcium mineral
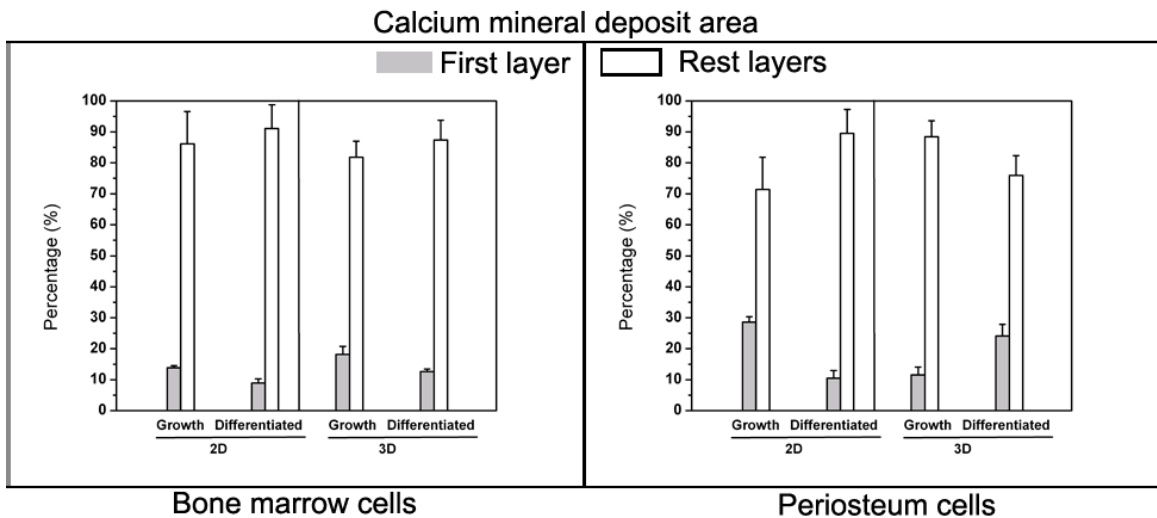
Figure 6-22 The percentage of calcium mineral in first layer VS rest layers

The percentage of chemical staining of calcium mineral in the first layer of these eight group cultures was compared with a three way ANOVA with means comparison using a tukey test (factor one is cell type, factor two is culture medium, factor three is culture modality (2D VS 3D)) (Figure 6-22). None of these three factors (cell type, culture medium and culture modality) was a factor having significant influence on the percentage of chemical staining of calcium mineral in the first layer. Specifically, there

was no significant difference between the percentage of chemical staining of calcium mineral in the first layer of the bone marrow and periosteum cell cultures, no significant difference between the percentage of chemical staining of calcium mineral in the first layer of the cultures with growth medium and differentiation medium, and no significant difference between the percentage of chemical staining of calcium mineral in the first layer of the cultures on 2D plastics and 3D hydrogel (p value in table 6-2). In all no difference of calcium distribution was found between these 8 groups.

Factors	Cell density	SPARC	BSP	ARS
Cell type	0.86	0.36	0.10	0.06
Culture medium	0.35	0.76	0.06	0.09
Culture modality	0.0001	0.06	0.85	0.62

Table 6-2 p value of distribution analysis

In all, my results of this part studies showed that for both bone marrow and periosteum there were no difference between the distribution of SPARC, BSP and mineral staining in the culture on 3D hydrogel with that on 2D plastic; while there was significant difference between the distribution of cell density on 3D hydrogel with that on 2D plastic. This proved partly my second hypothesis that cell density in bone marrow and periosteum 3D collagen fibronectin hydrogel cell cultures will exhibit a basal lateral deposition pattern while not on 2D conventional tissue plastic, while partly rejected my second hypothesis that extracellular matrix protein and mineral deposition in bone

122

marrow and periosteum 3D collagen fibronectin hydrogel cell cultures will exhibit a basal lateral deposition pattern while not on 2D conventional tissue plastic.

6.3.2 Nuclear morphologies of bone marrow and periosteum cells on 2D plastic and 3D hydrogel cultures

As shown in Figure 6-1, *in vivo* periosteum tissue exhibits cells at different osteogenic stage having different morphologies. The quantity of nuclei aspect ratio of these eight groups was compared with three way ANOVA with means comparison using a tukey test (factor one is cell type, factor two is culture medium, factor three is culture
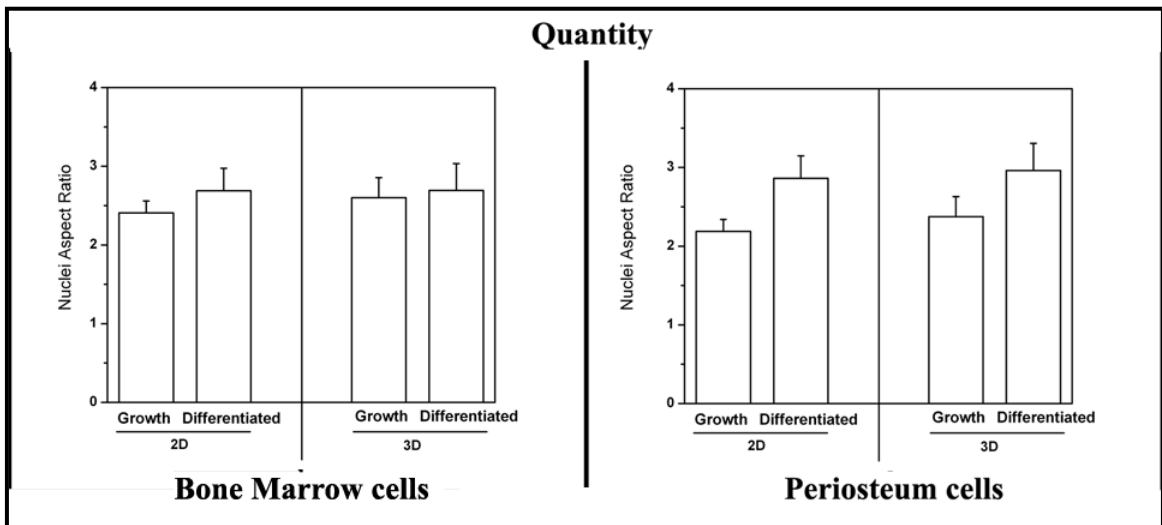
Figure 6-23 The quantity of nuclear aspect ratio of cells cultures on 2D plastic VS 3D hydrogel.

modality (2D VS 3D)) (Figure 6-23), none of these three factors (cell type, culture medium and culture material) was a factor having significant influence on the nuclear aspect ratio. Specifically, there was no significant difference found between the nuclear aspect ratio of the bone marrow and periosteum cell cultures (p = 0.35), no significant difference between the nuclear aspect ratio of the cultures with growth medium and

123

differentiation medium (p = 0.03), and no significant difference between the nuclei aspect ratio of the cultures on 2D plastics and 3D hydrogel (p = 0.11).

The distribution of cell nuclei distribution was shown in Figure 6-24. One way ANOVA was used to compare the aspect ratio of nuclei among all the five layers in each culture to test the hypothesis that cells at different osteogenesis stage have different nuclear morphology. For each culture, the result showed there was no significant difference of the aspect ratio of nuclei among the five layers, which suggest there was no different of nuclei morphology among the five layers in each culture. Therefore, it rejected my third hypothesis that cells at different osteogenesis stage have different nuclear morphology.
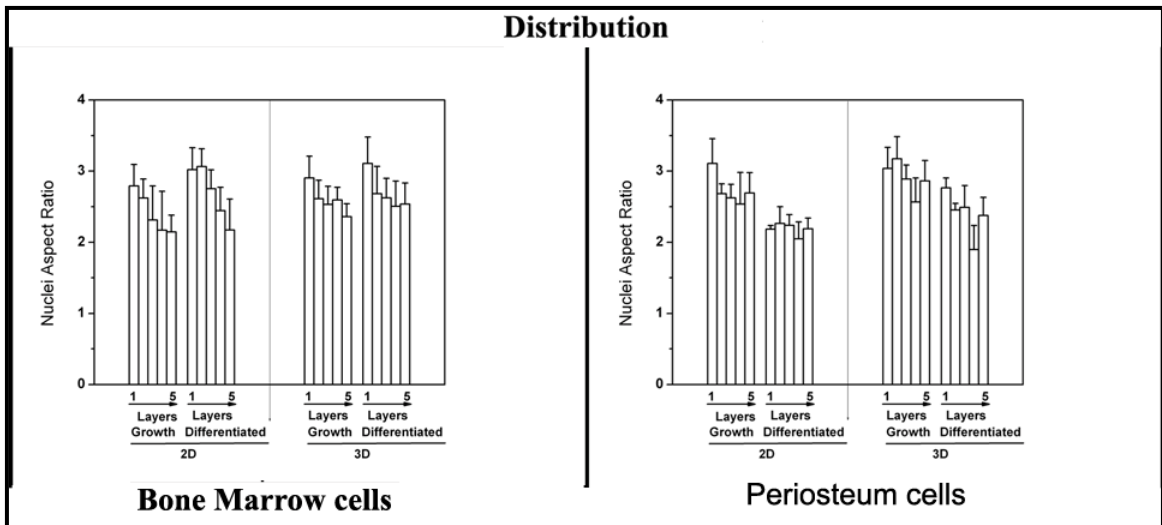
Figure 6-24 The distribution of nuclear aspect ratio of cells cultures on 2D plastic VS 3D hydrogel.

6.3.3 Osteogenesis of bone marrow and periosteum cells

124

All the results from above suggested that cell type was not a factor that has significant influence on the amount and distribution of cell density, SPARC, BSP deposit, calcium mineral deposit and nuclear morphology of the cell cultures. This proved my fourth hypothesis that osteo-progenitors derived from bone marrow and periosteum cells exhibit equivalent osteogenic capacity.

6.4 Discussion

Culture condition is an important component to be considered in my system. *In vivo*, bone formation cells lay on the osteoid layer to form bone (Figure 6-1), which is secreted by osteoblasts and becomes mineralization. Therefore, we propose that the chemicals in this layer and its structure are important for bone formation. To mimic this layer, an artificial osteoid layer was made from type I collagen and fibronectin. And the osteogenesis of primary bone cells cultured on this layer was compared with that on 2D plastic (Chapter VI). My results showed that there was significant increase of extracellular matrix (SPARC, BSP) and calcium mineral deposition in the culture on 3D collagen- fibronectin hydrogel than that on 2D plastic, which suggested that this artifical osteoid layer promoted osteogenesis of primary bone cells. This matches with previous studies showing that collagen [6, 22, 30, 33, 49, 65] and fibronectin [60] promoted osteogenesis of bone cells. Barralet et al. cultured bone marrow cells on type I collagen gels for 21-28 days and showed new osteoid-like tissue formation by these cells [6]. Wiesmann et al. cultured periosteal derived osteoblasts on Petri dishes as well as within 3D collagen constructs. They showed that these cells can form 'bone like' mineral

deposits in both 2- and 3-D environments and formed an extracellular matrix containing osteocalcin, SPARC (osteonectin), and newly synthesized collagen type I in both environments [89]

Moreover, the polarity of cells, extracellular matric and calcium mineral deposition on this 3D collagen fibronectin hydrogel was analyzed. My results showed the polarity of cell density distribution on 3D collagen fibronectin hydrogel and no polarity on the distribution of extracellular matrix and mineral deposition, which may because that overall very small amount extracellular matrix and calcium mineral deposited on 3D collagen fibronectin cultures, which suggest that my end time point is the initial differentiation time point (bone cells starts to deposit extracellular matrix and mineral); and no polarity would be generated at this time point of culture.

Cell source is one key component in bone tissue engineering [39, 66], until now, bone cell sources used in bone tissue engineering have included mesenchymal stem cells derived from bone marrow, perioteum and umbilical et al [5, 6, 13, 29, 30, 33, 39, 42, 51, 76-79, 89], and mature osteoblasts, such as trabecular bone obtained during iliac crest biopsies [60]. Osteo-progenitors derived from bone marrow and periostum are two popular cell types are used in bone tissue engineering. My results that osteo-progenitors derived from bone marrow and periosteum cells exhibit equivalent osteogenesis, which suggested that both cell types are appropriate for the use in this model system.

There were some limitations that should be addressed in future. Studies includes: (1) to investigate the polarity of cell cultures on 3D collagen fibronectin hydrogel, cultures

126

with extended culture time (6 week) will be needed. (2) Multiple experimental time points will be needed to investigate the cell osteogenesis status. (3)The amount of extracellular matrix in the culture medium needs to be measured to have a better comparison between the cultures on 3D collagen fibronectin hydrogel and 2D plastic. (4) The markers of cell osteogensis stage (e.g. alkaline phosphatase (osteoblast cells), E11 (pre-osteocyte) [9, 66]) will be stained on the serial slides of the culture to determine whether cells in the culture are at different osteogenesis stage. (5) F-actin [54] needs to be stained to determine the morphology of cells which enable us to investigate the relationship between cell morphology and cell osteogenesis status.

In all, the results in this Chapter indicate that bone marrow and periosteum cells exhibit similar osteogenesis on both 2D plastic and 3D hydrolgel, and that the 3D collagen-fibronectin hydrogel promoted osteoblasts osteogenesis. Applying this knowledge to our prospective bone tissue engineerin3D bioreactor system, we propose to use 3D collagen-fibronectin hydrogel as interface between cells and scaffolds to promote osteoblasts osteogenesis, and to use either bone marrow or periosteum cells as the cell source.

CHAPTER VII

DISCUSSIONS AND CONCLUSIONS

Large-sized bone defects and recalcitrant fractures require surgical intervention with grafting materials to provide the best potential for healing [1, 4]. Around 10 billion dollars in United States and 24 billion dollars worldwide are expended annually to treat large-sized cortical bone damage with graft materials, such as autografts, allografts and synthetic grafts [4, 39, 69]. However, even these graft materials have limitations and may seem unsuitable for some clinical needs. Cortical bone tissue engineering provides a promising approach to generate new graft materials that may satisfy these clinical needs [39, 66]. Yet, cortical bone tissue has not been produced *in vitro* to date using engineering approaches. In order to generate ample amounts of cortical bone with a tissue engineering approach, three key aspects need to be considered: 1) an optimal osteogenic cell source needs to be identified, 2) biocompatible scaffold materials with similar

128

mechanical and permeability properties as cortical bone needs to be identified thereby providing immediate functional bone capacity, and 3) optimal culture conditions (such as collagen scaffold)need to be identified that will promote osteogenesis of bone cells [66].

In this dissertation work I set out to develop a cortical bone tissue engineering system that would mimic the three cortical bone layers to promote functional cortical bone formation *in vitro*. Specifically, the tissue engineering bone model system proposed (Figure 2-2) would be composed of a biocompatible scaffold with similar mechanical strength and permeability as cortical bone; an artificial osteoid layer made of type I collagen and fibronectin in hydrogel format to mimic the osteoid layer and osteogenic bone cells mimic the bone cell layer. We expect a functional bone tissue can be generated from this system in the future. To set up this bone model system these three components need to be tested and selected.

7.1 Characterization of Scaffold material

Different biomaterials have been used in bone tissue engineering. They include metals (such as cobalt-chromium alloys, stainless steel and titanium), synthetic polymers (such as PMMA), ceramics, natural collagens and their bio-composites [39, 66, 95]. Among all these materials, some match the mechanical property (such as ceramics and metals), some match the permeability property (such as porous metals, porous polymer and porous ceramics), and some exhibit appropriate biocompatibility [66]. PMMA and 316L stainless steel were tested as candidate scaffolds since they are cost effective, easy to be manufactured into any shape and size needed, and more important have similar pore

size as cortical bone are reported to be biocompatible (Chapter III). To determine whether these two material scaffolds are appropriate for the use in our system, we measured their mechanical and hydraulic permeability properties, as well as their short term and long term- biocompatibility. My results showed that PMMA exhibited roughly similar hydraulic permeability as cortical bone and an appropriate biocompatibility for short term bone cell culture; and that 316L stainless steel exhibited roughly similar ultimate tensile strength and hydraulic permeability as cortical bone and an appropriate biocompatibility for both short term and long term bone cell culture. These biocompatibility results match with previous studies on the biocompatibility of stainless steel and PMMA; such as: Puleo et al. [61] showed that stainless steel exhibits good short term biocompatibility; and Ramachandran et al [71]. showed that osteoblasts exhibited phenotypic stability when cultured on PMMA suggesting that PMMA exhibits adequate biocompatibility. In the other hand, these results disagree with some other studies; such as Jocobs et al.[36] stated that 316 L stainless steel containing chromium (16-18%) and nickel (10-14%) was a probable source of long-term complications, and their findings suggested caution for its use as an implant; Chiu et al. [13] showed that PMMA inhibits the proliferation and osteogenic differentiation of bone marrow cells suggesting that PMMA may not always exhibit high levels of biocompatibility. The difference of the biocompatibility of stainless steel between mine and Jocobs' may come from the difference in the test methods: mine are *in vitro* experiment results while theirs are *in vivo* experiment results. The difference of biocompatibility of PMMA between mine and Chiu's may come from the difference of

the outcomes: mine are the proliferation rate of the cells while theirs are the osteogenesis properties. Therefore, based on my results, these two scaffold materials were appropriate for our system. Our first choice would be 316L stainless steel, and the second choice would be PMMA.

7.2 Hydraulic permeability of cortical bone

One criterion for the selection the scaffold material used in my bone model system is the hydraulic permeability of cortical bone. Because *in vivo* fluid flow is critically important for the nutrient and waste product transport, which is important to maintain osteocyte viability and regulate the physiological processes of bone remodeling and homoestasis [7, 98]. Until now, few studies have experimentally measured the hydraulic permeability of cortical bone in part because of the engineering challenges in measuring extreamly low permeabilities. These devices require high pressure tolerances in both the bone tissue holding chamber and other upstream components of the permeability device in order to accurately measure the permeability of cortical bone. Therefore, the hydraulic permeability of cortical bone and the contribution of bone components to its hydraulic permeability were studied in Chapter IV. My permeability results showed that the permeability of fresh cortical bone from endosteum side was below the detection limit of my device (4×10^{-17}); after removing the lipids from the porous compartment of cortical bone, its permeability was increased around 3 fold; after removing the collagen in the porous compartment of cortical bone, its permeability was increased another 5 fold; after removing the crystal minerals, its permeability was increased another 5 fold. These

results match with Li's study [46]. They reported that the radial permeability of adult canine tibial cortex was 5 x 10^{-17} m^2 and that the radial permeability of puppy bone was 6-fold higher than that of adult canines. In addition, they suggested that the periosteal portion of cortical bone was relatively impermeable as compared to the endosteal portion of cortical bone. My lipids results showed that the composition of the extracted lipids from porous compartment in cortical bone consisted of ~60% triacylglycerols, ~4% fatty acids, ~1% phospholipids and 11% cholesterol; which matched with previous reports measuring the lipid contents of human [19] or ox [45] cortical bone, respectively, and finding high levels of triacylglycerols and low levels of phospholipids. In addition my hydroxyproline results showed that the relative proportion of the porous to non-porous collagen content calculates to be 4.9%, which approximates the relative volume ratio of these two compartments of cortical bone; which match with previous report of porosity of cortical bone (2~10%) [9, 14]. These results suggested that we might be able to decrease the permeability of scaffold materials by coating them with lipids and / or collagen to adjust their overall permeability similar to that of cortical bone.

7.3 Glucose diffusion

Glucose supply always needs to be considered in bone tissue engineering since it is essential to maintain cell viability [66]. Under static culture conditions, glucose transport is only mediated by diffusion. To determine when glucose becomes limited in our system, the glucose concentration profile needed be calculated based on the diffusion coefficient of glucose in cortical bone. Therefore the diffusion coefficient of glucose in cortical bone

was experimental measured and mathematical modeling was established to generate the glucose concentration profile in Chapter IV. I can not measure the glucose diffusion coefficient with current diffusion chamber. With the measurement of the bone porosity, I can calculate the diffusion coefficient of cortical bone (3.15×10^{-9} cm^2/s) based on the correlation of porosity, tortuosity and permeability established by previous study [2, 73]. In addition, a mathematical model was established based on the transport principles to predict the glucose concentration in scaffold (here is cortical bone) and cell layers in my model system. Base on this model, the largest thickness bone tissue can be generated from this system on 300μm cortical bone was 50 μm. Thus, to generate more bone tissue, the glucose transport needs to be increased in this system, which can be done by applying mechanical load in this system.

7.4 Cell source and culture conditions

Cell source is one key component in bone tissue engineering, until now, bone cell sources used in bone tissue engineering have included mesenchymal stem cells derived from bone marrow, perioteum and umbilical et al, and mature osteoblasts, such as trabecular bone obtained during iliac crest biopsies[5, 6, 13, 29, 30, 33, 39, 42, 50, 51, 76-79, 89]. Osteo-progenitors derived from bone marrow and periostum are two popular cell types are used in bone tissue engineering. Previous Studies showed that both cell types have osteogenesis properties. Barralet et al. [6] cultured bone marrow cells on type I collagen gels for 21-28 days and showed new osteoid-like tissue formation by these cells. Sikavitsas et al. [78] cultured bone marrow cells in a flow perfusion bioreactor and

showed that such a fluid-flow bioreactor culture system minimized diffusion constraints and provided mechanical stimulation to the bone marrow cells, leading to the accumulation of a cancellous bone-like mineralized tissue. Wiesmann et al [89] cultured periosteal derived osteoblasts on Petri dishes as well as within 3D collagen constructs. They showed that these cells can form 'bone like' mineral deposits in both 2- and 3-D environments and formed an extracellular matrix containing osteocalcin, SPARC (osteonectin), and newly synthesized collagen type I in both environments. Koshihara et al [48] showed that periosteum cells are osteoblastic cells and could differentiat into osteocytes and deposited calcified mineral in response to 1, 25 dihydroxyvitamin D_3. To select the cell source used in my model system, osteogenesis of these two cell types were compared side by side on both 2D conventional tissue plastic and 3D collagen fibronetin hydrogel. Our results showed that there was no significant difference between the osteogenesis of these two cell types. Therefore either of these two cells can be used in our system.

Culture condition is another important component to be considered in my system. *In vivo*, bone formation cells lay on the osteoid layer to form bone (Figure 6-1), which is secreted by osteoblasts and becomes mineralization. Therefore, we propose that the chemicals in this layer and its structure are important for bone formation. To mimic this layer, an artificial osteoid layer was made from type I collagen and fibronectin. And the osteogenesis of primary bone cells cultured on this layer was compared with that on 2D plastic (Chapter VI). My results showed that there was significant increase of

extracellular matrix (SPARC, BSP) and calcium mineral deposition in the culture on 3D collagen- fibronectin hydrogel than that on 2D plastic, which suggested that this artifical osteoid layer promoted osteogenesis of primary bone cells. This matches with previous studies showing that collagen [6, 22, 30, 33, 49, 65] and fibronectin [60] promoted osteogenesis of bone cells. Moreover, the polarity of cells, extracellular matric and calcium mineral deposition on this 3D collagen fibronectin hydrogel was analyzed. My results showed the polarity of cell density distribution on 3D collagen fibronectin hydrogel and no polarity on the distribution of extracellular matrix and mineral deposition, which may because that overall very small amount extracellular matrix and calcium mineral deposited on 3D collagen fibronectin cultures, which suggest that my end time point is the initial differentiation time point (bone cells starts to deposit extracellular matrix and mineral); and no polarity would be generated at this time point of culture.

7.5 Future direction

1. Scaffold material

There were some limitations in characterizing the scaffold material that should be addressed in future, which include: (1) the long term biocompatibility of PMMA will be tested; (2) osteogenesis potential of bone cells cultured on these material will be measured basing on the deposition amount of extracellular matrix (alkaline phosphatase (expressed at early stage of differentiation), BSP (expressed at later stage of differentiation) and calcium mineral on these cultures with simple biochemistry methods;

specifically the amount of activity of alkaline phosphatase can be measured with alkaline

phosphatase assay kit (BioAssay System), amount of the BSP can be measured with west

blotting method and the mount of calcium mineral can be measured with a colorimetric

method; 3) Sample size will be increased to be able to exclude random variability.

<u>2. Hydraulic permeability of cortical bone</u>

There were some limitations in measuring the hydraulic permeability of cortical bone

that should be addressed in future, which include: (1) the hydraulic permeability of fresh

cortical bone will be measured. To do this there are two methods can be used: (a) with

current device, the bone wafers can be cut into several pieces of thinner wafers with same

thickness and the hydraulic permeability of these wafers will be measured at same

conditions; then the hydraulic permeability of bone wafers will be average of all these

measurements; (b) a new device with lower detection limit needs to be made. Right now

the detect limit of the present device results from the pressure limit of the holder made of

PVC. Therefore, the bone holder made from stainless steel with same design as proposed

in this chapter will increase the pressure limit of the bone holder thereby lower the

detection limit. Compare to method (a) the advantage of this method is that the hydraulic

permeability can be measured directly and the disadvantage is that some cost will be

applied on the new device. (2) Hydraulic permeability of the cortical bone from

periosteum side and the contribution of bone components to its permeability need to be

studied to understand the mechanism of the nutrient and waste transport underneath

periosteum layer, which is critical important for bone formation *in vivo*. To do this, a new

device with much lower detect limit needed. (3) Changes in ultrastructure of the remaining pericellular matrix after removing lipids and / or collagen may have effect on the changes on the permeability. To determine whether there is the change of ultrastructure, transmission electron microscopy (TEM) images of the wafers after collagenase and or acetone methonal treatment need to be compared with that of the wafers before treatments.

3. Glucose diffusion

There were some limitations in measuring the diffusion coefficient of glucose in cortical bone that should be addressed in future, which include: (1) the glucose diffusion coefficient in cortical bone will be measured with a more sensitive detection method needs to apply this system, such as using radiolabel chemicals. (2) Diffusion coefficient of oxygen will be studied to generate the oxygen concentration profile with this model system. (2) Diffusion coefficient of hydrophobic molecular (such as prostaglandin [64]) in cortical bone will be studied to better understand the nutrient transport inside the bone. (3) The diffusion coefficient of glucose in cortical bone under mechanical load will be studied to better understand the nutrient transport inside the bone. (4) Convection factors will be included in the model system to predict the glucose concentration profile in the system with mechanical load.

4. Cell source and culture condition

There were some limitations in selecting the cell source and culture conditions that should be addressed in future, which include: (1) Cultures with extended culture time (6

week) will be done to investigate the polarity of cell cultures on 3D collagen fibronectin hydrogel. (2) Multiple experimental time points will be done to investigate the cell osteogenesis status. (3)The amount of extracellular matrix in the culture medium will be measured to have a better comparison between the cultures on 3D collagen fibronectin hydrogel and 2D plastic. (4) F-actin will be stained to determine the morphology of cells which enable us to investigate the relationship between cell morphology and cell osteogenesis status.

7.6 Significance of this work

Clinically there is a need for bone graft alternatives. However there are no functional bone grafts that have been generated to meet this demand. My approach and system design provide a means for studies to be conducted towards the development of functional bone tissue *in vitro*. My ultimate goal is to generate a functional bone tissue on a biocompatible scaffold, which will be peeled off from the scaffold and used as bone scaffold material to treat large size bone defect. The data in this work provide the basis for future studies that may incorporate growth factors, mechanical stimuli and co-culture of different cells types in this bone model system to promote sustained bone formation *in vitro*.

REFERENCES

1. Attawia AM, Nicholson JJ, Laurencin TC. Co-culture system to assess biocompatibility of candidate orthopaedic materials. Clinical orthopaedics and related research research, 1999, 365: 230-236.

2. Backer LD, Baron G. Effective diffusivity and tortuosity in a porous glass immobilization matrix. Appl Microbiol Biotechnol. 1993, 39:281-284.

3. Bailey LO, Lippiatt S, Biancanello FS, Ridden SD, Washburn NR. The quantification of cellular viability and inflammatory response to stainless steel alloys. Biomatrials, 2005, 26: 5296-5302.

4. Banes AJ, Lee G, Graff R, Otey C, Archambault J, Tsuzaki M, Elfervig M, and Qi. J Current Opinion in Orthopaedics. 2001, 12:389-396.

5. Barralet JE, Wang L, Lawson M, Triffitt JT, Cooper PR, Shelton RM. Comparison of bone marrow cell growth on 2D and 3D aliginate hydrogels. Journal of materials science: materials in medicine. 2005, 16: 515-519.

6. Batorsky A, Liao J, Lund AW, Plopper GE, Stegemann JP. Encapsulation of adult human mesenchymal stem cells within collagen-agarose microenvironments. Published online 9 September 2005 in Wiley InterScience (www.interscience.wiley.com)

7. Beno T, Yoon Y, Cowin SC, Fritton SP. Estimation of Bone Permeability Using accurate microstructural measurements. Jouranl of biomechanics. 2006, 39: 2378-2387.

8. Berg RA. Determination of 3- and 4- hydroxyproline. Methods in Enzymology, 1982, Part A, 82: 372-398.

9. Bilezikian JP, Raisz LG, Rodan GA. Principles of bone biology. San Diego: Academic Press, c2002

10. Black, J.; Mattson, R.; and Korostoff, E. Haversian osteons: size distribution, internal structure, and orientation. J. Biomed. Mater. Res., 1974, 8: 299-319

11. Bordji K, Jouzeau TY, Mainard D, Payan E, Delagoutte JP, Netter P. Evaluation of the effect of three surface treatment on the biocompatibility of 316L stainless steel using human differentiated cells. Biomaterials, 1996, 17: 491-500.

12. Burger EH, Klein-Nulend J. Mechanotransduction in bone-role of lacunocanalicular network. FASEB J., 1999, 13(suppl.): S101-S112.

13. Chiu R, Ma T, Smith RL, Goodman SB. Polymethymethacrylate particles inhibits osteoblastic differentiation of bone marrow osteogenitor cells. Inc J biomed mater res, 2006, 77A: 850-856.

14. Cooper D, Turinsky A, Sensen, C, Hallgrimsson, B. Effect of voxel size on 3D micro-CT analysis of cortical bone porosity. Calcified Tissue International, 2007, 80:211-219.

15. Cooper RR, Milgram JW, Robinson RA. Morhpology of the osteon: an electron microscopic study. J Bone Joint Surg Am, 1966, 48: 1239 -1271.

16. Cowin SC. Mechanosensation and fluid transport in living bone. Journal Musculoskel Neuron Interact, 2002, 2(3): 256-260.

17. Cowin SC. Bone mechanics handbook. Boca Raton, FL: CRC press 2001

18. Dillaman RM, Roe RD, Gay DM. Fluid movement in bone: theoretical and empirical. J. biomechnics. 1991, 24: 163-177.

19. Dirksen TR, Marinetti GV. Lipids of bovine Enamel and dentin and human bone. Calc. Tiss. Res., 1970, 6:1-10.

20. Disegil JA. and Eschbachz. L. Stainless steel in bone surgery. Injury, Int.I. Care Injured 2000, 31: S-D2-6.

21. Donahue TL, Haut TR, Yellowley CE., Donahue HJ., Jacobs CR. Mechanosensitivity of bone cells to oscillating fluid flow induced shear stress may be modulated by chemotransport. Journal of Biomechanics, 2003, 36: 1363-1371.

22. Domaschke H, Gelinsky M, Burmeister B, Fleig R, Hanke T, Reinstorf A, Pompe A, Rosen-wolff A. in vitro ossification and remodeling of mineralized collagen I scaffold. Tissue engineering, 2006, 12(4): 415-423.

23. Duncan RL., Turner CH.. Mechanotransduction and functional response of bone to mechanical strain. Calcified Tissue Iternational. 1995, 57: 344-358.

24. El Haj AI, Walker LM, Preston MR, Publicover SJ. Mechanotransduction pathway in bone: calcium fluxes and the role of voltage-operated calcium channels. Medical & biological engineering & computing. 37: 403-409, 1999.

25. Gomes ME, Azevedo HS, Moreira AR, Ellä V, Kellomäki M, Reis RL. Starch-poly(epsilon-caprolactone) and starch-poly(lactic acid) fibre-mesh scaffolds for

bone tissue engineering applications: structure, mechanical properties and degradation behaviour.J Tissue Eng Regen Med. 2008 Jul;2(5):243-52.

26. Gordon JAR, Tye CE, Sampaio AV, Underhill TM, Hunter GK, Goldberg HA. Bone sialoprotein expression enhanced osteoblast differentiation and matrix mineralization *in vitro*. Bone, 2007, 41: 462-473.

27. Hanagata N, Takemura T, Monkawa A, Ikoma T, Tanaka J. Pre-adsorbed type –I collagen structure-dependent changes in osteoblastic phenotype. Biochemical and biophysical Research communications, 2006, 344: 1234-1240.

28. Helmus NM, Gibbons FD, Cebon D. Biocompatibility: meeting a key functional requirement of next-generation medical devices. Toxicologic pathology, 2008, 46:70-80

29. Hillsley MV, Frangos JA. Review: bone tissue engineering: the role of interstitial fluid flow. Biotechnology and Bioengineering, 1994, 43: 573-581.

30. Hottori K, Yoshikawa T, Takakura Y, Aoki H, Sonobe M and Tomita N. Bio-artificial periosteum for severe open fracture-An experimental study of osteogenic cell/collagen sponge composite as a bio-artificial periosteum. Bio-Medical materials and engineering, 2005, 15:127-136.

31. Hsieh YF, Robling AG., Ambrosius WT, Burr DB and Turner CH. Mechanical loading of diaphyseal bone *in vivo*: The strain threshold for an osteogenic response varies with location. Journal of Bone and Mineral Research, 2001, 16(12): 2291-2297.

32. Huang H, Kamm RD, Lee RT. Cell mechanics and mechanotransduction: pathways, probes, and physiology. Am J Physiol Cell Physiol. 2004, 287: C1–C11.

33. Ignatius A, Blessing H, Liedert A, Schmidt C, Neidlinger-Wilke C, Kaspar D, Friemert B, Claes L. Tissue engineering of bone: effect of mechanical strain on osteoblastic cells in type 1 collagen matrices. Biomaterials, 2005, 26:311-318.

34. Inman CL, Warren GL, Hogan HA, and Bloomfield SA. Mechanical loading attenuates bone loss due to immobilization and calcium deficiency. Journal application physiology. 1999, 87(1): 189-195.

35. Jackson AR, Yuan TY, Huang CC, Travascio F, Gu WY. Effect of compressionand anisotropy on the diffusion of glucose in annulus fibrosus. Spine 2008; 33: 1-7

36. Jocobs AM, Gloft LM. Podiatric metallurgy and the effects of implanted metals on living tissues. Clin podiatry, 1985, 2:121-141.

37. Johnson RL, Tabin CJ. Molecular models for vertebrate limb development. Cell, 1997, 90: 979-990.

38. Jundt G, Bergh-iusert KH, Termine JD, Schulz A. Osteonectin- a differentiation marker of bone cells. Cell Tissue Res. 1987, 248 (2): 409-415

39. Khan YK, Yaszemski MJ, Mikos AG, Laurencin CT. Tissue Engineering of Bone: Material and Matrix Considerations. J Bone Joint Surg Am, 2008, 90:36-42.

40. Kraft CN, Burian B, Diedrich O, Wimmer MA. Implication of orthopedic fretting

143

corrosion particles on skeletal muscle microcirculation. Journal of materials science: materials in medicine, 2001, 12 : 1057-1062.

41. Kraft CN, Diedrich O, Pourian B, Schmitt O, Wimmer MA. Microvascular response of striated muscle to metal debris- a comparative in vivo study with titanium and stainless steel. J. Bone Joint Surg (Br), 2003, 85(B): 133-141.

42. Koshihura Y, kawamura M, Endo S, Tsutsumi C, Kodama H, Higaki S. establishment of human osteoblastic cells dedrived from periosteum in culture. In vitro cellular & developmental biology. 1989, 25(1): 37-43

43. Lang SB, Stipanich N, Soremi EA. Diffusion of glucose in stressed and unstressed canine femur *in vitro*. Annals New York academy of sciences. 1974, 238: 139-148.

44. Leblond CP, Wilkinson GW, Belanger LF, Robichon J. Radio-autographic visualization of bone formation in the rat. Am J. Anat., 1950, 86(2): 289-341.

45. Leach AA. The lipids of ox compact bone. Biochem J. 1958, 69(3): 429-432.

46. Li GP, Bronk JT, An KN, Kelly PJ. Permeability of cortical bone of canine tibia. Microvasc Res., 1987, 34: 302-310.

47. Livingston T, Ducheyne P,Garino. *In vivo* evaluation of a bioactive scaffold for bone tissue engineering. J Biomed Mater Res. 2002, 62: 1–13.

48. Maroudas A, Stockwell RA, Nachemson A, Urban J. Factor involved in the nutrition of the human lubar intervertebral disc: cellularity and diffusion of glucose in vitro. J Anat, 1975, 120(1): 113-130.

49. Masi L, Fanchi A, Santucci M, Danielli D, Arganini L, Giannone V, Formigli L, Benvenuti S, Tanini A, Beghe F, Mian M, Brandi ML. Adhesion, growth and matrix production by osteoblasts on collagen substrata. Calcif Tissue int. 1992, 51: 202-212.

50. Mauney JR, Sjostorm S, Blumberg J, Horan R, O'Leary JP, Vunjak-Novakovic G, Volloch V, Kaplan DL. Mechanical stimulation promotes osteogenic differentiation of human bone marrow stromal cells on 3-D partially demineralized bone scaffolds in vitro. Calcified tissue international, 2004, 74(5):458-68.

51. Meinel L, Karageorgiou V, Fajardo Snyder RB, Shinde-Patil V, Zichner L, Caplan D, Langer R, and Vunjak-Novakovic G. Bone tissue engineering using human mesenchymal stem cells: effect of scaffold material and medium flow. Annals of biomedical engineering, 2004, 32(1): 112-122,.

52. Mishra S. and Knothe Tate ML, Effect of lacunocanalicular architecture on hydraulic conductance in bone tissue: implications for bone health and evolution. The Anatomical record. 2003: 273A: 752-762.

53. Montanaro L, Cervellati M, Campoccia D, Prati C, Breschi L, Arciolo CR. No genotoxicity of a new nickel-free stainless steel. Int J. Artif Organs, 2005, 28(1): 58-65.

54. Moursi AM, Damsky CH, Lull J, Zimmerman D, Doty SB, Aota S. Globus RK. Fibronectin regulates calvarial osteoblast differentiation. Journal of Cell Science. 1996, 109: 1369-1380.

55. Moursi AM, Winnard AV, Winnard PL, Lannulti JJ, Seghi, RR. Enhanced osteoblast response to a polymethylmetacrylate hydroxyapatite composite. Biomaterials, 2002, 23:133-14

56. Muellar, K. H.; Trias, A.; and Ray, R. D. Bone density and composition: Age-related and pathological changes in water and mineral content. J. Bone and Joint Surg., 1966, 48-A: 140-148.

57. Mullender M., Haj AJE, Yang Y, van Dulin MA,. Hurger EH, Klein-Nulend J. Mechanotransduction of bone cells *in vitro*: mechanobiology of bone tissue. Medical & biological engineering & computing, 2004, 42, 14-21.

58. Murshid SA, KamiokaH, Ishihara Y, Ando R, Sugawara Y, Takano-yamamoto T. Actin and microtubule cytoskeletons of the processes of 3D-cultured MC 3T3-E1 cells and osteocytes. J. bone miner metab. 2007, 25: 151-158.

59. Petrov N. and. Pollack SR. Comparative analysis of diffusive and stress induced nutrient transport efficiency in the lacunar-canalicular system of osteons. Biorheology, 2003, 40: 347-353.

60. Pietrazk WS, Woodell-May J. The composition of human cortical allograft bone derived from FDA/AATB-screened donor. J. Craniofac. Surg., 2005, Jul, 16(4):579-85.

61. Puleo DA, Holleran LA, Doremus RH, Bizios R. Osteoblast response to orthopedic implant materials in vitro. J. biomed mater res, 1991, 25(6):711-23

62. Qi J, Chi L, Faber J, Koller B, Banes AJ. ATP reduces gel compaction in osteoblast-population collagen gels. J, Appl Physiol, 2007, 102 (3): 1152-1160

63. Ramachandran R, Goodman SB, Smith RL. The effect of titanium and polymethylmathacrylate particles on osteoblast phenotypic stability. J biomed mater res, 2006, 77A: 512-517.

64. Raisz LG. Prostaglandins and bone: physiology and pathophysiology. Osteoarthritis & Cartilage. 1999, 7(4):419-21.

65. Rattner A, Sabido O, Le J, Vico L, Massoubre C, Frey J, Chamson A. Mineralization and alkaline phosphatase activity in collagen lattices populated by human osteoblasts. Calcif Tissue Int. 2000, 66: 35-42.

66. Bronner F, Farach-Cason MC, Mikos AG. Engineering of Functional skeletal tissues. London, Springer. C2007

67. Robinson LG, Pugh ER. The determination of serum cholesterol. US Armed Forces Medical Journal. 1957, 9(4): 501-507.

68. Ronald HAD, Verbeeck MH, L. I.F.J.M. De Ridder, Schacht EH, Cornelissen MJ. Calcification as an indicator of osteoinductive capacity of biomaterials in osteoblastic cell cultures. Biomaterials, 2005, 26: 4964-4974.

69. Sander EA, Nauman EA. Permeability of Musculoskeletal Tissues and Scaffolding Materials: Experimental Results and Theoretical Predictions. Critical Reviews in Biomedical Engineering, 2003, 31(1): 1-26.

70. Setlana V. Komarova, Fasoil I. Ataullakhanov, and Ruth K. Globus Bioenergetics and mitochondrial transmembrane potential during differentiation of cultured osteoblasts. Am J Physiol Cell Physiol 279: C1220-C1229, 2000.

71. Seidl DKL, Neidlinger-Wilke C, Claes L. *In vitro* effect of dynamic strain on the proliferative and metabolic activity of human osteoblast. J. Musculoskel Neuron Interact, 1(2): 161-164, 2000.

72. Seidl DKW, Neidlinger-Wilke C, Ignatius A, Claes L. Dynamic cell stretching increases human osteoblast proliferation and CICP synthesis but decrease osteocalcin synthesis and alkaline phosphatase activity. Journal of biomechanics, 33:45-51, 2000.

73. Shen L, Chen Z, Critical review of the impact of tortuosity on diffusion. Chemical Engineering Science. 62 :3748 – 3755, 2007

74. Shimko DA, Nauman EA. Development and Characterization of a porous poly (methacrylate) scaffold with controllable modulus and permeability. Journal of Biomedical material Research. Part B. Applied Biomaterial, 2007, 80B 360-369.

75. Shimko DA, White KK, Nauman EA and Dee KC. A device for long term, *in vitro* loading of three-dimensional natural and engineering tissues. Annals of biomedical engineering. 2003, 31:1347-1356.

76. Shin H, Zygourakis K, Farach-Carson MC, Yaszemski MJ, Mikos AG. Attachment, proliferation, and migration of marrow stromal osteoblasts cultured on biomimetic hydrogels modified with an osteopontin-derived pepetide. Biomaterial, 2004, 25: 895-906.

77. Shin M, Yosimoto H, Vacanti JP. *In vivo* bone tissue engineering using mesenchymal stem cells on a novel electropun nanofibrous scaffold. Tissue Engineering. 2004, 10(12):33-41.

78. Sikavitsas VI, Bancroft GN, Holttorf HL, Jansen JA, and Mikos AG. Mineralized matrix deposition by marrow stromal osteoblasts in 3D perfusion culture increases with increasing fluid shear forces. PNAS, 100(25): 14683-14688, 2003(December).

79. Sikavitsas VI, Bancroft GN, Mikos AG. Formation of three- dimensional cell/polymer constructs for bone tissue engineering in a spinner flask and a rotating wall vessel bioreactor. Inc J. biomed mater Res. 2002, 62: 126-148.

80. Simonds WF, Koski G, Streaty RA, Hjelmeland LM, Klee WA. Solubilization of active opiate receptors. Proc Natl Acad Sci USA, 1980, 77(8) : 4623-4627

81. Stegemann H, Stalder K. Determination of hydroxyproline. Clinica Chimica Acta, 1967, 18: 267-273.

82. Takahashi T, Ueda S, Takahashi K, Scow RO. pH-dependent multilamellar structures in fetal mouse bone: possible involvement of fatty acids in bone

mineralization. American Journal Physiology, 1995, 266 (cell physiology. 35), C590-C600.

83. Turner CH, Forwood MR, RHO JY, Yoshikawa T. Mechanical loading thresholds for lamellar and woven bone formation. Journal of bone and mineral research, 1994, 9(1): 87-97.

84. Turner CH, Owan I, and Takano Y. Mechanotransduction in bone: role of strain rate. American Journal of Physiology, 1995, 269 (Endocrinol, Metab. 32), E438-E442.

85. Venugopal J, Low S, Choon AT, Kumar TSS, Ramakrishna S. Mineralization of osteoblasts with electrospun collagen/hydroxyapatite nanofibers. J mater sci: mater med

86. Wahl DA, Sachlos E, Liu C, Czernuzka. Controlling the processing of collagen-hydroxyapatites scaffolds for bone tissue engineering. Journal of bone and mineral research, 2001, 16(9):

87. Watson KE, Parhami F, Shin V. Demer LL. Fibronectin and collagen I matrixes promote calcification of vascular cells in vitro, whereas collagen IV matrix inhibitory. Thromb Vasc Biol, 8:1964-1971. 1998.

88. Weinger JM, Holtrop ME. An ultrastructural study of bone cells: the occurrence of microtubules, microfilaments and tight junctions. Callc. Tiss. Res. 1974, 14: 15-29, 1974

89. Wiesmann HP, Nazer N, Klatt C, Szuwart T, Meyer U. Bone tissue engineering

by primary osteoblast-like cells in monolayer system and 3-Dimensional collagen gel. J Oral Maxillofac Surg, 61: 1455-1462, 2003

90. Winet H. A bone fluid flow hypothesis for muscle pump-driven capillary filtration: II proposed role for exercise in erodible scaffold implant incorporation. European Cells and Materials, 2003, 6: 1-11.

91. Wuthier RE. Lipids of matrix vesicles. Fed. Proc, 1976, 35(2):117-121.

92. Yang C, Hillas PJ, Baez JA, Nokelainen M, Balan J, Tang J, Spiro R, Polarek JW. The application of recombinant human collagen in tissue engineering. biodrugs, 18(2): 103-119, 2004

93. Yang Z, Yu X, Huang F, Xie H. The influence of type 1 collagen on the cell behavior of human embryonic periosteous osteoblasts. Jounal of WCUMS 32(1): 1-4, 2001.

94. Yu X, Botchwey AE, Levine EM, Pollack SR, and Laurencin CT. Bioreactor-based bone tissue engineering; the influence of dynamic flow on osteoblast phenotypic expression and matrix mineralization. PNAS, 101(31): 11203-11208, 2004.

95. Zaffe D. Some Considerations on biomaterials and bone. Micron. 36(7-8): 583-92, 2005.

APPENDIX

APPENDIX 1: The schematic of permeability device